Kinetics of free radical homo- and copolymerisations investigated with pulsed laser methods

DISSERTATION

for the award of the degree
"Doctor rerum naturalium"
of the Georg-August-Universität Göttingen

within the doctoral program chemistry
of the Georg-August University School of Science (GAUSS)

submitted by
ENNO MEYER
from Hannover

Göttingen, 2023

Thesis Advisory Committee:

Prof. Dr. Philipp Vana

apl. Prof. Dr. Thomas Zeuch

Prof. Dr. Dirk Schwarzer

Members of the Examination Board

Reviewer:

Prof. Dr. Philipp Vana, Institut für Physikalische Chemie

Second Reviewer:

apl. Prof. Dr. Thomas Zeuch, Institut für Physikalische Chemie

Further Members of the Examination Board:

Prof. Dr. Dirk Schwarzer, Max-Planck-Institut für multidisziplinäre Naturwissenschaften

Jun.-Prof. Dr. Daniel Obenchain, Institut für Physikalische Chemie

Jun.-Prof. Dr. Anna Krawczuk, Institut für Anorganische Chemie

Dr. Tim Schäfer, Institut für Physikalische Chemie

Date of the Oral Examination: 08.02.2024

There shall, in that time, be rumors of things going astray, erm, and there shall be a great confusion as to where things really are, and nobody will really know where lieth those little things with the sort of raffia work base that has an attachment. At this time, a friend shall lose his friend's hammer and the young shall not know where lieth the things possessed by their fathers that their fathers put there only just the night before, about eight o'clock.

— Unknown prophet, circa 30 A.D.

Abstract

Free-radical polymerisation is the most important polymerisation process due to its simplicity and robustness. It is therefore necessary to understand the kinetics of the involved reactions in order to plan a polymerisation, be it on lab scale or industrial scale. Three different topics are investigated in this thesis:

First, the copolymerisation of styrene (Sty) with maleic anhydride (MAn) which is interesting from a kinetic standpoint because MAn does not homopolymerise. Thus, several reaction steps can be neglected and the kinetic treatment is simplified. By using the Single–pulse pulsed–laser–polymerisation with EPR spectroscopy (SP–PLP–EPR) technique developed by Buback, hitherto unknown chain-length dependent termination rate coefficients can be extracted. However, it was not possible to investigate this system with SP–PLP–EPR due to a to small signal-to-noise ratio (S/N). However some preliminary calculations had been performed which are shown.

Second, since petrol-based monomers are not sustainable, bio-based alternatives are of great interest. A well-known bio-based monomer family is itaconic acid and its corresponding esters. The propagation and termination kinetics of a few of the homologues have been already investigated in earlier publications. However, for the diethyl and di-*n*-propyl ester no data exist. Consequently, this gap was closed by measuring the propagation rate coefficient with Pulsed laser polymerisation–size exclusion chromatography (PLP–SEC) and the chain-length dependent termination rate coefficent with the already mentioned SP–PLP–EPR methods. Both rate coefficients were determined for a range of temperatures.

The third topic deals with the kinetics of copolymerisations and a rarely investigated property of copolymerisations, the propagating radical fraction (PRF) which describes the composition of radical functionalities during a copolymerisation. This observable was measured for three different copolymerisation systems with stationary EPR spectroscopy and subsequent fitting of the copolymerisation EPR spectra with *easyspin*. The equation describing the PRF was fitted to obtain kinetic parameters. This yielded unplausible results. Consequently, a new data evaluation method, called 'determining reactivity ratios with a conjoined scalable fit (DRACO)', was created which combines the kinetic information of multiple observables in order to make the results more reliable. In this case, the composition of the final copolymer, the overall propagation rate coefficient $\langle k_\mathrm{p} \rangle$ and the previously described PRF were used. The method finds kinetic parameters which describe the combination of all observables best instead of the still widespread practice of fitting each property separately. DRACO can be easily adapted to include other or more observables. The version developed in this work can use the explicit penultimate model, the implicit penultimate model or the terminal model, but other models can be easily implemented. This approach yielded plausible results which can now be considered the new best values.

Contents

1. Introduction and motivation

Since the first polymers were discovered by Baekeland and Staudinger at the beginning of the 20$^{\text{th}}$ century polymer chemistry has grown to an important field in modern chemistry.[1,2] Polymeric products are omnipresent in todays world. Applications include for example beverage bottles, packaging material and car parts. But also more specialised, high-end applications exist, for example in medical syringes or aviation parts. Most polymers are produced with the free radical polymerisation because this is the easiest and most robust polymerisation method. Different solvents and monomers can be easily polymerised and the tolerance towards impurities is the highest for any polymerisation method.

The production of plastic products amounted to 390.7 Mt in 2022, of which 90.2 % are produced from fossil sources, 8.3 % are recycled and only 1.5 % are bio-based.[3] Fossil-based plastic is obviously not sustainable. Only bio-based plastics are a sustainable source of plastics and thus their percentage of the total plastic production should be increased significantly. A prominent example for a monomer which can be synthesised from renewable sources is itaconic acid.[4–12] From itaconic acid which hardly polymerises, its corresponding esters can be synthesised easily, which do yield polymers. Here the diethyl ester is especially interesting due to the bioavailability of ethanol. However the kinetics of the itaconic acid esters are not completely understood, especially for the diethyl ester, no rate coefficients have been determined up to now. This work aims to change that by investigating the propagation and termination kinetics of diethyl itaconate in order to lay the foundation for usage in large-scale polymerisation. Up to now some applications of itaconates in unsaturated polyester resins exist but that is far from being on a significant scale.[13,14] In order to investigate the propagation kinetics,

the IUPAC-recommended PLP–SEC method developed by Olaj is used.[15] This method is based on the application of several laser pulses to a monomer sample which induces chain growth. The resulting molar weight distribution then shows distinct peaks which can be correlated to the propagation rate coefficient. For the termination, the SP–PLP–EPR method is used which was developed by Buback.[16] This method allows direct time-resolved observation of the radical concentration and is thus the best method to investigate termination kinetics. The underlying model for chain-length-dependent termination is the 'composite model' by Smith, Russell and Heuts.[17]

Many commercial plastic products are copolymers, i.e. consisting of more than one monomer. The kinetics of copolymerisations are significantly more complex than for homopolymerisation and there is still no universally accepted model for copolymerisations. Rate coefficients (or rather the ratio of rate coeffients) obtained from experimental data typically have a large uncertainty and vary strongly between results from different labs. This work introduces a new data evaluation method based on earlier work by Schweer and Riemann.[18,19]. This method combines several data sets to be fitted simultaneously and can be easily expanded to include more data. Also the physical model can be easily changed. The method was applied to three different comonomer systems: Sty/DMA, Sty/DEI and Sty/MMA, the last system being one of the most investigated copolymerisation systems and the one where the failure of the up to then widely accepted terminal model was shown first.[20]

2. Theory

2.1. Ideal polymerisation kinetics

Ideal polymerisation kinetics are described in countless textbooks and reviews. A free radical polymerisation requires at least two different chemicals: The initiator and the monomer. The initiator is a labile molecule such as peroxides or azo compunds, while the monomer is a molecule with an olefinic double bond. Typical monomers of commercial interest are acrylates, methacrylates and styrene. Further compounds can be added to modify the properties of the product, such as a chain transfer agent. As they will not be used within this thesis, they are not discussed in great detail. Optionally the reaction can be performed in an inert solvent. In ideal polymerisation kinetics, a few simplifying assumptions are made:[21]

1. The radical concentration is stationary.

2. All reactions are irreversible.

3. Monomer is consumed only in the propagation step.

4. All rate coefficients are independent of conversion and chain length.

5. Chain termination occurs only via combination or disproportionation.

Only three reactions are considered in ideal kinetics: initiation, propagation and termination. Each of these will be described briefly.

2.1.1. Initiation

The initiation step consists of the homolytic cleavage of an initiator molecule, yielding two primary radicals (eq. 2.1). This cleavage can be induced either thermally or by photolysis. The primary radicals then attacks the double bond of a monomer molecule and add to it, shifting the radical functionality to the former double bond (eq. 2.2).

$$\mathrm{I_2} \xrightarrow[h\nu,\Delta]{k_\mathrm{d},f} 2\mathrm{I}^{\cdot} \tag{2.1}$$

$$\mathrm{I}^{\cdot} + \mathrm{M} \xrightarrow{k_\mathrm{i}} \mathrm{P_1}^{\cdot} \tag{2.2}$$

In practice, depending on the viscosity of the reaction mixture, solvent, intermolecular forces etc., not all primary radicals initiate chain growth, but some recombine with the other primary radical to give the inverse reaction of eq. 2.1. To account for this, k_I is modified by a factor f, the initiator efficiency, which runs from 0 to 1. The rate law for the first step is:

$$\frac{\mathrm{d}\, c_{\mathrm{I}\cdot}}{\mathrm{d}\, t} = 2 \cdot k_\mathrm{d} \cdot f \cdot c_{\mathrm{I}_2} \tag{2.3}$$

The second step is typically very fast, significantly faster than the propagation. It can consequently be neglected in the kinetic treatment.

2.1.2. Propagation

The newly formed monomer radical then undergoes a chain reaction, adding more monomer molecules and shifting the radical functionality in the same fashion as before. The radical functionality is always located at the end of the chain, the so-called active end. This is the reaction step which is responsible for the creation of a polymer.

$$\mathrm{P_n}^{\cdot} + \mathrm{M} \xrightarrow{k_\mathrm{p}} \mathrm{P_{n+1}}^{\cdot} \tag{2.4}$$

$$\frac{\mathrm{d}\, c_\mathrm{M}}{\mathrm{d}\, t} = -k_\mathrm{p} \cdot c_\mathrm{M} \cdot c_{\mathrm{P_n}^\cdot} \tag{2.5}$$

2.1.3. Termination

When two macroradicals encounter each other, the termination reaction occurs, destroying both active ends. This can happen either via recombination (eq. 2.6), creating one dead polymer chain with the combined length of both macroradicals or via disproportionation (eq. 2.7), where one of the macroradicals abstracts a hydrogen atom from the other macroradical, leaving two dead polymer chains, of which one has an olefinic bond at the end. This olefinic bond is of no interest to the kinetics, however.

$$\mathrm{P_n}^\cdot + \mathrm{P_m}^\cdot \xrightarrow{k_\mathrm{t,comb}} \mathrm{P_{n+m}} \tag{2.6}$$

$$\mathrm{P_n}^\cdot + \mathrm{P_m}^\cdot \xrightarrow{k_\mathrm{t,dis}} \mathrm{P_n} + \mathrm{P_m} \tag{2.7}$$

Since both termination reactions occur simultaneously, one can define k_t as the sum of $k_\mathrm{t,comb}$ and $k_\mathrm{t,dis}$. The corresponding law is:

$$\frac{\mathrm{d}\, c_{\mathrm{P_n}^\cdot}}{\mathrm{d}\, t} = -2 \cdot k_\mathrm{t} \cdot c^2_{\mathrm{P_n}^\cdot} \tag{2.8}$$

It is noteworthy that termination is second order in the radical concentration and thus especially sensitive to it. Also some literature does not include the factor of 2 but incorporates it into the rate coefficient. In this work the IUPAC-recommended form of explicitly using the factor of 2 is used.

Assuming stationary conditions, the rate of radical termination and rate of radical formation are identical:

$$2 \cdot k_\mathrm{d} \cdot f \cdot c_{\mathrm{I_2}} = 2 \cdot k_\mathrm{t} \cdot c^2_{\mathrm{P_n}^\cdot} \tag{2.9}$$

Inserting this in eq. 2.5, one obtains the polymerisation rate:

$$-\frac{\mathrm{d}\, c_\mathrm{M}}{\mathrm{d}\, t} = R_\mathrm{p} = k_\mathrm{p} \cdot c_\mathrm{M} \cdot \sqrt{\frac{k_\mathrm{d} \cdot f \cdot c_{\mathrm{I_2}}}{k_\mathrm{t}}} \tag{2.10}$$

From this it can be seen that knowing the initiator decay rate coefficient and initiator efficiency one can determine the ratio $\frac{k_\mathrm{p}}{\sqrt{k_\mathrm{t}}}$ by measuring the conversion as a function of time, a method which has been employed widely in literature. For further reading the reader is referred to reference [22].

2.2. Side reactions

Naturally, in a real polymerisation many more reactions occur which can influence the kinetic description. Most prominent examples of this are transfer reactions where the radical functionality is transferred to either a different molecule or polymer chain or within the polymer chain itself. The latter is also known as backbiting. Transfer can occur to solvent molecules, monomer or a separately added chain transfer agent (CTA) which is usually a thiole. A CTA is added to control the obtained chain length distribution. Backbiting and transfer to other polymer chains can generate a tertiary radical (a so called mid-chain radical (MCR)) which has strongly different kinetic properties than the usual secondary radicals. Typically due to the radical now being tertiary and therefore more stable, k_p is strongly reduced for these MCR and k_t is reduced as well due to steric hindrance. However for this work, these side reactions are not relevant.

2.3. Diffusion control in radical polymerisations

Most reaction steps in a polymerisation are bimolecular reactions, consequently two different molecules have to encounter each other for a reaction to take place. It is therefore necessary to look into diffusional properties. As the viscosity of the reaction mixture increases with the conversion χ, all diffusional effects are conversion-dependent, especially in bulk polymerisations.

2.3.1. Diffusion control of initiation

As mentioned earlier, the two primary radicals can recombine which is expressed by the initiator efficiency f. At higher viscosities, escaping the solvent cage becomes more and more difficult and thus f decreases. This is called the 'cage effect'.

2.3.2. Diffusion control of termination

Termination is diffusion-controlled already at zero conversion as can be shown by several reasons:[23]

1. The Smoluchoswki equation (eq. 2.12) gives an accurate prediction for the termination rate of small radicals.[24–26]
2. k_t is inversely proportional to the viscosity.
3. k_t decreases with pressure, showing a positive activation volume.[23]

The Stokes-Einstein equation (eq. 2.11) describes the self-diffusion coefficient D_i where i denotes the chain length:[27]

$$D_\mathrm{i} = \frac{k_\mathrm{B} \cdot T}{6 \cdot \pi \cdot r_\mathrm{i} \cdot \eta} \tag{2.11}$$

D_i depends on the hydrodynamic radius r_i which is chain-length-dependent and the viscosity η. The Smoluchowski equation describes the diffusion rate coefficient:[28]

$$k_\mathrm{D} = 4\pi \cdot P_\mathrm{Spin} \cdot N_\mathrm{A} \cdot (D_\mathrm{A} + D_\mathrm{B}) \cdot R_\mathrm{c} \tag{2.12}$$

Here P_Spin denotes the spin factor and R_c the capture radius. Inserting the Stokes-Einstein equation and using $P_\mathrm{Spin} = 0.25$ and $D_\mathrm{A} = D_\mathrm{B}$, this is simplified to:[26]

$$k_\mathrm{D} = \frac{R \cdot T \cdot R_\mathrm{c}}{6 \cdot \eta \cdot r_\mathrm{i}} \tag{2.13}$$

For small molecules like monomers assuming a spherical radical is a good approximation. For spherical radicals, $R_\mathrm{c} = 2 \cdot r_1$ is valid. Inserting this into eq. 2.13

one obtains the so-called 'diffusion limit' which is the maximum possible value of $k_t^{1,1}$.

$$k_t^{1,1} = \frac{R \cdot T}{3 \cdot \eta} \tag{2.14}$$

At higher conversion, the 'Trommsdorff effect' or 'gel effect' starts to take effect. It describes the decrease in k_t with increasing viscosity. As the diffusion of macroradicals becomes more and more hindered, termination is suppressed and thus the concentration of macroradicals begins to rise, increasing the polymerisation rate and also increasing the reaction temperature which further increases the reaction rate, potentially leading to an explosion. This can be prevented by performing the polymerisation in solution.

2.3.3. Diffusion control of propagation

Also for the propagation step, a macroradical and a monomer molecule have to encounter each other. However, monomer is under typical conditions in a vast excess compared to macroradicals, so that it is ubiquitous. Diffusion has a minor influence and propagation is chemically controlled. In this regime, k_p can be described by eq. 2.15.[29]

$$\frac{1}{k_p} = \frac{1}{k_p^0} + \frac{1}{k_p^\chi} \tag{2.15}$$

Here k_p^0 denotes k_p at zero conversion and k_p^χ denotes the conversion-dependent k_p which in turn is calculated by eq. 2.16.

$$k_p^\chi = \frac{k_p^{\chi,0}}{\eta_{rel}} \tag{2.16}$$

$k_p^{\chi,0}$ is the rate coefficient of a very fast transportation process at zero conversion. It typically has a value of around $10^{11}\,\mathrm{L\,mol^{-1}\,s^{-1}}$. η_{rel} is the reduced viscosity, indicating the increased viscosity during the polymerisation.[29]

$$\eta_{rel} = \frac{\eta(\chi)}{\eta_0} \tag{2.17}$$

Here η_0 denotes the viscosity at zero conversion. Due to the high value of $k_\mathrm{p}^{\chi,0}$ the second term in eq. 2.15 has no influence up to high conversions and consequently k_p can be assumed to be conversion-independent.

For very high conversions (higher than for the Trommsdorff effect), the so-called 'glass effect' starts to influence the propagation. The monomer diffusion becomes hindered, so that the whole reaction mixture becomes 'frozen'. The macroradicals then can terminate only by growing through the solution ('reaction diffusion') and eventually encountering each other. Propagation and termination rate are greatly reduced in this conversion regime.

2.4. Chain-length dependence of rate coefficients

2.4.1. Chain-length dependence of propagation

For k_p, a chain-length dependence is found only for small chain lengths up to roughly $i = 10$. The chain-length-dependence can be interpreted in terms of transition state theory (TST) as the reduction of internal mobility in the transition state (TS) which lowers the entropy-governed pre-exponential Arrhenius factor. For higher chain lengths this effect becomes significantly less pronounced and converges to the long-chain coefficient k_p^∞. Mathematically the chain-length-dependent k_p can be described by:

$$k_\mathrm{p}{}^i = k_\mathrm{p}^\infty \cdot \left(1 + C_1 \cdot \exp\left(-\frac{\ln(2)}{i_{1/2}} \cdot (i-1)\right)\right) \tag{2.18}$$

$$C_1 = \frac{k_\mathrm{p}^1 - k_\mathrm{p}^\infty}{k_\mathrm{p}^\infty} \tag{2.19}$$

C_1 describes the magnitude of decrease of k_p and $i_{1/2}$ can be understood as a 'half life chain length', indicating the chain lengths which are affected by the chain-length dependence.. Typical values are $C_1 = 10$ and $i_{1/2} = 1$ which means that k_p for monomer radicals is up to one order of magnitude higher than the long-chain limit.

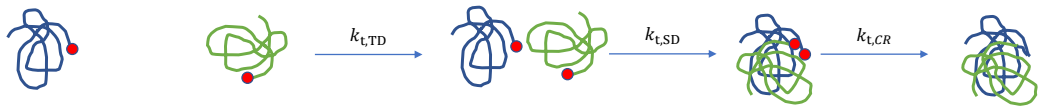

Figure 2.1.: Mechanism of the three substeps of the termination reaction according to Benson and North.[30]

2.4.2. Chain-length dependence of termination

Termination is perhaps the reaction step for which the chain-length dependence is best investigated. In order to understand the chain-length dependence, it is necessary to look into the mechanism of the termination reaction. Benson and North proposed a three-step procedure: First center-of-mass diffusion of two macroradicals to each other (translational diffusion (TD)) occurs, followed by a reorientation of the coiled macroradicals so that both radical functionalities can make contact (segmental diffusion (SD)) and the last step is the chemical reaction. Typically the chemical reaction is very fast and thus not of interest for the kinetics. For short chains, translational diffusion is rate determining while for chains longer than a crossover-chainlength i_c segmental diffusion becomes rate determining. The termination rate coefficient is thus comprised of three separate k_t:[29]

$$\frac{1}{k_t} = \frac{1}{k_{t,TD}} + \frac{1}{k_{t,SD}} + \frac{1}{k_{t,CR}} \tag{2.20}$$

The chain-length dependence of k_t for two identical chain lengths is described by a power-law:

$$k_t^{i,i} = k_t^{1,1} \cdot i^{-\alpha} \tag{2.21}$$

However this power-law does not capture the change in the rate-determining diffusion process. Smith, Russell and Heuts formulated two separate power-laws for the short- and long-chain regime where the crossover-chainlength i_c determines when the other diffusion mechanism becomes rate-determining.[17] $k_t^{1,1}$ is the termination rate coefficient of two monomeric radicals (which has to be below the diffusion limit in eq. 2.14 and should have the same activation energy as the fluidity). k_t^0 is a hypothetical rate coefficient for two coiled monomer radicals which is of course

a purely theoretical concept. The α_s and α_l parameters describe the strength of the chain-length dependence.

$$k_t^{i,i} = k_t^{1,1} \cdot i^{-\alpha_s} \quad ; i \leq i_c \tag{2.22}$$

$$k_t^{i,i} = k_t^{1,1} \cdot i_c^{-\alpha_s+\alpha_l} \cdot i^{-\alpha_l} = k_t^0 \cdot i^{-\alpha_l} \quad ; i > i_c \tag{2.23}$$

Typical values for i_c can vary from small chain-lengths as 20 for vinyl acetate (VAc) to values well above hundred (270 for 2-ethylhexyl methacrylate (2-EHMA).[31,32] For all monomers except methacrylates, i_c was found to be temperature-independent. For methacrylates the temperature-dependence might be correlated to the hindered internal rotation which makes the polymer chains more rigid at low temperatures. α_s is predicted from theory to be around 0.5-0.6 and α_l at 0.1-0.2.[17,33–38]

Termination for radicals with different chain lengths

The composite model treats only macroradical termination for identical chain lengths. In a continuously initiated polymerisation radicals of all different chain lenghts are present and can terminate with each other. To determine the termination rate coefficient for this scenario, three approaches exist:[23]

1. geometric mean model (GMM)
2. harmonic mean model (HMM)
3. diffusion mean model (DMM)

$$k_t^{i,j} = k_t^{1,1} \cdot \sqrt{i \cdot j}^{-\alpha} \quad \text{GMM} \tag{2.24}$$

$$k_t^{i,j} = k_t^{1,1} \cdot \left(\frac{2 \cdot i \cdot j}{i + j} \right)^{-\alpha} \quad \text{HMM} \tag{2.25}$$

$$k_t^{i,j} = \frac{1}{2} \cdot k_t^{1,1} \cdot \left(i^{-\alpha} + j^{-\alpha} \right) \quad \text{DMM} \tag{2.26}$$

The DMM is most accurate for small molecules where translational diffusion is dominant, while the HMM is more accurate for larger macroradicals where segmental diffusion becomes rate-determining.[39,40] The GMM however can not be

correlated to a physical process but was shown to model the segmental diffusion well.[39] All of these models collapse into the already described power-law (eq. 2.21) for $i = j$.

2.5. Kinetics of copolymerisations

In a copolymerisation, where two (or more) monomers are present, the kinetics are far more complicated than in a homopolymerisation. The general concepts of initiation, propagation and termination still apply, however each of these steps becomes more complex. A detailed understanding is necessary because the reaction kinetics influence properties such as copolymer composition, sequence distribution and reaction rate, all of which are necessary to know in order to obtain the desired product. Most models neglect chain length dependence of the rate coefficients which will be also done here.

In a copolymerisation both monomers are consumed at different rates. This leads to a drift in the composition of the reaction mixture, the so-called 'composition drift'. In certain cases, for a well-defined comonomer composition, an azeotropic copolymerisation can be realised, where both monomers are consumed at the same rate, hence no composition drift occurs. For the experiments conducted in this work, a composition drift is suppressed by polymerising only to small conversions.

2.5.1. Initiation in copolymerisations

The initiation step is largely unaffected by the presence of another monomer. The decay of the initiator is not influenced, but the primary radicals can have a preference for one of the monomers. This is however not of great interest for the kinetics.

2.5.2. Propagation in copolymerisations

This is the most interesting step in a copolymerisation because it influences properties like the composition of the copolymer and reaction rate the most. A number of models for this step exist, which are described in greater detail in reference [21]. Here only the models which were used in this work shall be described. A number of general assumptions are valid for most of these models:

1. Long-chain assumption: It is assumed that the chains are long enough to neglect chain-length-dependent effects.

2. Neglect of remote substituent effects: It is assumed that substituents that are further away than a certain position relative to the radical are negligible. This reduces the number of different chains that need to be considered from N_{M}^{i} to N_{M}^{d} where N_{M} is the number of different monomers, i the chain length and d the relative position in the chain.

3. Neglect of side reactions

Terminal model

The terminal model (TM) was introduced independently by Mayo and Lewis as well as Alfrey and Goldfinger in 1944.[41,42] In this model the remote substituent effect is neglected for all monomers that are not at the very end of the active macroradical. In a binary copolymerisation this means only two different types of macroradicals exist, those with monomer 1 or with monomer 2 at the end. Each of these can add another monomer 1 or 2, giving rise to four different reactions, each with a different propagation rate coefficent.

$$\mathrm{R{-}M_i} + \mathrm{M_j} \xrightarrow{k_{\mathrm{P}}^{\mathrm{ij}}} \mathrm{R{-}M_i{-}M_j} \qquad \mathrm{i,j} = 1 \text{ or } 2 \tag{2.27}$$

These four propagation rate coeficients are grouped in two reactivity ratios (RR) r_i (often also called 'copolymerisation parameters').

$$r_\mathrm{i} = \frac{k_\mathrm{p}^\mathrm{ii}}{k_\mathrm{p}^\mathrm{ij}} \qquad \mathrm{i} \neq \mathrm{j} \text{ and } \mathrm{i},\mathrm{j} = 1 \text{ or } 2 \tag{2.28}$$

These RR thus denote the ratio of homopropagation to crosspropagation.

An expression for the copolymer composition was derived by Mayo and Lewis as well as Alfrey and Goldfinger:

$$\frac{F_1}{F_2} = \frac{f_1}{f_2} \cdot \frac{r_1 f_1 + f_2}{r_2 f_2 + f_1} \tag{2.29}$$

This can be rearranged to directly give the fraction of units of monomer 1 in the copolymer:

$$F_1 = \frac{r_1 f_1^2 + f_1 f_2}{r_1 f_1^2 + 2 \cdot f_1 f_2 + r_2 f_2^2} \tag{2.30}$$

Nowadays, usually fits are performed directly onto eq. 2.29 or eq. 2.30. In earlier times when computers were not as widely used, this equation was linearised using the Fineman-Ross method or the Kelen-Tüdos method which is an improvement over the Fineman-Ross method.[43–46]

In 1985 Fukuda derived an expression for the overall copolymerisation propagation rate coefficient $\langle k_\mathrm{p} \rangle$.[20]

$$\langle k_\mathrm{p} \rangle = \frac{r_1 f_1^2 + 2 f_1 f_1 + r_2 f_2^2}{\frac{r_1 f_1}{k_\mathrm{p}^{11}} + \frac{r_2 f_2}{k_\mathrm{p}^{22}}} \tag{2.31}$$

Fukuda also found that for the Sty/MMA system the RR obtained by fitting the copolymer composition differ substantially from the RR obtained from fitting $\langle k_\mathrm{p} \rangle$ and that each observable is poorly described by the set of RR obtained from the other observable, thus establishing a failure of the TM which was later shown to be generally true, not only for the Sty/MMA system.

Penultimate model

Merz initially described an extension of the TM and Fukuda delivered a full description of this model which is called penultimate model (PUM).[47,48] Here the remote substitutent effect is neglected only after 2 monomer units which in a binary copolymerisation means that four different types of chains are present and eight different propagation reactions need to be considered.

$$\mathrm{R{-}M_i{-}M_j} + \mathrm{M_k} \xrightarrow{k_\mathrm{p}^{\mathrm{ijk}}} \mathrm{R{-}M_i{-}M_j{-}M_k} \qquad \mathrm{i,j,k} = 1 \text{ or } 2 \tag{2.32}$$

The eight propagation rate coefficients are grouped in six RR:

$$r_1 = \frac{k_\mathrm{p}^{111}}{k_\mathrm{p}^{112}} \qquad r_2 = \frac{k_\mathrm{p}^{222}}{k_\mathrm{p}^{221}} \tag{2.33}$$

$$r_1' = \frac{k_\mathrm{p}^{211}}{k_\mathrm{p}^{212}} \qquad r_2' = \frac{k_\mathrm{p}^{122}}{k_\mathrm{p}^{121}} \tag{2.34}$$

$$s_1 = \frac{k_\mathrm{p}^{211}}{k_\mathrm{p}^{111}} \qquad s_\mathrm{B} = \frac{k_\mathrm{p}^{122}}{k_\mathrm{p}^{222}} \tag{2.35}$$

The additional RR are used to calculate the adjusted parameters $\overline{r}$ and $\overline{k_\mathrm{p}}$.

$$\overline{r_1} = r_1' \cdot \left(\frac{r_1 f_1 + f_2}{r_1' f_1 + f_2} \right) \tag{2.36}$$

$$\overline{k_\mathrm{p}^{11}} = k_\mathrm{p}^{111} \cdot \left(\frac{r_1 f_1 + f_2}{r_1 f_1 + \frac{f_2}{s_1}} \right) \tag{2.37}$$

The equations for the copolymer composition and $\langle k_\mathrm{p} \rangle$ are very similar to their TM counterparts, except that now $\overline{r}$ and $\overline{k_\mathrm{p}}$ are used instead of the TM versions.

$$F_1 = \frac{\overline{r_1} \cdot f_1^2 + f_1 \cdot f_2}{\overline{r_1} \cdot f_1^2 + 2 \cdot f_1 \cdot f_2 + \overline{r_2} \cdot f_2^2} \tag{2.38}$$

$$\langle k_\mathrm{p} \rangle = \frac{\overline{r_1} f_1^2 + 2 f_1 f_2 + \overline{r_2} f_2^2}{\frac{\overline{r_1} f_1}{\overline{k_\mathrm{p}^{11}}} + \frac{\overline{r_2} f_2}{\overline{k_\mathrm{p}^{22}}}} \tag{2.39}$$

The PUM offers increased flexibility because of the increased number of adjustable parameters and typically fits data sets of copolymer composition and $\langle k_\mathrm{p} \rangle$ satisfactorily. However this can also be a case of overfitting. The obtained RR often have limited physical meaning because of this. Having more data points helps combat the overfitting problem. Also some approximations and fitting approaches have been used to help with this issue. Most notable is the approximation $r = r' = \overline{r}$ suggested by Fukuda.[20] Using this approximation, the model is then called the 'implicit PUM' as opposed to the 'explicit PUM' which does not have any approximations. The assumption in the implicit PUM is essentially that the reactivity of a macroradical does not depend on which monomer it is reacting with thus only the overall reactivity depends on the penultimate unit but not the selectivity.

Several fitting approaches are possible, for example:

1. Determine r_1 and r_2 according to the terminal model by fitting the copolymer composition and carry them over to the penultimate model and consider them fixed in the following fit for $\langle k_\mathrm{p} \rangle$.

2. Fit the copolymer composition to obtain r_1, r_2, r_1' and r_2' according to the PUM. Use these values as fixed in fitting $\langle k_\mathrm{p} \rangle$.

3. Introduce further approximations such as $r_1 \cdot r_2 = s_1 \cdot s_2$ and/or $s_1 = s_2$.[48]

More approaches are possible and most of them can be combined. All of these approaches reduce the dimensionality of the problem and influence the accuracy of the results. Because man-made assumptions are brought into this and the obtained RR can not be clearly assigned to a straightforward model, these approaches are disregarded in this work and only the explicit PUM, the implicit PUM and the TM are used in this work. For more details the reader is referred to reference [49].

2.5.3. Termination in copolymerisation

Also termination is fairly complicated in a copolymerisation. Walling proposed a simple model, introducing the cross-termination factor ϕ.[50]

$$\phi = \frac{k_{\mathrm{t,ij}}}{\sqrt{k_{\mathrm{t,ii}} \cdot k_{\mathrm{t,jj}}}} \tag{2.40}$$

ϕ describes the preference of cross-termination over homo-termination. This implies chemical control of the termination reaction which is not the case for homopolymerisations and there is no reason why it should for copolymerisations. Consequently, diffusion-controlled models were developed. A simple and straightforward model is to take a linear combination of homo-termination rate coefficients weighted with their fractions in the copolymer.[51]

$$k_{\mathrm{t,copo}} = F_1 \cdot k_{\mathrm{t},11} + F_2 \cdot k_{\mathrm{t},22} \tag{2.41}$$

This approach has also been defined in the inverse form:[52]

$$\frac{1}{k_{\mathrm{t,copo}}} = \frac{F_1}{k_{\mathrm{t},11}} + \frac{F_2}{k_{\mathrm{t},22}} \tag{2.42}$$

Fukuda later proposed an approach based on the terminal model method, using radical population fractions instead of the composition of the copolymer and applied the geometric mean and algebraic mean to this,leading to eq. 2.43 (gmm) and eq. 2.44 (amm).

$$\sqrt{k_{\mathrm{t,copo}}} = \phi_1 \cdot \sqrt{k_{\mathrm{t},11}} + \phi_2 \cdot \sqrt{k_{\mathrm{t},22}} \tag{2.43}$$

$$k_{\mathrm{t,copo}} = \phi_1 \cdot k_{\mathrm{t},11} + \phi_2 \cdot k_{\mathrm{t},22} \tag{2.44}$$

Here ϕ_{i} denotes the radical population fraction, i.e. the fraction of macroradicals with monomer i ath the chain end. It is not to be confused with the Walling cross-termination factor.

All of the up to now discussed models do not consider chain length dependence of k_{t}. Olaj *et al.* investigated the copolymerisation of Sty with methyl methacrylate (MMA) and found a higher termination rate coefficient for the copolymerisation

than for the homopolymerisations which was surprising.[53] This phenomenon was attributed to increased chain flexibility from the alternating composition.

2.6. The SP–PLP–EPR method

The SP–PLP–EPR method which was developed by Buback is currently the most powerful method for investigation of termination kinetics as it allows a time-resolved direct observation of the radical concentration.[16] The method requires two steps: First an electron paramagnetic resonance (EPR) spectrum of the sample is recorded under continuous initiation to identify the magnetic field position where the peak maxima are. Second, the magnetic field position is fixed to the peak maximum and a single laser pulse is applied to generate radicals and their decay is monitored time-resolved.

Using initiation with a short laser pulse, all macroradicals are formed at the same time and thus have the same chain length. The chain length can be correlated to the time after the laser pulse:

$$i = k_\mathrm{p} \cdot c_\mathrm{M} \cdot t = \frac{t}{t_\mathrm{p}} \tag{2.45}$$

Expressions for the radical concentration as a function of time can be obtained by inserting the short- and long-chain expressions for $k_\mathrm{t}^{\mathrm{i,i}}$ from the composite model (eqs. 2.22 and 2.23) and eq. 2.45 in the differential rate law of termination (eq. 2.8) and integrating. One obtains:

$$\frac{c_{\mathrm{R},0}}{c_\mathrm{R}(t)} - 1 = \frac{2 \cdot k_\mathrm{t}^{1,1} \cdot c_{\mathrm{R},0} \cdot t_\mathrm{p}^{\alpha_\mathrm{s}}}{1-\alpha_\mathrm{s}} \cdot t^{1-\alpha_\mathrm{s}} \quad ; i \leq i_\mathrm{c} \tag{2.46}$$

$$\frac{c_{\mathrm{R},0}}{c_\mathrm{R}(t)} - 1 = \frac{2 \cdot k_\mathrm{t}^{0} \cdot c_{\mathrm{R},0} \cdot t_\mathrm{p}^{\alpha_\mathrm{l}}}{1-\alpha_\mathrm{l}} \cdot t^{1-\alpha_\mathrm{l}} \quad ; i > i_\mathrm{c} \tag{2.47}$$

By logarithmising these equations one obtains a useful linear form for data evaluation.

$$\log\left(\frac{c_{\mathrm{R},0}}{c_{\mathrm{R}}(t)}-1\right)=\log\left(\frac{2\cdot k_{\mathrm{t}}^{1,1}\cdot c_{\mathrm{R},0}\cdot t_{\mathrm{p}}^{\alpha_{\mathrm{s}}}}{1-\alpha_{\mathrm{s}}}\right)\cdot(1-\alpha_{\mathrm{s}})\cdot\log(t)\quad ;i\leq i_{\mathrm{c}} \tag{2.48}$$

$$\log\left(\frac{c_{\mathrm{R},0}}{c_{\mathrm{R}}(t)}-1\right)=\log\left(\frac{2\cdot k_{\mathrm{t}}^{0}\cdot c_{\mathrm{R},0}\cdot t_{\mathrm{p}}^{\alpha_{\mathrm{l}}}}{1-\alpha_{\mathrm{l}}}\right)\cdot(1-\alpha_{\mathrm{l}})\cdot\log(t)\quad ;i>i_{\mathrm{c}} \tag{2.49}$$

Two linear regions should be seen in the plot, both of which are fitted separately with a straight line. It can be seen that for obtaining the α parameters and i_{c} knowledge of the initial radical concentration directly after the laser pulse $c_{\mathrm{R},0}$ is not necessary as the ratio $\frac{c_{\mathrm{R},0}}{c_{\mathrm{R}}(t)}$ can be replaced with the ratio of intensities $\frac{I_{\mathrm{R},0}}{I_{\mathrm{R}}(t)}$. α_{s} and α_{l} can be obtained from the slopes of both linear regions while the absolute termination rate coefficients $k_{\mathrm{t}}^{1,1}$ and k_{t}^{0} are obtained from the intercept with the ordinate.

In order to extract $k_{\mathrm{t}}^{1,1}$ and k_{t}^{0} however, exact knowledge of the initial radical concentration is necessary. A calibration procedure has to be performed.

2.6.1. Calibration procedure

It consists of two steps. In the first step, solutions of 2,2,6,6-Tetramethylpiperidin-1-oxyl (TEMPO) as a stable radical in the respective monomer (and solvent, if applicable) with varying concentrations are prepared and their EPR spectrum is measured. By determining the double integral of these spectra and correlating it with the TEMPO concentration, one obtains the first of two calibration factors:

$$c_{\mathrm{R}}=h_1\cdot\iint I(B) \tag{2.50}$$

In the second step, EPR spectra of the actual samples under investigation are required. The measurement is performed to identify the peak maxima anyway. Now the intensity at the magnetic field position at which the measurement is performed (typically the maximum) is correlated with the double integral of this

spectrum.

$$\iint I(B) = h_2 \cdot I(B_{\max}) \tag{2.51}$$

A combination of these two steps gives the final correlation:

$$c_{\mathrm{R}}(t) = h_1 \cdot h_2 \cdot I(B_{\max}, t) \tag{2.52}$$

2.7. PLP–SEC

The PLP–SEC method was developed by Olaj for determination of propagation rate coefficients k_{p}.[15] The principle of the method is to apply short laser pulses to a sample with photoinitiator repeatedly with a defined time span between the pulses. Each laser pulse generates radicals which can propagate in the dark time. With each new laser pulse, the radical concentration is increased drastically which leads to immediate termination. The resulting molecular weight distribution thus has peak at a chain length of $i = k_{\mathrm{p}} \cdot c_{\mathrm{M}} \cdot t$ where t is the time between two laser pulses. Because not all radicals terminate when the next laser pulse arrives, but are terminated at one of the subsequent pulses, multiple maxima are observed which should be evenly spaced with double, triple etc. of the molar mass of the first peak. The peaks are typically difficult to identify. Also it was shown that the correct result is obtained by using the inflection point on the low molecular weight side of the peak.[15,54,55] Thus it is easier to identify the peaks as maxima in the first derivative of the molecular weight distribution. This is shown schematically in fig. 2.2. The rate coefficient k_{p} is then given by eq. 2.45.

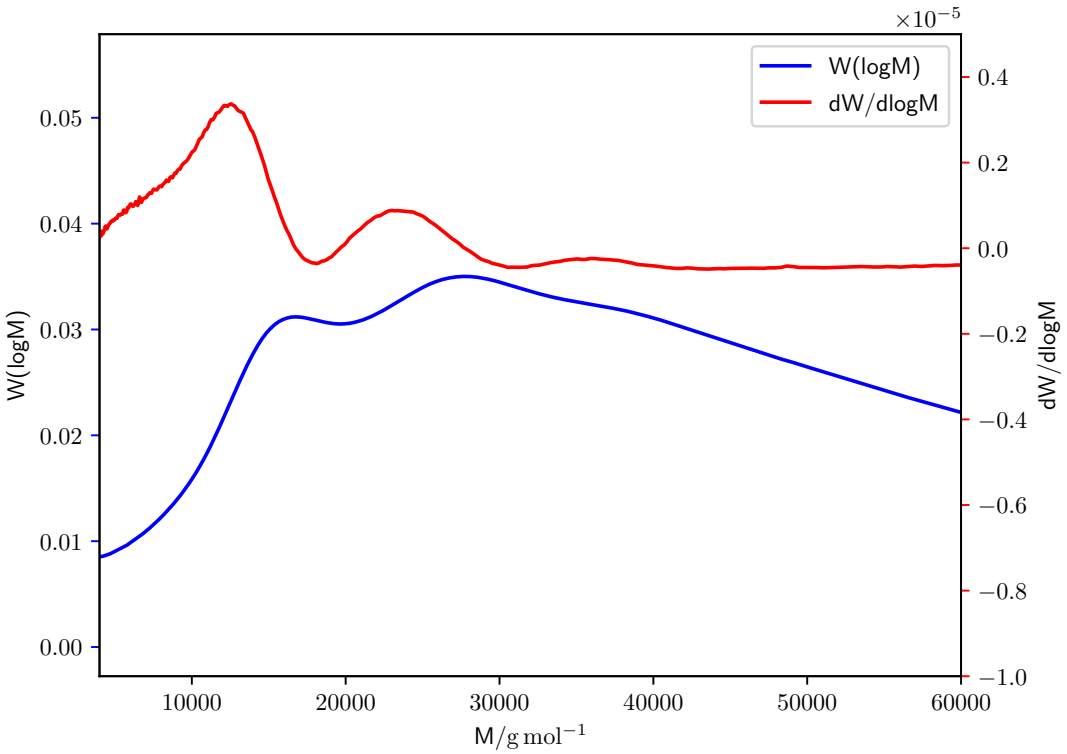

Figure 2.2.: Excerpt from an exemplary molecular weight distribution and its first derivative in a PLP–SEC experiment using bulk diethyl itaconate (DEI) at 303.15 K, a laser repetition rate of 1 Hz and 0.027 mol L^{-1} of 2,2-Dimethoxy-2-phenylacetophenone (DMPA) as photoinitiator.

3. Experimental

3.1. Chemicals

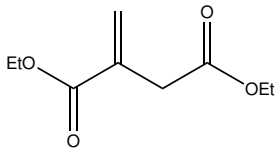

Diethyl itaconate was purchased from TCI (98 %) and the inhibitor TBC was removed by passing through a column filled with aluminium oxide (Alfa Aesar, activated basic, Brockmann Grade I).

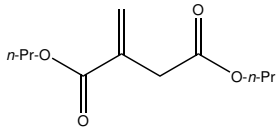

Di-*n*-propyl itaconate was synthesised from itaconic acid (TCI, 99 %) and a ten-fold excess of *n*-propanol (Merck, 99.5 %). The excess *n*-propanol was removed with a rotary evaporator under reduced pressure, the product was neutralised with aqueous sodium hydrogencarbonate solution and dried over calcium chloride. The purity of the product was determined with NMR spectroscopy to be over 95 %.

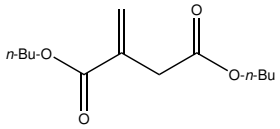

Di-*n*-butyl itaconate was purchased from TCI (97 %) and the inhibitor was removed by passing through a column filled with inhibitor remover (Sigma-Aldrich).

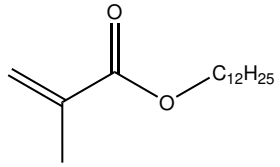

Dodecyl methacrylate was purchased from TCI (97 %) and the inhibitor was removed by passing through a column filled with inhibitor remover (Sigma-Aldrich).

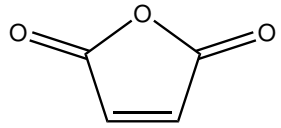

Maleic anhydride was purchased from Sigma-Aldrich (99 %) and was used as received.

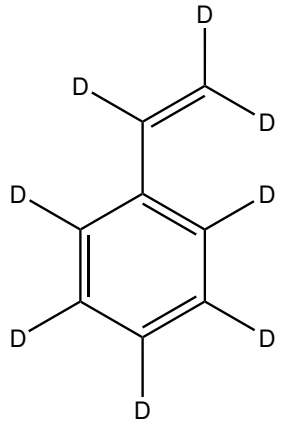

Styrene-d8 was purchased from abcr (98 atom % D, in a sealed glass ampule under argon atmosphere) and the inhibitor was removed by passing through a column filled with inhibitor remover (Sigma-Aldrich).

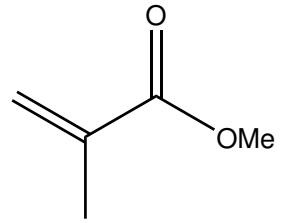

Methyl methacrylate was purchased from Sigma-Aldrich (99 %) and the inhibitor was removed by passing through a column filled with inhibitor remover (Sigma-Aldrich).

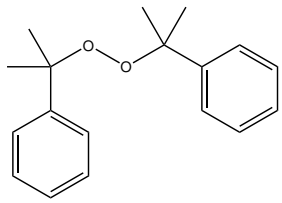

Dicumylperoxide was purchased from Aldrich (98 %) and was used as received. It was stored at 7 °C isolated from light.

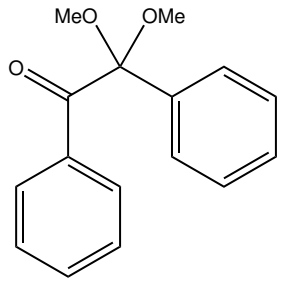

2,2-Dimethoxy-2-phenylacetophenone was purchased from Aldrich (99 %) and was used as received. It was stored isolated from light.

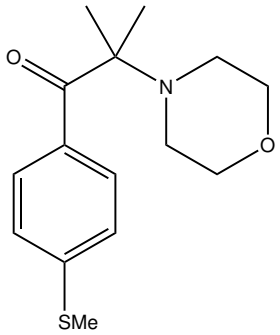

2-Methyl-4′-(methylthio)-2-morpholinopropiophenone was purchased from Aldrich (98 %) and was used as received. It was stored isolated from light.

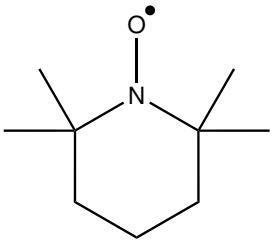

2,2,6,6-Tetramethylpiperidin-1-yl)oxyl was purchased from Aldrich (98 %) and used as received.

3.2. Quantum chemical calculations

Relevant conformers were identified using the 'crest' program by Grimme.[56] The conformers were then optimised using ORCA 4.1.2. No Counterpoise-correction has been applied. Infrared spectra were calculated with the harmonic approximation. For the rate coefficient calculations, the most stable conformers of the reactants and products were identified using crest and optimised. Then a nudged-elastic-band calculation was performed to identify the transition state which was then optimised with the keyword 'OptTS'.

3.3. PLP–SEC

Pulsed laser polymerisations were carried out in cylindrical double-walled cuvettes (Starna, 65.14Q/10, Spectrosil quartz glass, 10 mm optical path length) which can be tempered using a thermostat with an ethylen glycole:water (4:1) mixture. The samples consisting of monomer with dissolved photoinitiator were degassed by a stream of argon for at least 10 min and then tempered for another 10 min.

The laser used for irradiation is an ATLEX-I (ATL Lasertechnik GmbH, 351 nm wavelength, 7 mJ maximum pulse energy, 1000 Hz maximum repetition rate, 20 ns pulse length) XeF exciplex laser. The laser beam is led through a system of four lenses, first two plane concave lenses (ThorLabs, UV-protected quartz, anti-reflective coating for 290-370 nm; lens 1: LK4326-UV, $f_l = -25.0$ mm; lens 2: LK-4385-UV, $f_l = -75.0$ mm) and then two plane convex lenses (lens 3: ThorLabs, UV-protected quartz, anti-reflective coating for 290-370 nm, LJ4395-UV, $f_l = 100.0$ mm; lens 4: Melles Griot, UV-protected quartz, V-type anti-reflective coating for 351 nm, SCX-25.4-101.7-UV-248-355, $f_l = 25.4$ mm). This lens system widens the laser beam from 4×6mm to 16×16mm to ensure that the sample is completely irradiated. The samples were used for size-exclusion chromatography without separation of polymer since separation was not possible.

Size-exclusion chromatography was performed using a sequence of one pre-column (PSS SDV, 8×50 mm, 5 µm particle size) and three separation columns (PSS SDV, 8×300 mm, 5 µm particle size, pore sizes of 10^6, 10^5 and 10^3 Å). An Agilent autosampler (Model 1260, ALS G1329B) was used. The eluent was tetrahydrofuran with a flow rate of 1 mL min^{-1} pumped by an Agilent Iso-pump (Model 1260, G1310B). A polystyrene ($M_n = 474 - 2\,520\,000$ g mol^{-1}) and poly(methyl methacrylate) (($M_n = 800 - 1\,600\,000$ g mol^{-1})) calibration was used and an universal calibration was performed using the Mark-Houwink parameters from reference [57].

3.4. SP–PLP–EPR

3.4.1. Sample preparation

Samples were prepared by degassing all monomers and solvents with several freeze-pump-thaw cycles under exclusion of light with aluminium foil. Then the photoinitiator was added in a glovebox with an argon atmosphere and 50 µL of the sample was filled in EPR tubes (Wilmad Suprasil, 3 mm outer diameter, 2 mm inner diameter). For the Sty/DMA copolmyerisation, bigger sample tubes were

used (Wilmad Suprasil, 5 mm outer diameter, 4 mm inner diameter) and also a bigger sample volume of 200 µL was used.

3.4.2. Experimental setup

The setup consists of a Bruker Elexsys-II 500 T EPR spectrometer (X-band, approximately 9.4 GHz) equipped with a Bruker ER 41122SHQE-LC cavity, coupled to a Nd:YAG laser (Litron Laser Ltd., LPY774G-30, third harmonic at 355 nm) with a pulse controller (Quantum Composer 9314, Scientific Instruments). A beam shutter is placed in the beam path and is also coupled to the pulse controller to allow a single laser pulse to be irradiated onto the sample for the SP–PLP–EPR experiments. Temperature control was achieved by a Bruker ER 4131VT unit. For measurements below room temperature, liquid nitrogen was evaporated and led into the cavity. To avoid condensation of air humidity, gaseous nitrogen was also flushed through the cavity. For all experiments, the modulation amplitude was 3 G and the modulation frequency was 100 kHz. The receiver gain was 60 and the attenuation was 20 dB. The calibration procedure to obtain absolute radical concentrations is described in section 2.6.1.

3.5. Determination of the propagating radical fraction

Comonomer mixtures were prepared as all other EPR samples. A photoinitiator concentration of 0.1 mol L^{-1} Dicumylperoxide (DCP) was chosen to generate a high number of radicals for a good S/N. The sample was irradiated in the EPR spectrometer with a repetition rate of 30 Hz and several scans (10-20) were coadded. The PRF was determined by fitting the obtained copolymerisation spectrum with a sum of the homopolymerisation spectra. For this, the 'easyspin' software package for MATLAB was used. An exemplary script can be found in the appendix. From the obtained weights of the involved radical species, the PRF is calculated as a simple fraction.

3.6. Density and viscosity measurements

The density of DEI and di-*n*-propyl itaconate (DPI) was measured using a gas pycnometry system (Micromeritics, AccuPyc II). No temperature control was available for that instrument, consequently only room temperature density was measured.

The viscosity of DEI was measured with an Anton Paar AMVn falling ball viscosimeter at various temperatures.

4. Copolymerisation of styrene with maleic anhydride

The copolymer of Sty and MAn is a promising candidate for nanoencapsulation of drugs and drug delivery because of its amphiphilic properties. Also applications in nanoparticle synthesis or proteine encapsulation are known. A vast number of studies have been investigating this copolymer.[58–65] Also from a kinetic standpoint this copolymerisation is of great interest because the cross-propagation is extremely dominant in this system, so that an mostly alternating copolymer is created. Also MAn does not homopolymerise in a radical polymerisation (however it does in an anionic polymerisation[66,67]). This simplifies the kinetic treatment, because homopropagation steps of MAn can be neglected. In this work, a thorough examination of the copolymerisation termination kinetics was attempted via the SP–PLP–EPR method.

The reason why the cross-propagation is so dominant in this system, is still a point of discussion. Most of literature agrees on the presence of a complex of both monomers and that the propagation step incorporates this complex as a unit, thus leading to an alternating copolymer, while others view this simply in the general kinetic treatment that cross-propagation steps are fast and the homopolymerisation step of MAn has a rate coefficient of 0, without the need of an additional complexation model. In this work, it was tested via quantum chemistry, if such a complex is present and how its binding energy is, in order to assess whether it is stable under usual polymerisation conditions. Also it was checked whether one of the vibrational bands is shifted in the complex versus as

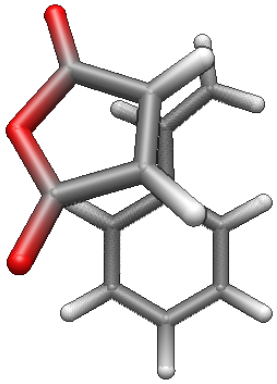

Figure 4.1.: Structure of the complex between Sty and MAn obtained using *crest*. Both molecules are aligned in a parallel, but shifted fashion.

	gas phase	acetone
$E_{\mathrm{dis}}/\mathrm{kJ\,mol^{-1}}$	3.8	-1.2

Table 4.1.: Electronic dissociation energies of the Sty-MAn complex in the gas phase and in acetone at 0 K at B3LYP/def2-TZVP level of theory. The results are not counterpoise-corrected.

lone monomers. This way the complex formation could be verified with infrared spectroscopy.

First, the structure of the most stable complex between the two monomers was identified using the *crest*-program by Grimme[56]. The structure consists of a parallel, but shifted alignment of both rings, indicating strong interactions between the electron-rich Sty and the electron-poor MAn. This alignment also brings both double bonds in close proximity, enabling a propagation step that incorporates both molecules at once.

Next, this structure and each of the monomers were optimised with B3LYP/def2-TZVP in order to obtain accurate energies. This was performed once in the gas phase and once using the CPCM solvent model for acetone, since literature reports already exist for EPR studies in acetone.[68] A counterpoise-correction was not employed.

It is visible in table 4.1 that the complex is unstable in acetone which is due to the strong stabilisation of MAn in acetone, which is stronger than the stabilisation in the complex. To estimate the fraction of molecules bound in the complex, a simple Maxwell-Boltzmann distribution of the form $f(E) = 2 \cdot \sqrt{\frac{E}{\pi}} \cdot \left(\frac{1}{RT}\right)^{\frac{3}{2}} \cdot \mathrm{e}^{-\frac{E}{RT}}$ was used. All molecules with an energy higher than the complex dissociation energy were considered unbound and those with an energy below the dissociation energy were considered bound. The fraction of bound molecules is then given by $\frac{\int_0^{E_{\mathrm{dis}}} f(E)}{\int_0^{\infty} f(E)}$. This model can only give a rough estimate and should not be considered precise. Since the dissociation energy in acetone is negative, this analysis was performed only with the gas phase value. For a temperature of 50 °C which is a typical temperature for free radical polymerisations one obtains a fraction of 41 % bound molecules. This is congruent with the results of Tsuchida *et al.*, who found values of 31 %.[69] This shows that a significant portion of the monomers indeed are bound in a complex.

The next step is to try to prove the existence of this complex experimentally. In order to do so, the infrared spectra of both monomers and the complex were calculated using the harmonic approximation in the gas pahse as well as in acetone. If a band in the spectrum of the complex significantly differs from the sum of the monomer spectra, this can be used to prove the existence of said complex.

It can be seen that no significant band shift occurs, only minor shifts. Considering that in condensed phase all bands undergo significant broadening, showing the existence of the complex is virtually impossible. It might be achieved using supersonic jet expansions coupled with IR spectroscopy in order to obtain sharp IR spectra. However the conditions are nowhere near comparable to the conditions used in classical polymerisations, strongly limiting the transferrability of results obtained with supersonic jet expansions.

While the existence of the complex was proven theoretically, this does not prove the involvement of the complex in the actual propagation step. To allow for theoretical modeling of the polymerisation, it was attempted to investigate the termination kinetics using the SP–PLP–EPR method. In the literature, a few studies regarding the EPR spectra of this copolymerisation can be found.[70–72] These have been

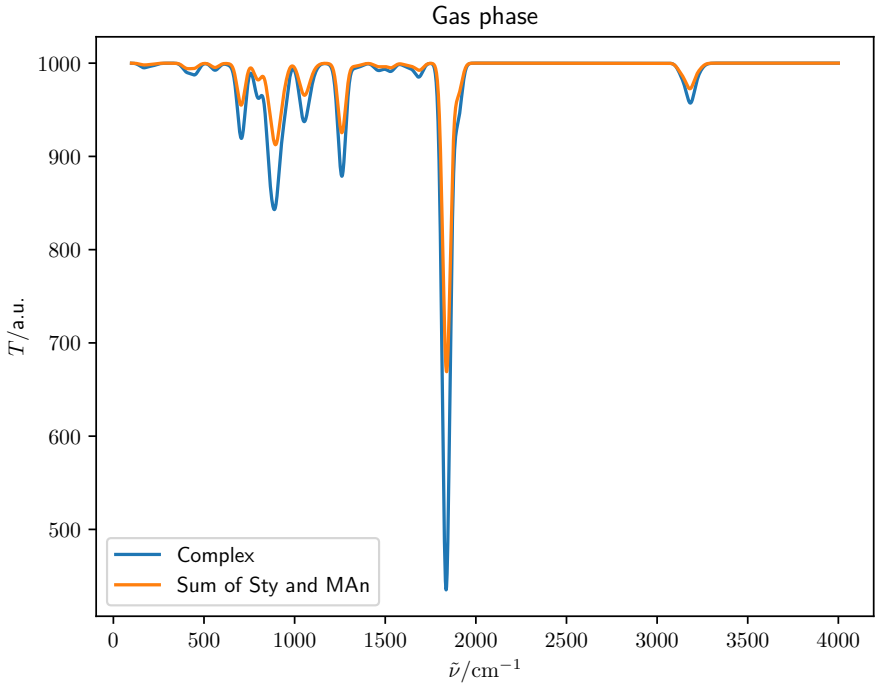

(a) IR spectra in the gas phase

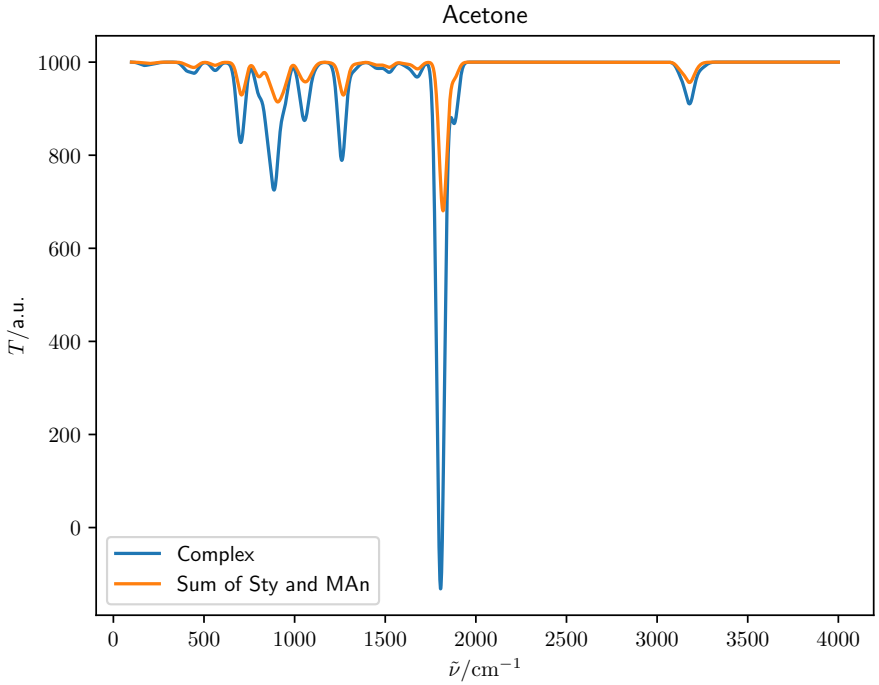

(b) IR spectra in Acetone

Figure 4.2.: Calculated infrared spectra of the complex between both monomers and the sum of the Sty and MAn spectra. Calculations were performed in the gas phase as well in acetone solution on B3LYP/def2-TZVP level of theory.

performed in bulk as well as in solution, mostly acetone. This is also the reason why acetone was chosen as solvent for the quantum chemical calculations. In this work, it was found that MAn is insoluble in Sty, hence a solvent was necessary. Since previous studies already used acetone, this was an obvious first choice. Just as in previous studies, a total comonomer concentration of $2\,\mathrm{mol\,L^{-1}}$ was chosen. However the previous studies also found that the EPR spectra are mainly comprised of the solvent radicals.[70,71]

Again quantum chemistry was employed to predict spectra, this time the EPR spectra. For this, the basis set EPR-II was used, which is optimised for EPR calculations.[73] The EPR spectra of both monomeric units were calculated. Also it was tested whether a different penultimate unit has significant influence on the spectrum by comparing the EPR spectrum of the MAn monomer to a dimer of Sty and MAn with the radical centered on MAn. It can be seen in fig. 4.3 that the differences in the spectra are extremely small, too small to be identified in real, noisy spectra. It can be safely concluded that identification of penultimate units by EPR spectroscopy is (at least in this system) not possible.

The high dipole moment of acetone thwarted any attempts to obtain meaningful EPR spectra. First room temperature was tested. Critically coupling the cavity proved difficult and the S/N was orders of magnitude worse than necessary for SP–PLP–EPR measurements. Approximately 100 scans were necessary to obtain meaningful spectra, while SP–PLP–EPR requires the S/N to be high enough that one scan suffices. Upon decreasing the temperature, the signal-to-noise ratio stayed this low up to the freezing point. In frozen solution, the S/N improved by several orders of magnitude, which can be attributed to the fact that termination reactions are largely suppressed, as they are diffusion-controlled. However suppressing termination reactions is unhelpful for studying termination reactions. In the frozen state, no useful kinetic information can be obtained. The obtained spectra are shown in fig. 4.4.

It was then tested whether a different, less polar solvent increases the S/N enough to facilitate SP–PLP–EPR measurements. A quick test of solvents showed 1,2-dimethoxyethane (DME) to be the solvent with the lowest dipole moment which

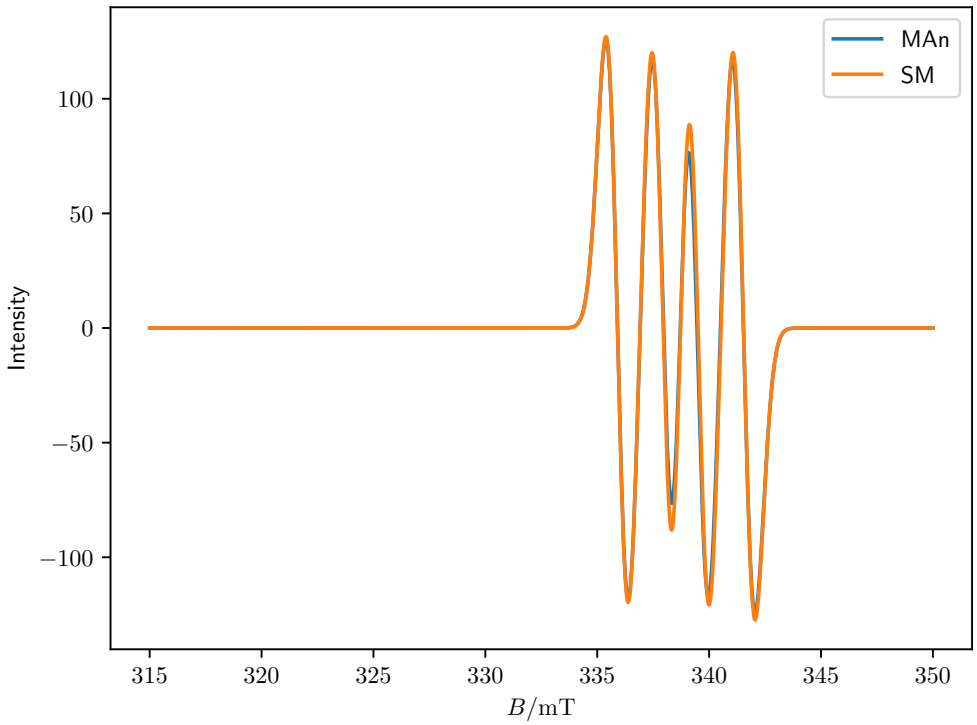

Figure 4.3.: Calculated EPR spectra for a MAn radical and a dimer of Sty with MAn with the radical centered on the MAn. The spectra were calculated with B3LYP/EPR-II.

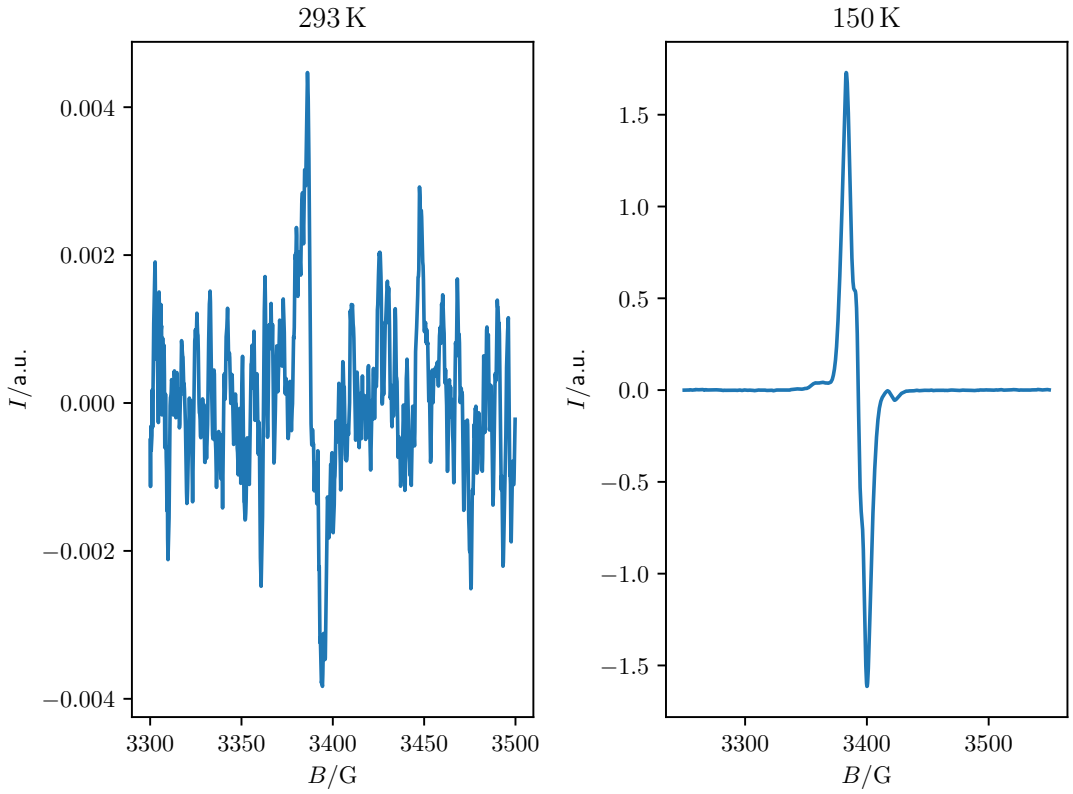

Figure 4.4.: EPR spectra of a Sty/MAn solution (10:90 at a total concentration of $2\,\mathrm{mol\,L^{-1}}$ in acetone) at 293 K and 150 K.

still dissolves MAn. It was consequently selected for further experiments. However, the results were the same as for acetone: The S/N was approximately the same and upon freezing the solution, it increased dramatically.

Consequently, it was not possible to conduct SP–PLP–EPR measurements.

5. Free radical polymerisation kinetics of itaconates

Up until now, most polymer products are produced from petrol-based monomers which is disadvantageous for several reasons.[3] As petrol-based products they are non-sustainable, although in the last decades more efforts were made to recycle used polymer products. Also the fossil sources for plastic are still cheaper than bio-based alternatives but as their supply is limited, it is immediately apparent that they are not a long-term solution. Additionally, the price of crude oil can vary strongly, especially when for example geopolitical crises occur. In the last years, bio-based polymers have gained more attention, especially in the production of unsaturated polyester resins. These require addition of a reactive diluent, which typically is Sty. This has several disadvantages, from an economical and ecological point of view. Due to its high vapour pressure, Sty is released into the atmosphere in significant amounts which is a loss of resources. Also Sty is known to be a potent air pollutant, contributing to the greenhouse effect and also to be cancerogenic. It is therefore desirable to use different reactive diluents instead. Diluents based on itaconic acid have shown to be suitable for this purpose.[13,14] Itaconic acid can be produced by microorganisms, namely *Aspergillus terreus*, and is therefore a very promising candidate as it is sustainable and not dependent on crude oil.[4–12]

To fully utilise itaconate derivatives, the polymerisation kinetics need to be known in detail. A sensible starting point is the homopolymerisation of the itaconates, before moving on to more complex cases as in the application with polyester resins. So far, a few studies exist on the kinetics of the homopolymerisation of different itaconic acid esters, most of them focusing on the propagation step.[74–81] Buback

et al. also investigated the termination kinetics of di-*n*-butyl itaconate (DBI).[82] It would be helpful to have data for k_p and k_t for a complete homologue series of itaconate esters.

This work focuses on examining the homopolymerisation kinetics of two different itaconates: diethyl itaconate (DEI) and di-*n*-propyl itaconate (DPI). As mentioned, in a previous publication Buback *et al.* already investigated DBI with SP–PLP–EPR.[82]

When evaluating the SP–PLP–EPR measurements, the propagation rate coefficient k_p gives access to additional observables. This propagation rate coefficient was determined in a separate series of experiments for the temperature range from 293.15-343.15 K with the well-known IUPAC-recommended PLP–SEC-method introduced by Olaj *et al.*.[15] Literature data for k_p exist only for solution in benzene at 50 °C and 60 °C by Otsu and Sato.[78,79] Both Otsu and Sato determined k_p from the reaction rate and the radical concentration, a method that is not used anymore. Since the values found by Otsu at 60 °C are lower than those found by Sato at 50 °C and this is physically unreasonable, a reevaluation using a better method is beneficial. As the measurements of k_p are independent from the SP–PLP–EPR measurements and the data is useful also on their own, these measurements will be presented separately in the following sections.

5.1. Propagation kinetics of DEI and DPI

The results of this section have been published in literature.[83] In addition to PLP–SEC experiments, it was attempted to obtain theoretical values for the reaction rate coefficient of the propagation step. This was achieved by performing quantum chemical calculations with the program package ORCA (version 4.1.2).[84,85] This program features an 'NEB-TS' algorithm which is capable of finding transition states by interpolating between the reagent and product structures which have to be given to the program.

5.1.1. Quantum chemical calculation of the propagation rate coefficient

The calculations have only been performed for DEI, for reasons of computational power. In order to obtain an Arrhenius expression for k_p, TST is used, as recommended by Coote.[86] In TST, k_p as a function of temperature, can be expressed as follows:

$$k(T) = \kappa \cdot c^{(1-m)} \cdot \frac{k_\mathrm{B}T}{h} \cdot \frac{Q^\ddagger}{\prod_\mathrm{i} Q_\mathrm{i}} \cdot \exp\left(-\frac{E_0}{RT}\right) \tag{5.1}$$

Here Q are the partition functions of the respective species, c the inverse of the volume used in the translational partition function, E_0 the electronic barrier height and m the molecularity of the reaction (2 in this case). κ denotes a factor to account for tunneling. This was not considered in this work, so it is set to 1 and will be left out in the following. As it is usually easier to calculate and also easier to grasp, this can be reformulated using thermodynamical properties:

$$k(T) = c^{(1-m)} \cdot \frac{k_\mathrm{B}T}{h} \exp\left(\frac{\Delta S^\ddagger}{R}\right) \cdot \exp\left(-\frac{\Delta H^\ddagger}{RT}\right) \tag{5.2}$$

Now the pre-exponential factor A and the activation energy can be calculated separately:

$$A = c^{(1-m)} \cdot \exp(m) \cdot \frac{k_\mathrm{B}T}{h} \exp\left(\frac{\Delta S^\ddagger}{R}\right) \tag{5.3}$$

The pre-exponential factor depends mainly on the entropy of activation $\Delta S^\ddagger$ which is the sum of translational, rotational and vibrational entropy:

$$S_{trans} = R\left(\ln\left(\left(\frac{2\pi M k_B T}{h^2}\right)^{\frac{3}{2}} \frac{k_B T}{p}\right) + 1 + \frac{3}{2}\right) \tag{5.4}$$

$$S_{rot} = R\left(\ln\left(\frac{\pi^{\frac{1}{2}}}{\sigma_r}\left(\frac{T^{\frac{3}{2}}}{\Theta_{r,x}\Theta_{r,y}\Theta_{r,z}}\right)\right) + \frac{3}{2}\right) \tag{5.5}$$

$$S_{vib} = R\sum_i \left(\frac{\frac{h\nu_i}{k_B T}}{\exp\left(\frac{h\nu_i}{k_B T}\right) - 1} - \ln\left(1 - \exp\left(\frac{h\nu_i}{k_B T}\right)\right)\right) \tag{5.6}$$

The Arrhenius activation energy E_A consists of the electronic barrier height E_0, a zero-point vibrational energy correction ZPVE, a temperature correction $\Delta\Delta H^\ddagger$ and accounts for the molecularity:

$$E_\mathrm{A} = E_0 + \mathrm{ZPVE} + \Delta\Delta H^\ddagger + mRT \tag{5.7}$$

$$\mathrm{ZPVE} = \frac{1}{2}\sum_\mathrm{i} h\nu_\mathrm{i} \tag{5.8}$$

$$\Delta\Delta H = R \cdot \sum_\mathrm{i} \frac{\frac{h\nu_\mathrm{i}}{k_\mathrm{B}}}{\exp\left(\frac{h\nu_\mathrm{i}}{k_\mathrm{B}T}\right) - 1} + \frac{5}{2}RT + \frac{3}{2}RT \tag{5.9}$$

ν_i denotes the individual vibrational frequencies. Since in this work harmonic frequencies were calculated, they were corrected to account for anharmonicity. Radom and Martin reported scaling factors for different levels of theory with different approaches, for varying frequency regions.[87,88] In this work, the average scaling factor of these approaches was used which amounts to 0.900 64 for UHF/6-31G(d) and 0.9870 for B3LYP/def2-TZVP.

As itaconates are 1,1-substituted ethylene derivatives, both sides of the olefinic bond are inequivalent. The attacking radical can be centered on both of the former olefinic carbon atoms. Also, the attack on the monomer can happen at both ends of the olefinic bonds. This gives rise to four different combinations. To discriminate between the combinations, radical stability and steric hindrance can be used. Radical stability favors the radical functionality to be centered at the substituted, tertiary carbon (favoring reactions A and B in fig. 5.1), both in the attacking radical and the product. Steric hindrance favors an attack on the unsubstituted carbon which results in the product having the radical on the substituted carbon (favoring reactions A and C in fig. 5.1). As both effects favor reaction A, only this one was investigated. This can be improved by calculating the Arrhenius parameters for all reaction patterns and Boltzmann-weighing them.

Regarding the choice of level of theory, it should be noted that the geometry and frequencies are rather insensitive to the level of theory, so a cheap one can be chosen. The electronic barrier height however is sensitive to the level of theory.

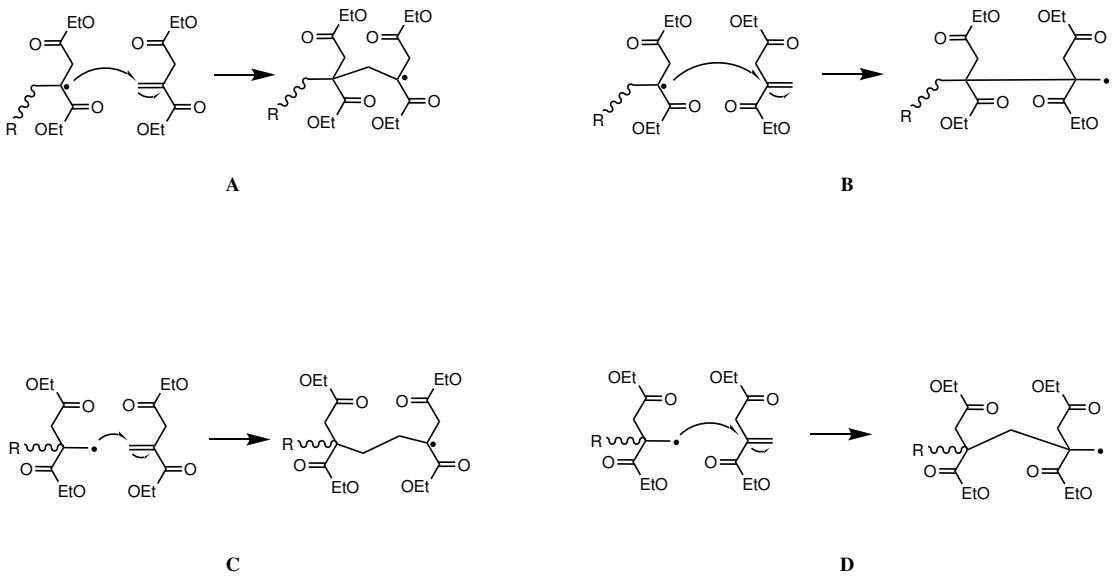

Figure 5.1.: Different propagation reactions for 1,1-substituted ethylenes such as itaconates. The attacking radical can be centered on the tertiary carbon (reactions A and B) or on the primary carbon (reactions C and D). Also the monomer which is being attacked can be attacked either at the primary position (reactions A and C, resulting in a tertiary radical) or at the tertiary position (reactions B and D, resulting in a primary radical). Reaction A is heavily favored by reasons of radical stability as well as steric hindrance.

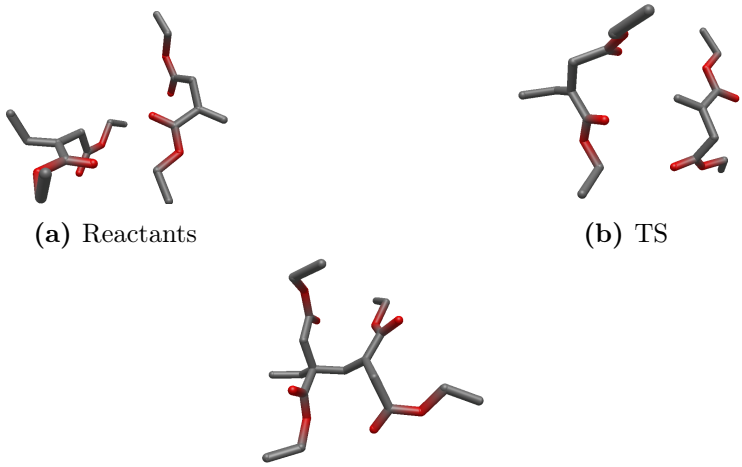

(a) Reactants **(b)** TS

(c) Product

Figure 5.2.: Structure of the reactants, TS and product of the propagation step of DEI on UHF/6-31G(d) level of theory.

A high one should be chosen here, preferrably CCSD(T).[86] For reasons of computational power, only UHF/6-31G(d) and B3LYP/def2-TZVP were used. The structures of the reactants and the product were found by using the *crest*-program by Grimme and then optimised with UHF/6-31G(d) or B3LYP/def2-TZVP using ORCA 4.1.2.[56] In order to find the TS, a nudged-elastic-band calculation was performed. As this was computationally extremely costly, this was performed only on UHF/6-31G(d). The resulting raw TS structure was then optimised with either UHF/6-31G(d) or B3LYP/def2-TZVP, see fig. 5.2.

The structures of the reactants and the product both show an orthogonal alignment of both monomeric units, to minimise steric repulsion. For the propagation step to take place, the molecules need to be aligned to facilitate overlap of the involved orbitals as can be seen in the TS structure. It is untypical that the TS structure differs so strongly from the reactants, because exothermic reactions such as this normally show an early TS, meaning the structure of the TS is similar to that of the reactants.

Resulting parameters from the employed methods are compared in table 5.1. The obtained activation energies differ only by $0.4\,\mathrm{kJ\,mol^{-1}}$, which is very close to each other, considering the difference in theory levels. The pre-exponential factors

Table 5.1.: Computational results for the electronic barrier height E_0, the pre-exponential factor A and the activation energy E_A on UHF/6-31G(d) and B3LYp/def2-TZVP level of theory. The vibrational frequencies were used unscaled as well as scaled by their respective correction factors.

Method	E_0/kJ mol^{-1}	A/L mol^{-1} s^{-1}	E_A/kJ mol^{-1}
UHF/6-31G(d) unscaled	12.7	$2.0 \cdot 10^3$	22.6
UHF/6-31G(d)	12.7	$3.3 \cdot 10^3$	22.3
B3LYP/def2-TZVP unscaled	13.8	$1.4 \cdot 10^4$	22.7
B3LYP/def2-TZVP	13.8	$1.5 \cdot 10^4$	22.7

however differ by approximately one order of magnitude. Comparing to other families of monomers such as acrylates, it can be seen that the pre-exponential factor is about two to three orders of magnitude smaller.[89] This can be explained by the bulky side chains which hinder the approach of a new monomer.

5.1.2. PLP–SEC experiments

Itaconates propagate and terminate extremely slowly. This has to be reflected in the choice of the pulsed laser polymerisation (PLP) parameters. Slow propagation requires a long dark time between two consecutive pulses, so that sufficiently long polymer chains can be formed. However, long dark times can be problematic when investigating propagation kinetics with PLP. When dark times become too long, many growing chains will terminate naturally in between pulses. Therefore, the PLP shape will be less pronounced or even vanish, impeding the determination of k_p. Fortunately, the slow termination rate of itaconates allow for extended dark times without disrupting the PLP mechanism.

Preliminary measurements were conducted to choose a suitable photoinitiator. Davis *et al.* have used azobisisobutyronitrile (AIBN) in a very similar study with dimethyl itaconate (DMI).[74] This has been unsuccessful in this study. No polymer was obtained using AIBN as photoinitiator. Davis used a Nd:YAG laser

at 355 nm with a pulse energy of 5-30 mJ per pulse as opposed to this work where a XeF exciplex laser at 351 nm with a pulse energy of 1-6 mJ per pulse was employed. However, 2,2-Dimethoxy-2-phenylacetophenone (DMPA) and 2-Methyl-4′-(methylthio)-2-morpholinopropiophenone (MMMP) which are suitable photoinitiators for the SP–PLP–EPR method both were usable.[90] DMPA was chosen for this study because of a slightly better yield.

The XeF laser used in this work allows for repetition rates between 1-1000 Hz and a defined number of pulses. To access frequencies smaller than 1 Hz, the burst mode was used. Using bursts of 1 pulse and a pause of the users choice between the bursts, effectively lower repetition rates can be achieved. This approach however leads to loss of control of the number of pulses. Since the number of pulses only influences the conversion and needs to be high enough to obtain a sufficient amount of polymer for analysis but low enough as to not influence the monomer concentration significantly, an exact control is not necessary. In this work, laser repetition rates between 0.5-2 Hz were used.

In order to consider the results reliable, the obtained k_p have to be independent of photoinitiator concentration, laser repetition rate and and also the different inflection points should give the same k_p. The last requirement corresponds to the second inflection point being located at double the molar mass of the first one and the third one at triple the molar mass. This implies that k_p is chain-length independent.

For each temperature, two solutions of DMPA in DEI with different concentrations were prepared in order to check the independence of the results from the initiator concentration. From each of those solutions two experiments were performed, one with a higher laser repetition rate and one with a lower one. This was done to check whether the results meet the criterion of being independent from the laser repetition rate. The laser energy declined over the time of the irradiation process. The values given in table 5.2 refer to the energy at the beginning and the end of the irradiation, respectively. They should be considered estimates rather than exact values. In order to extract the molar masses, the molar mass distributions were numerically differentiated and the maxima and zero points which correspond

Table 5.2.: PLP data for DEI. Molar masses are given in g/mol. inf refers to the inflection points, while p refers to peak maxima. A maximum for the third peak could not be extracted for any of the experiments.

c_I/mol L^{-1}	T/K	# pulses	E/mJpp	ν/Hz	M_{inf1}	M_{p1}	M_{inf2}	M_{p2}	M_{inf3}
0.022	343.15	2000	6.9-5.2	1.0	25 400	36 700	42 800	52 700	-
0.022	343.15	2000	5.2-5.1	2.0	15 400	21 800	27 700	-	-
0.040	343.15	2000	4.9-4.2	1.0	26 600	-	42 800	-	-
0.040	343.15	2000	4.5-4.4	2.0	15 200	-	28 000	-	-
0.026	333.15	1000	2.5-1.0	0.5	43 000	-	73 800	-	108 800
0.026	333.15	4000	1.0-0.7	1.0	25 100	-	44 900	-	65 600
0.047	333.15	2400	0.8-0.7	0.5	44 700	-	79 100	-	116 500
0.047	333.15	4000	1.3-0.7	1.0	23 600	-	44 500	-	-
0.022	323.15	2000	7.2-5.2	1.0	20 000	25 100	36 400	-	54 300
0.022	323.15	2000	5.2-4.2	0.5	35 700	43 900	63 100	72 000	96 100
0.061	323.15	2000	4.2-3.8	1.0	19 780	25 550	36 500	44 000	-
0.061	323.15	2000	3.8-3.4	0.5	35 100	43 220	61 120	69 420	-
0.033	313.15	2000	7.2-5.6	1.0	16 320	20 940	30 050	35 980	-
0.051	313.15	2000	4.3-4.8	1.0	15 700	-	29 800	39 200	-
0.051	313.15	2000	4.8-3.5	0.5	29 100	36 500	52 300	67 800	-
0.027	303.15	2000	7.1-6.0	1.0	12 510	16 800	23 310	27 780	35 790
0.027	303.15	2000	5.7-4.8	0.5	23 500	28 400	42 900	49 100	65 000
0.046	303.15	2000	4.8-5.0	1.0	12 490	16 830	23 420	27 900	-
0.046	303.15	2000	4.8-3.6	0.5	23 100	27 800	42 900	48 600	64 200

to inflection points and maxima, respectively, were determined manually. However, only the inflection points were used for the data analysis (as recommended by Olaj *et al.*) and the maxima are given only for the sake of completeness.[15,54,55] For determination of k_{p} the monomer concentration at the measurement temperatures is needed. As the monomer is used in bulk, the concentration can be simply calculated using the density and the molar mass:

$$c = \frac{\rho}{M} \tag{5.10}$$

Since only a gas pycnometry system without temperature control was available, room temperature densities were used for the whole temperature range. The following densities were obtained: $1.044\,\mathrm{g\,mL^{-1}}$ (DEI) and $1.025\,\mathrm{g\,mL^{-1}}$ (DPI). The obtained PLP data are collected in table 5.2.

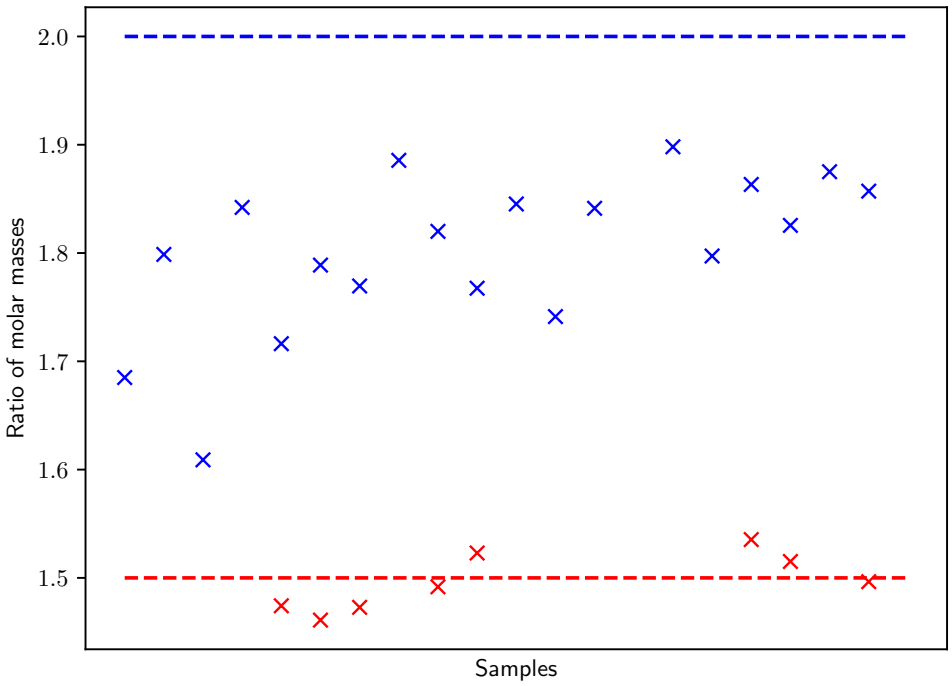

Figure 5.3.: Ratio of molar masses of the inflection points for DEI. Blue points show the ratio of the second inflection point to the first one, while red points show the ratio of the third inflection point to the second one.

Table 5.3.: Obtained Arrhenius parameters for DEI.

$A/\mathrm{L\,mol^{-1}\,s^{-1}}$	$E_\mathrm{A}/\mathrm{kJ\,mol^{-1}}$
$(1.1 \pm 0.3) \cdot 10^4$	17.5 ± 0.6

Figure 5.3 shows the ratio of inflection point positions for all samples. However not for all samples a distinct third inflection point could be observed. The ratio of the second inflection point to the first one is systematically smaller than the ideal value of 2, while the ratio of the third inflection point to the second one fits to the expected value of 1.5 quite well. This has been observed in a number of studies as well.[91–94] This phenomenon might be interpreted in terms of a chain-length-dependency of k_p. However as of today only a chain-length-dependency up to chain lengths of 5 units is accepted.[95,96] The same effect has also been observed for many other systems using PLP–SEC. It is not yet clear whether this is a real chain-length-dependency effect or an artefact from the size-exclusion chromatography.[97,98]

In fig. 5.4 it is visible that k_p is independent of initiator concentration but not of laser repetition rate. Higher repetition rate leads to higher values of k_p. This might be reasoned again by chain-length-dependency. Higher repetition rate leads to shorter chains which have an increased k_p compared to longer chains.

A typical Arrhenius fit (see fig. 5.5) is used to obtain the activation energy and the pre-exponential factor which are listed in table 5.3. The experimentally obtained pre-exponential factor is in very good agreement with the results from B3LYP/def2-TZVP (compare table 5.1). The experimental activation energy however is about $5\,\mathrm{kJ\,mol^{-1}}$ higher than the prediction. This is an overall very good agreement, considering the simple theoretical model used. Likely this good agreement is owed to error compensation because it is unlikely that the simple model and the only moderate level of theory yield an accurate description of the problem.

The same fashion of experiments was conducted for DPI, but here two stock solutions of DMPA in DPI were prepared which were used for all temperatures. Furthermore, the laser energy was not explicitly monitored but was in a similar

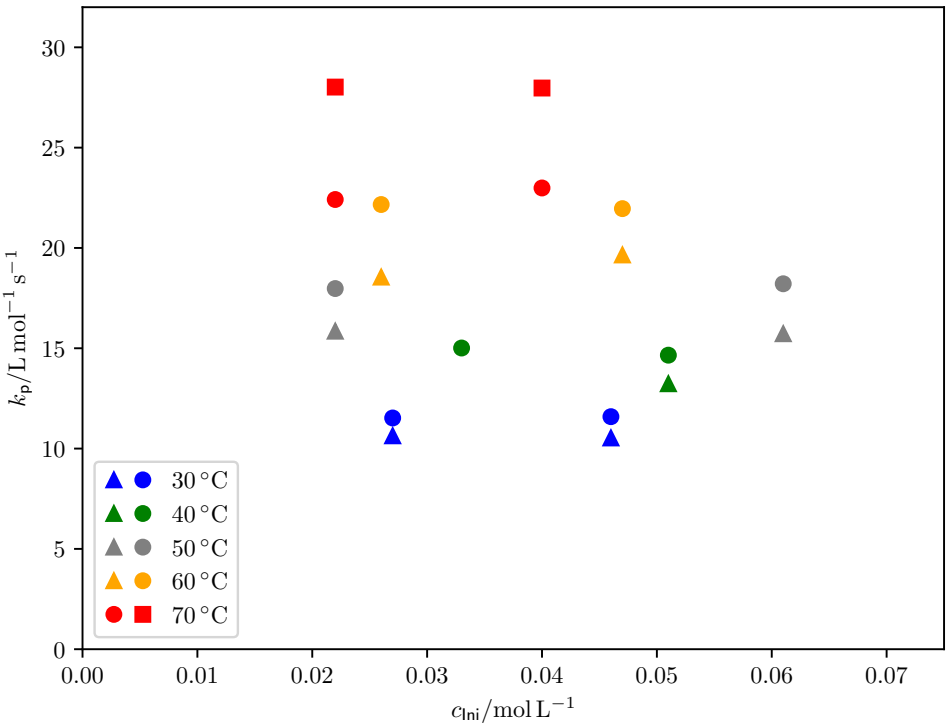

Figure 5.4.: Values of k_p for DEI as a function of photoinitiator concentration. An average of the k_p values obtained from the different inflection points is used here. Triangles refer to a laser repetition rate of 0.5 Hz, while circles refer to 1 Hz, and squares to 2 Hz.

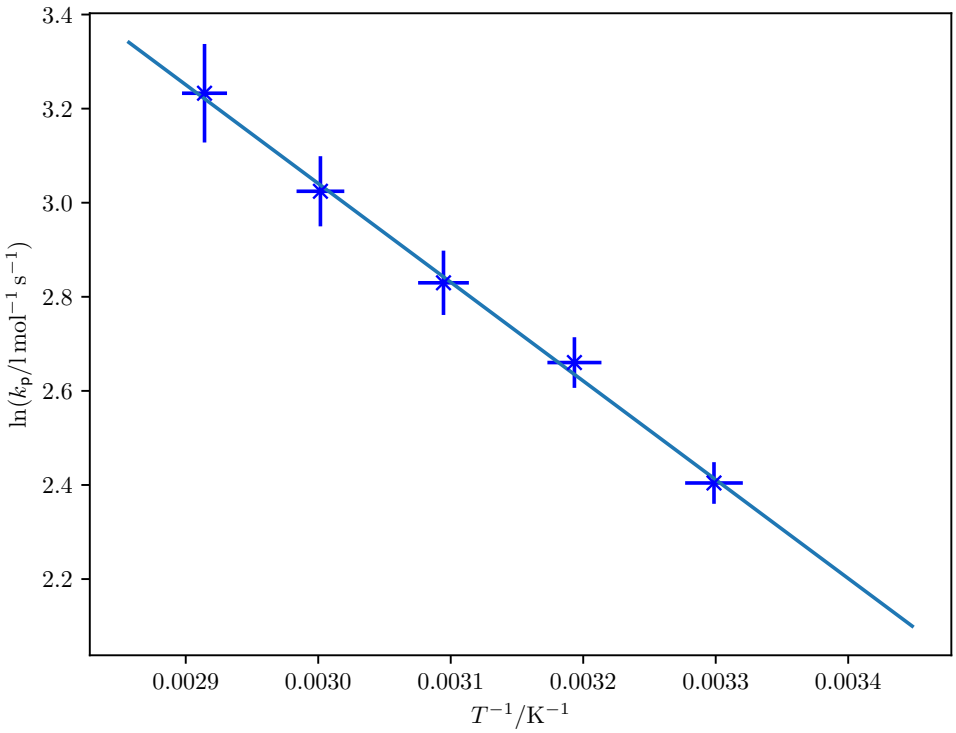

Figure 5.5.: Arrhenius fit for k_p of DEI. The uncertainties in $\ln(k_p)$ stem from the standard deviation of the obtained k_p values while for the uncertainty in T^{-1} an uncertainty of $\Delta T = 2\,\mathrm{K}$ was assumed.

Table 5.4.: PLP data for DPI. Molar masses are given in g/mol. inf refers to the inflection points, while p refers to peak maxima.

c_I/mol L^{-1}	T/K	ν/Hz	M_{inf1}	M_{p1}	M_{inf2}	M_{p2}	M_{inf3}	M_{p3}
0.074	333.15	0.25	70 800	85 600	129 100	145 900	-	-
0.049	333.15	0.25	70 200	83 900	127 900	142 600	193 900	-
0.074	333.15	0.50	41 300	48 500	72 800	84 700	111 900	-
0.049	333.15	0.50	41 100	50 200	72 500	83 400	110 000	-
0.074	323.15	0.25	61 800	-	115 200	-	-	-
0.049	323.15	0.25	61 200	-	113 500	-	-	-
0.074	323.15	0.50	33 930	41 500	61 600	-	-	-
0.049	323.15	0.50	35 000	42 500	61 000	-	-	-
0.074	313.15	0.25	47 200	60 100	92 800	-	-	-
0.049	313.15	0.25	50 500	61 300	93 400	-	136 800	-
0.074	313.15	0.50	26 200	-	49 800	-	-	-
0.049	313.15	0.50	28 400	-	48 400	-	-	-
0.049	303.15	0.50	19 400	-	39 100	-	-	-
0.074	293.15	0.25	12 100	-	22 400	-	32 700	-
0.049	293.15	0.25	12 400	-	20 700	-	32 100	35 900
0.074	293.15	0.50	16 100	-	29 600	-	-	-
0.049	293.15	0.50	14 300	-	30 100	-	-	-

Table 5.5.: Obtained Arrhenius parameters for DPI.

A/L mol^{-1} s^{-1}	E_A/kJ mol^{-1}
$(1.2 \pm 0.7) \cdot 10^4$	18.0 ± 1.7

range as for the DEI experiments. The PLP data is collected in table 5.4 and the tests for independence of k_p from the number of the evaluated peak and from repetition rate and initiator concentration are shown in figs. 5.6 and 5.7. Again, an Arrhenius fit is used (fig. 5.8) and the results are shown in table 5.5.

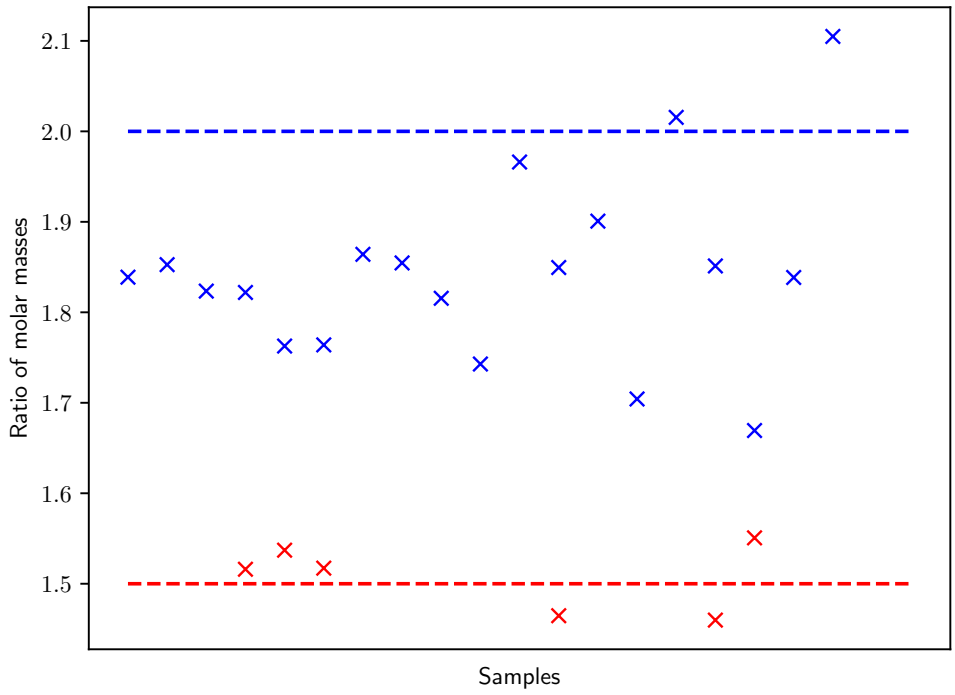

Figure 5.6.: Ratio of molar masses of the inflection points for DPI. Blue points show the ratio of the second inflection point to the first one, while red points show the ratio of the third inflection point to the second one.

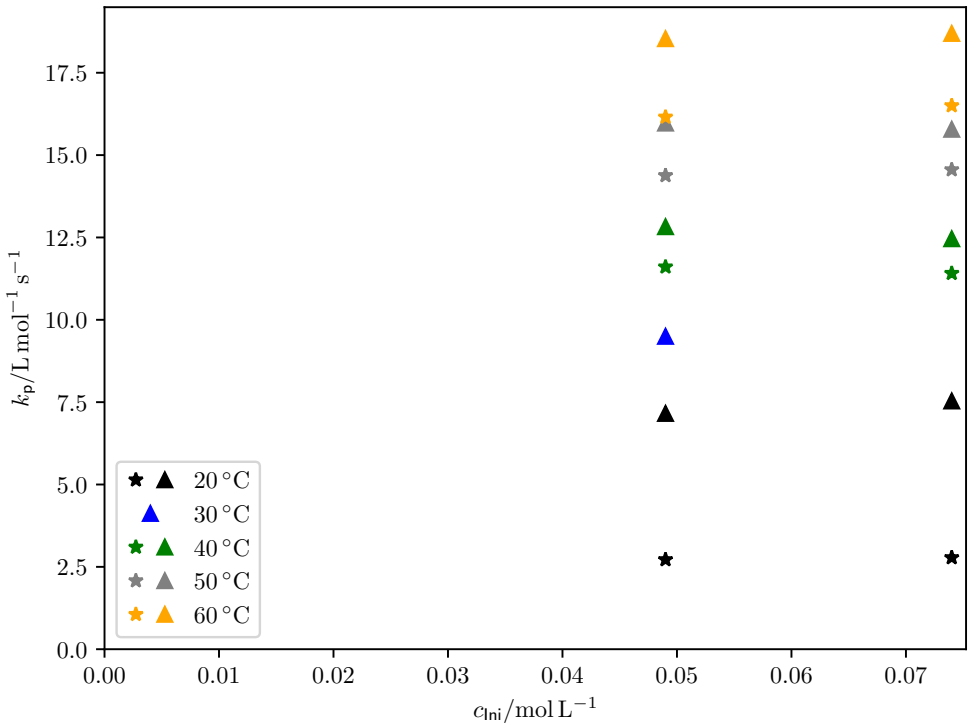

Figure 5.7.: Values of k_p for DPI as a function of photoinitiator concentration. An average of the k_p values obtained from the different inflection points is used here. Stars refer to a laser repetition rate of 0.25 Hz, while triangles refer to 0.5 Hz.

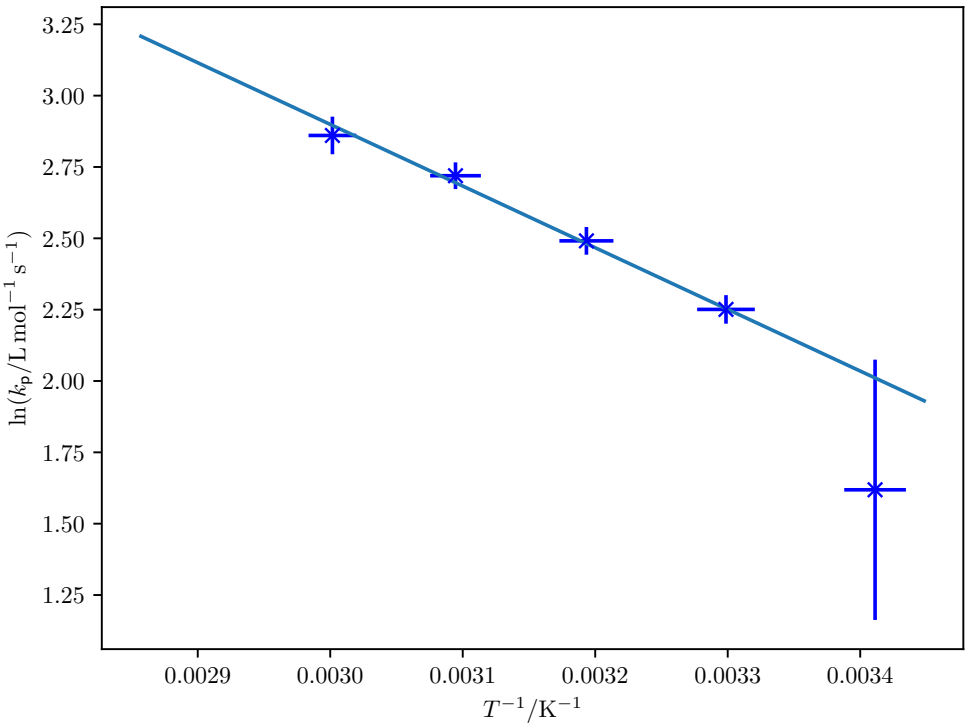

Figure 5.8.: Arrhenius fit for k_p of DPI. The uncertainties in $\ln(k_p)$ stem from the standard deviation of the obtained k_p values while for the uncertainty in T^{-1} an uncertainty of $\Delta T = 2\,\mathrm{K}$ was assumed. For 30 °C only one measurement exists, so the standard eviation was assumed to be similar to that of the other measurements.

5.1.3. Comparison with other monomers

The obtained Arrhenius parameters for DEI and DPI will be compared to other itaconates as well as other monomer families in the following.

Inspecting the values in table 5.6, one notices that low values of A are accompanied by low values of E_A. This makes it difficult to identify trends. Haehnel *et al.* investigated linear alkyl methacrylates and found the same effect of accompanied Arrhenius parameters.[99,100] They stated that in order to identify trends, not the Arrhenius parameters, but k_p at a given temperature should be used. In the case of linear methacrylates, a linearly increasing k_p at 50 °C was found. This was reasoned by Haehnel *et al.* by prestructuring of the monomer. With longer side chains, the attractive forces between them increase, leading to aligned side chains as the monomer molecules are stacked on each other. This alignment also leads to alignment of the olefinic bonds of neighboring molecules, reducing the distance between them. This facilitates the propagation step, since less rearrangement is necessary.[99,100]

In the case of itaconates the opposite trend is observed, k_p decreases linearly with size of the ester chain. This can be explained also by prestructuring. While methacrylates have only one ester side chain, itaconates have two. This allows for different alignment patterns. A stacked alignment just as for the previously discussed methacrylates is possible, but also a shifted, zig-zag motif exists (see fig. 5.9). This way the repulsion of the central moieties is eliminated, but the attraction of the side chains is retained. Each of the side chains of one monomer molecule is stacked with the side chain of a different molecule. This alignment reduces the distance of the olefinic bonds, hindering the propagation. Apparently, for itaconates the zig-zag motif is preferred. This can be verified by molecular dynamics simulations in the future.

k_p of other monomer families has values differing a few orders of magnitude from itaconates. In table 5.7 it can be seen that between the different families of monomers the values of A differ by several orders of magnitude. With less bulky substituents on the olefinic bond or no substitution at all, A increases which can

Table 5.6.: Comparison of Arrhenius parameters for the propagation step for several itaconic acid esters in bulk. DMI = dimethyl itaconate, DBI = di-*n*-butyl itaconate, DCHI = dicyclohexyl itaconate.

Substance	$A/10^5\,\mathrm{L\,mol^{-1}\,s^{-1}}$	$E_\mathrm{A}/\mathrm{kJ\,mol^{-1}}$
DMI[74]	2.2	24.9
DMI[75]	7.3	27.8
DEI (this work)	0.11	17.5
DPI (this work)	0.12	18.0
DBI[75]	0.33	21.3
DCHI[75]	0.99	26.5
DCHI[76]	0.17	22.0

Table 5.7.: Typical values of Arrhenius parameters and k_p for different monomer families. Several orders of magnitude are spanned.

Family	$A/10^4\,\mathrm{L\,mol^{-1}\,s^{-1}}$	$E_\mathrm{A}/\mathrm{kJ\,mol^{-1}}$	$k_\mathrm{p}(50\,^\circ\mathrm{C})/\mathrm{L\,mol^{-1}\,s^{-1}}$
Itaconates	2-20	18-28	5-25
Methacrylates[101]	100-800	20-23	800-2500
Acrylates[101]	1600-1800	17-18	20 000-32 000

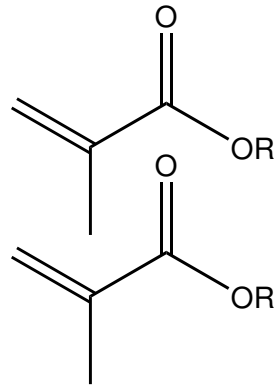

(a) Aligned olefinic bonds in methacrylates

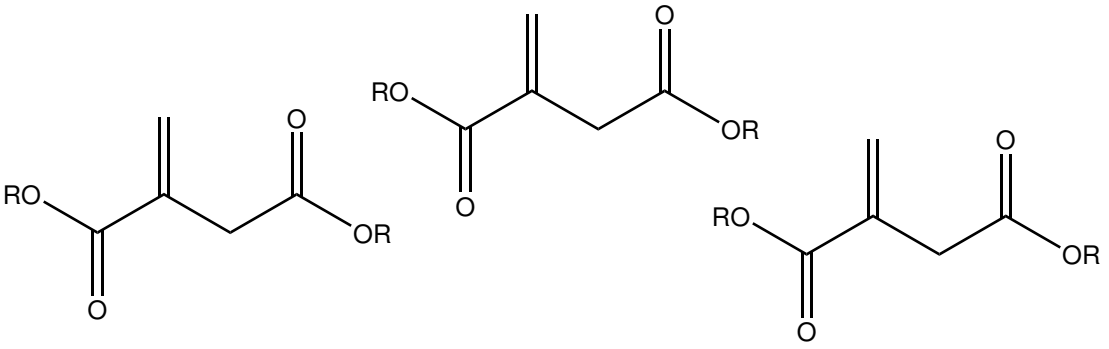

(b) Shifted zig-zag motif in itaconates

Figure 5.9.: Alignment mechanisms of monomers. The first one aligns the olefinic bonds, facilitating an easier propagation step. The second increases the distance of the olefinic bonds, decreasing the proapgation rate coefficient.

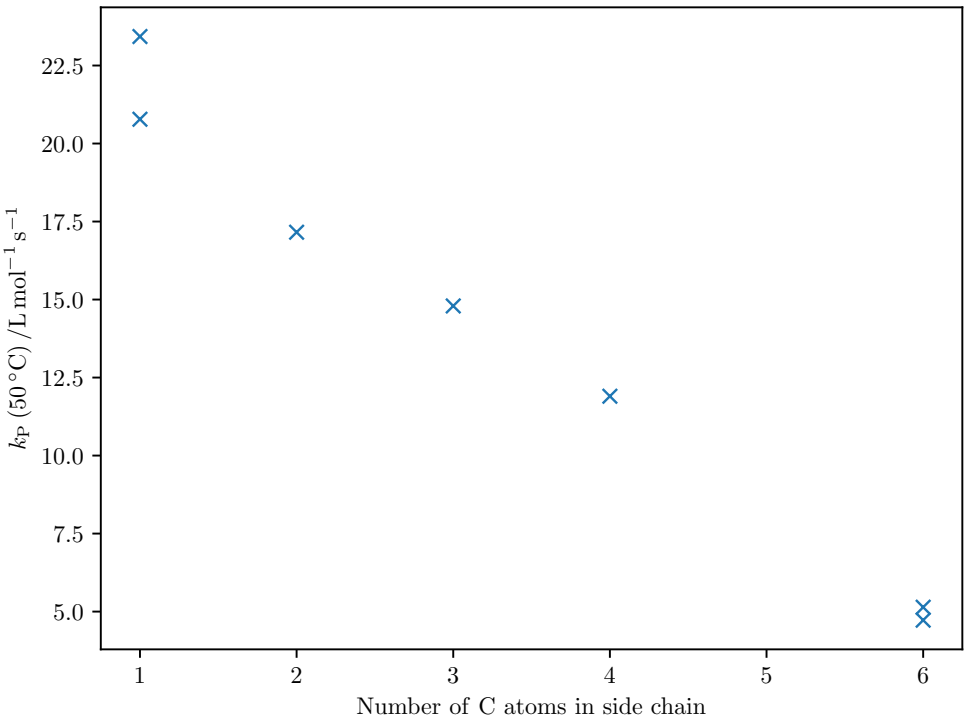

Figure 5.10.: Values of k_p at 50 °C for several itaconate esters using the Arrhenius parameters from table 5.6.

readily be reasoned by less steric repulsion and decreased propagating radical stability. The activation energies show a less clear picture which is due to the high scatter for the itaconate values. The resulting $k_p(50\,°C)$ values also span several order of magnitudes, roughly following the trend of A, since the values of E_A are comparable. It is clearly visible that itaconates are extremely slowly propagating compared to typical commercially used monomer families such as acrylates and methacrylates. As mentioned at the beginning of the chapter, itaconates are interesting in terms of replacement of petrol-based monomers. The low k_p values are discouraging for this as slow propagation means longer reaction times, possibly shorter polymer chains. But in order to fully assess the situation, also termination kinetics need to be taken into account. Consequently, the termination kinetics will be examined using SP–PLP–EPR.

5.2. Temperature dependence of the termination kinetics of DEI

The SP–PLP–EPR method which was developed by Buback is currently the most powerful method for the examination of termination kinetics. In a series of publications the SP–PLP–EPR method was used to determine the composite model parameters for different monomers. In this work the temperature dependence of the termination kinetics, namely the parameters describing the chain-length-dependence of k_t, α_s and α_l, the crossover-chainlength i_c as well as the termination rate coefficient of monomeric radicals $k_t^{1,1}$ and k_t^0 was examined. All measurements were performed in bulk.

5.2.1. Composite-model parameters

DEI shows a distinct 5-line EPR spectrum, typical for itaconates. This form has been observed earlier in a number of publications for different itaconates.[77–82,102–104]

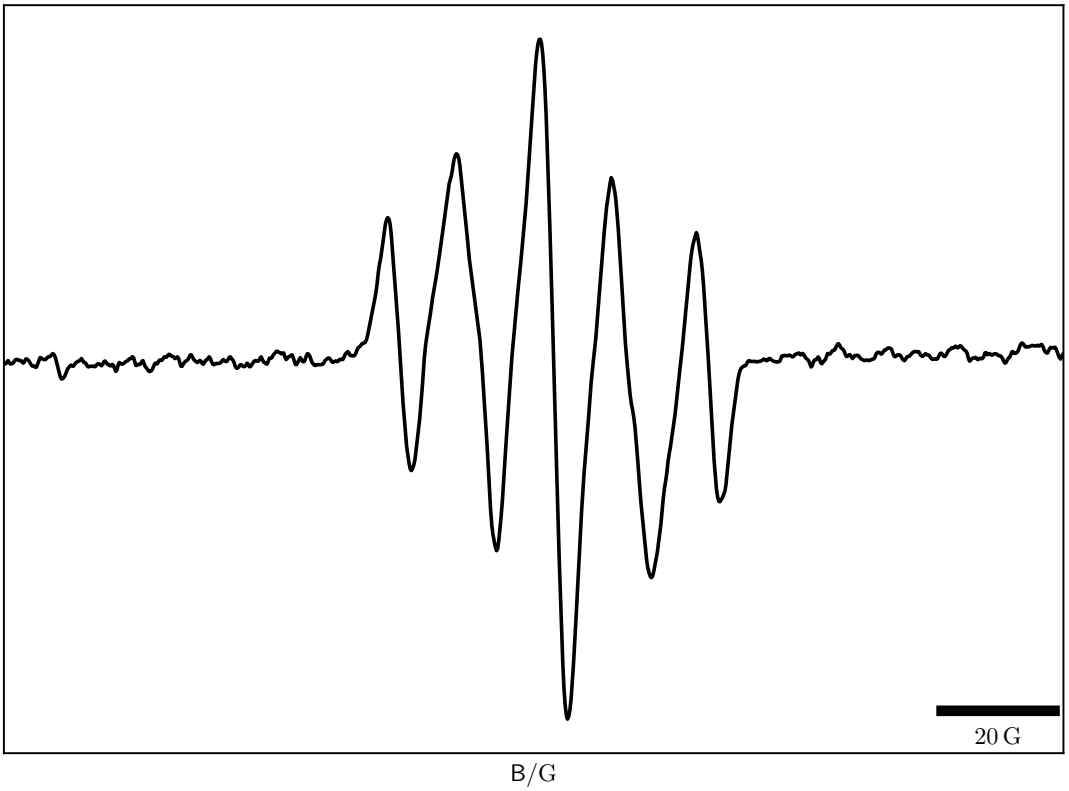

Figure 5.11.: EPR spectrum of a DEI polymerisation at 293 K with 0.1 mol L^{-1} of DMPA as photoinitiator and a laser repetition rate of 30 Hz.

Table 5.8.: Determined hyperfine coupling constants for DEI at 293 K. It can not be clearly assigned which hyperfine coupling constant belongs to which pair of hydrogen atoms, consequently no assignment is given.

# and pos. of atoms	a/G
2H	13.1
2H	11.6

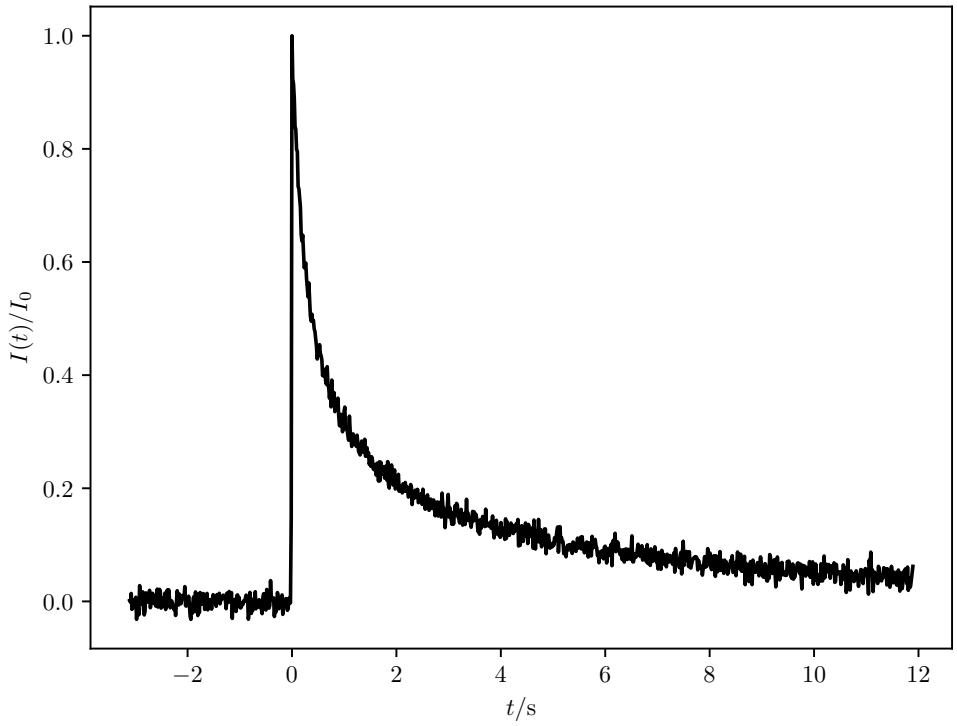

Figure 5.12.: SP–PLP–EPR measurement of DEI in bulk at 273 K. The intensity has been normalised to the peak intensity. The magnetic field position corresponds to that of the center peak in fig. 5.11.

The hyperfine coupling constants can be easily obtained from this by fitting with *easyspin*

After measuring the spectrum and identifying the peak with maximum intensity, the field position is fixed at that maximum intensity peak, a single laser pulse is applied and the decay of intensity is measured as a function of time as shown in fig. 5.12.

According to eqs. 2.48 and 2.49 from this a double-logarithmic plot (see fig. 5.13) can be done to obtain the composite model parameters, where α_s and α_l are obtained from the slopes of the two linear regimes, i_c from the intersection of both straight lines and $k_\mathrm{t}^{1,1}$ as well as k_t^0 from the intersection with the ordinate for both

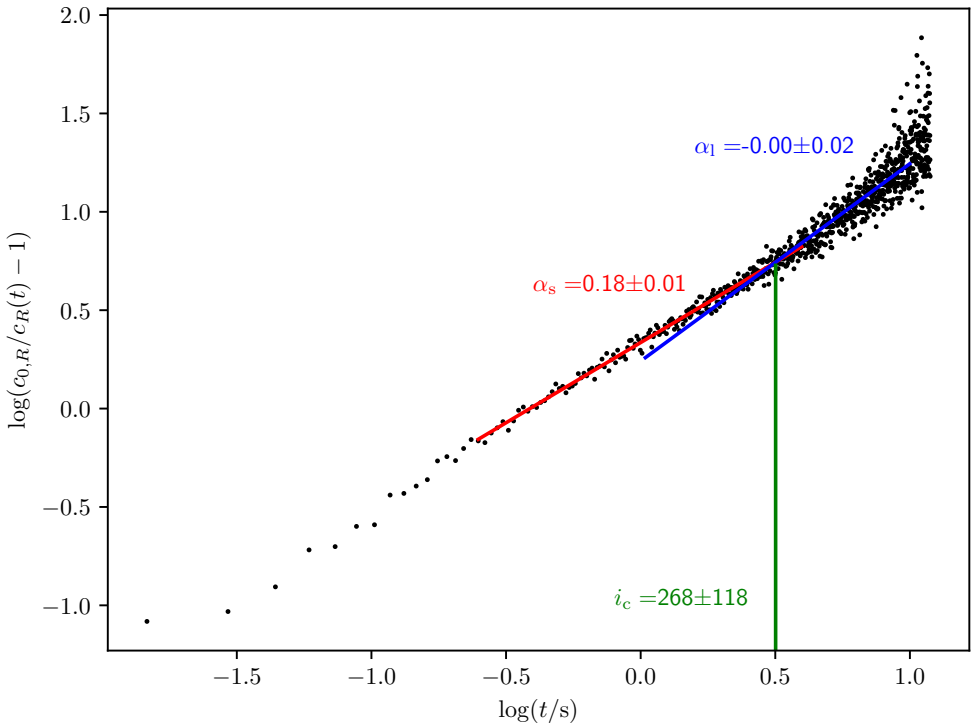

Figure 5.13.: Exemplary double-logarithmic plot for extracting the composite model parameters using a measurement of DEI in bulk at 273 K. The α values are extracted from the slopes of the linear regions, i_c from the abscissa position of the intersection of both linear regions. $k_t^{1,1}$ as well as k_t^0 are obtained from the ordinate intercepts of the respective linear regions (not shown here).

straight lines. This analysis was performed for a number of temperatures.

In the past, several different monomers have been investigated in this fashion, for example Sty, DBI, pentyl methacrylate as well as sodium methacrylate. For all of these monomers, α_s and α_l (if reported) were shown to be temperature-independent.[32,82,105–107] Also the typical values for α_s are around 0.5-0.7 an for α_l around 0.1-0.2. The values for DBI found by Kattner are $\alpha_s = 0.57 \pm 0.05$ and $\alpha_l = 0.17 \pm 0.08$ at 50 °C.[32] Significantly lower values were found in this work, even though one would expect DEI and DBI to have similar values as the only difference is the length of the ester side chains. For α_l even negative values are ob-

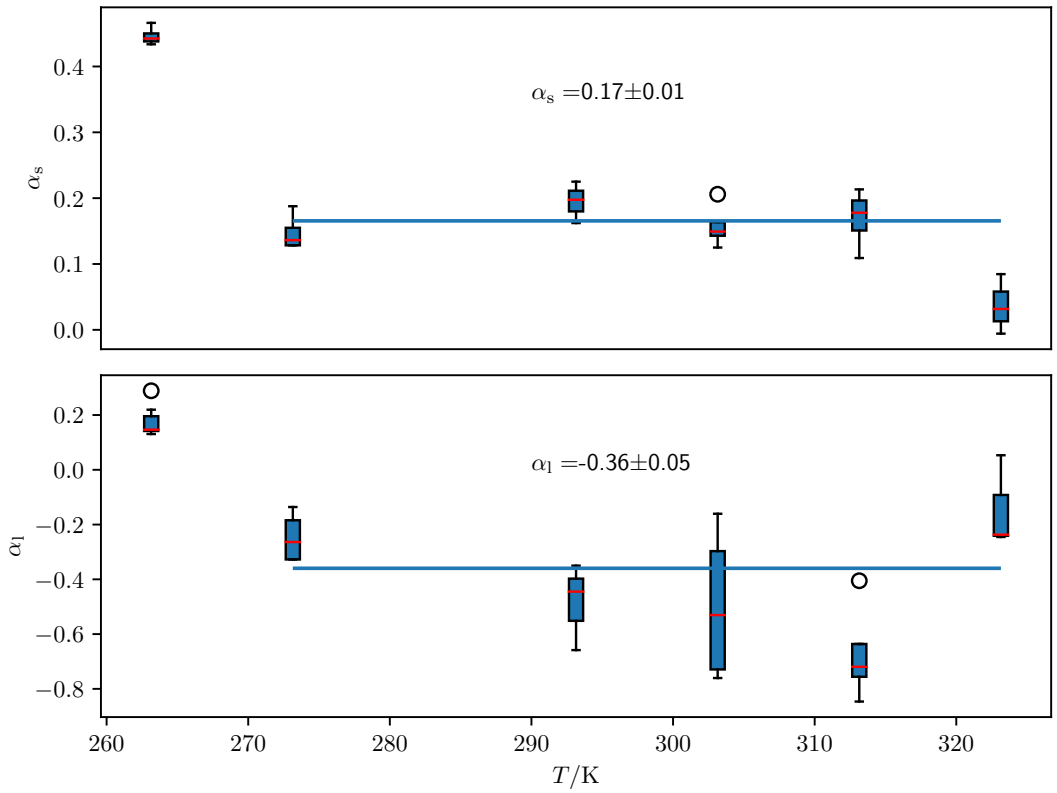

Figure 5.14.: Temperature dependence of α_s and α_l for the DEI bulk homopolymerisation. The data points deviate from the literature-known range.

tained. Negative values imply that k_t increases with increasing chain length which contradicts the composite model and the well established fact that termination is diffusion-controlled. This unusual finding might be explained by a number of things. First of all, backbiting comes to mind. If the EPR spectrum of the primary propagating radical is superimposed by a tertiary radical, the EPR peaks of this tertiary radical can influence the observed time trace. As a tertiary radical of DEI is more sterically hindered, termination can be assumed to be slower and thus tertiary radicals typically accumulate during the measurement. However in previous investigations of DBI no hints of backbiting were found and as DBI belong to the same monomer family it can be safely assumed that the backbiting behaviour is similar.[82,108] Additionally, by personal communication with H. Kattner, two more factors were identified which influence the results: Laser artefacts and the intensity at the laser pulse. When the laser pulse illuminates the sample during a time-dependent measurement, often a spike in the EPR intensity is observed. This spike can influence the intensity to positive or negative values, with the latter being more striking to the eye. This phenomenon is called the 'laser artefact'. Laser artefacts can occur temporally random and if a scan with a laser artefact is averaged together with other scans, this falsifies the averaged measurement, rendering it unusable. However, laser artefacts appear more frequent in certain spectral positions, namely the maximum peak intensity. H. Kattner therefore recommended measuring slightly next to the peak maximum where laser artefacts are far less common. The cause for this behaviour is unknown. Furthermore during the course of a time-dependent SP–PLP–EPR experiment, the photoinitiator in the sample is being consumed. This leads to decreasing intensities which shows in the peak intensity decreasing. However the shape of the decay after the laser pulse is largely unaffected by this lower starting intensity. Consequently, when averaging several scans, the peak intensity is systematically underestimated. It was tested in which direction the results are influenced by this error source. This was done by using a measurement of DBI at 50 °C and performing the double-logarithmic data analysis in order to obtain α_s, α_l and i_c, but the peak intensity was manually defined and varied instead of being the actually measured peak intensity. These results are compared to literature values.[82]

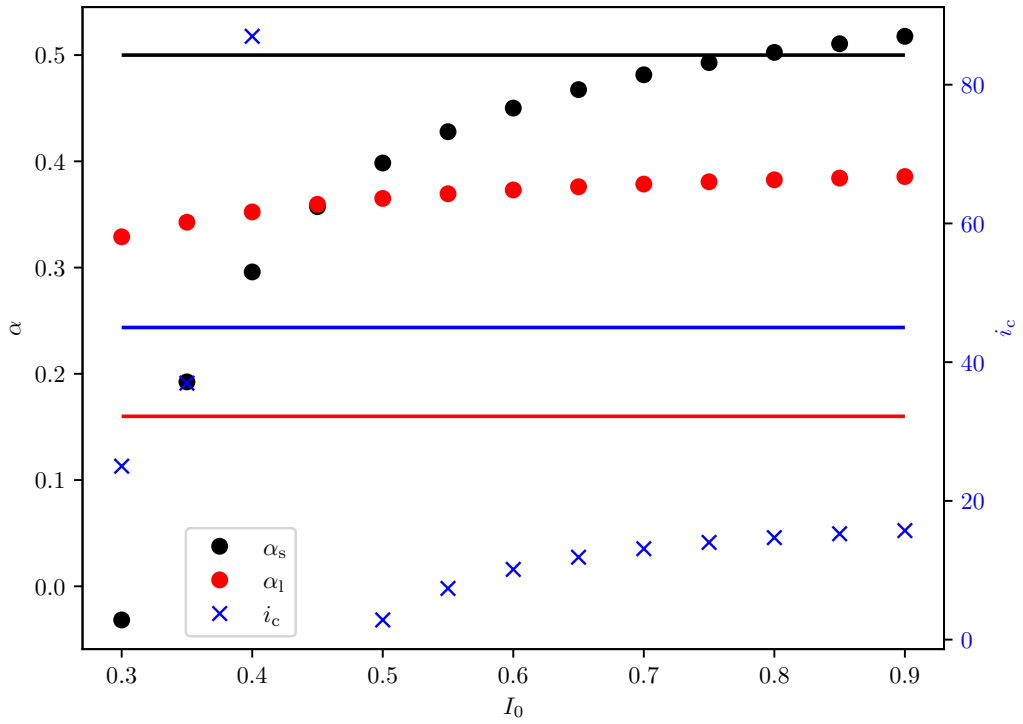

Figure 5.15.: Influence of peak intensity variation on the results for a data evaluation according to eqs. 2.48 and 2.49 with DBI at 50 °C. Literature results are shown as horizontal lines. For i_c a singularity can be seen at $I_0 = 0.45$ where $\alpha_s \approx \alpha_l$, which leads to parallel lines and consequently no intersection point.

In fig. 5.15 it can be seen that with increasing peak intensity the results for both α values and the crossover chain length i_c approach a constant value. For α_s this coincides with the literature value satisfactorily, while for α_l the result is significantly higher than the literature value and for i_c significantly lower. The behaviour of approaching a constant value is similar for all properties though. As the peak intensity might be distorted by undetected laser artefacts and/or averaging too many scans, it might be a worthwhile idea to report only the results for very large peak intensity as these are more robust.

The data presented here were measured with alredy taking H. Kattners recommendations into account. Data which were measured with laser artefacts present and too many scans (and therefore a significant decrease in I_0) are not reported here. The peak intensity however was not artificially changed. Based on the fact that previous studies all found α_s and α_l to be temperature-independent, this was also assumed here. A fit including the uncertainties of α_s and α_l respectively was performed using orthogonal distance regression. The uncertainties of the individual data points are not shown in the graph however for reasons of visual clarity. The data points for 263.15 K were not considered in the fit as they deviate strongly from the rest of the results. It might be investigated in future work whether this is a real physical effect or just an erroneous measurement.

One obtains $\alpha_s = 0.17 \pm 0.01$ and $\alpha_l = -0.36 \pm 0.05$. These values deviate significantly from values for other monomers, also for the closely related DBI. The results seem not trustworthy, especially the negative value for α_l. Theoretical calculations predict a value of $\alpha_s = 0.5 - 0.66$ and $\alpha_l = 0.16$.[17,36] Interestingly, the results for 263.15 K are close to these predictions, but are the only ones of this dataset which fulfill this expectation. The obtained value for α_s is coherent with the prediction for α_l which arises the suspicion that the chain-length-regimes were incorrectly identified. However comparing to earlier work by Buback *et al.* one can see that the time scales of the regimes in an SP–PLP–EPR experiment for DBI are nearly identical to the ones chosen in this work for DEI.[82] Both monomers have a similar k_p, so similar time frames should be expected. This points to the measurements being valid while contradicting the known behaviour.

monomer	α_s	α_l	reference
MMA	0.63 ± 0.15	-	[109]
MMA	0.65 ± 0.04	0.15 ± 0.03	[110, 111]
n-BMA	0.65 ± 0.10	0.20 ± 0.05	[112]
tert-BMA	0.56 ± 0.10	0.20 ± 0.05	[112]
PnMA	0.56 ± 0.08	0.16 ± 0.04	[89]
2-EHMA	0.61 ± 0.09	0.19 ± 0.05	[113]
DMA	0.65 ± 0.08	0.17 ± 0.04	[113]
BzMA	0.50 ± 0.07	0.21 ± 0.06	[108]
Sty	0.51 ± 0.05	0.16 ± 0.05	[106]
Sty	0.53 ± 0.04	0.15 ± 0.03	[114]
VAc	0.57 ± 0.05	0.16 ± 0.07	[31]
VAc	0.60 ± 0.04	0.15 ± 0.03	[115]
VPiv	0.67 ± 0.15	0.16 ± 0.07	[31]
MA	0.78 ± 0.04	0.15 ± 0.03	[35]
MA	0.31 ± 0.04	0.31 ± 0.03	[116]
MA	0.78 ± 0.04	0.26 ± 0.03	[117]
DEI	0.17 ± 0.01	-0.36 ± 0.05	this work
DBI	0.5 ± 0.1	0.16	[82]
DBI	0.57 ± 0.05	0.17 ± 0.08	[32]

Table 5.9.: Power-law exponentsα_s and α_l from the composite model for several monomers. MMA = methyl methacrylate, BMA = butyl methacrylate, PnMA = n-pentyl methacrylate, 2-EHMA = 2-ethylhexyl methacrylate, DMA = dodecyl methacrylate, BzMA = benzyl methacrylate, Sty = styrene, VAc = vinyl acetate, VPiv = vinyl pivalate, DEI = diethyl itaconate, DBI = di-*n*-butyl itaconate.

5.2.2. Crossover-chainlength

In previous investigations for most of the monomers no temperature dependence of i_c was found. Mostly acrylates and methacrylates were examined. Interestingly, a sigmoidal temperature dependence was observed for 2-EHMA and dodecyl methacrylate (DMA), however not for other methacrylates.[105] The cause for this is not yet clear. One might hypothetise that for other methacrylates the sigmoidal transition is in a temperature region that was not examined but is in principle present for all methacrylates. This is however just a hypothesis which needs verification by additional experiments. Especially interesting is the influence of a solvent on this temperature dependence.

Buback found for DBI a value of $i_c = 45 \pm 10$ and confirmed this in a later separate study.[82,118] In this previous work, for each temperature several data points exist and the associated uncertainty is the standard deviation of these points. This approach however neglects that each value itself also has an uncertainty. i_c is determined from the abscissa position of the intersection of both straight lines in the double-logarithmic plots. For each of the slopes and ordinate intersections of the straight lines an associated uncertainty is known from the fit procedure. Consequently the uncertainty of i_c can be calculated straightforward using Gaussian propagation of errors. Strictly speaking this is not correct as the slope and intercept of a straight line are correlated, but this is neglected here. Due to the logarithmic abscissa, this leads to significantly higher uncertainties but neglecting the uncertainty of the individual data points would lead to an artificially more accurate result than is actually true. So in this work the uncertainty for each single result was calculated by Gaussian propagation of errors and the uncertainty for the temperature-independent average was obtained by using orthogonal distance regression as the fitting algorithm which can handle uncertainties in both the dependent and independent variable (although only the uncertainties of the dependent variable were considered here). One obtains $i_c = 60 \pm 5$ for DEI. However the uncertainties are so large (roughly 50 %) that a different model might be chosen with the same legitimisation. It is therefore not possible to draw any definite insights from these data.

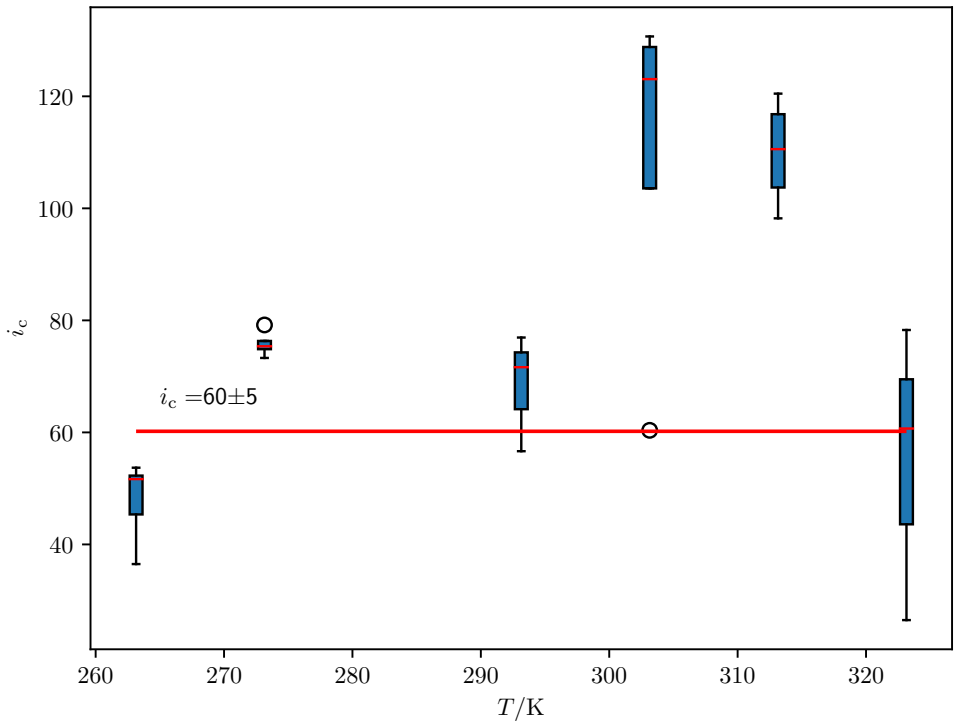

Figure 5.16.: Crossover-chainlength i_c as a function of temperature for DEI in bulk. Very large scatter between the measurements for each temperature and also between the different temperatures can be seen.

monomer	i_c	reference
Sty	18	[114]
Sty	30 ± 10	[106]
VAc	26	[115]
VAc	20 ± 10	[31]
VPiv	110 ± 30	[31]
MA	15	[35]
MA	30	[117]
MA	35 ± 10	[33]
NaMA	79 ± 10	[32]
BA	65 ± 20	[33]
MMA	100	[110,111]
MMA	100	[109]
n-BMA	50 ± 15	[112]
t-BMA	70 ± 15	[112]
PnMA	67 ± 10	[89, 105]
DEI	60 ± 5	this work
DBI	45 ± 10	[32, 107]

Table 5.10.: Crossover-chainlengths from the composite model for several monomers. Sty = styrene, VAc = vinyl acetate, VPiv = vinyl pivalate, MA = methyl acrylate, NaMA = sodium methacrylate, BA = butyl acrylate, MMA = methyl methacrylate, BMA = butyl methacrylate, PnMA = n-pentyl methacrylate, DEI = diethyl itaconate, DBI = di-*n*-butyl itaconate.

Riemann found a sigmoidal temperature dependence of i_c for 2-EHMA and DMA, decreasing with increasing temperature.[105] For all other monomers and especially other methacrylates, no temperature dependence was found. It is not yet clear what causes this effect. A likely explanation lies in the flexibility of the polymer chain. i_c marks the chain length, at which segmental diffusion becomes rate-determining. When dealing with rigid chains, virtually no entanglement of the polymer chains occurs and thus a very high i_c is observed. 2-EHMA and DMA have rather long, aliphatic side groups which can interact with each other, giving rise to stiffness of the chain because the side groups align. Upon increasing the temperature, the side groups start to move more freely which enables entanglement and thus lowers i_c. This hypothesis can be further examined by molecular dynamics simulations.

5.2.3. Termination rate coefficients

In order to obtain the rate coefficients $k_t^{1,1}$ and k_t^0 from the intercepts of the straight lines a 2-step calibration procedure is required. The first step correlates radical concentration with the double integral of the spectrum. The second step correlates the double integral with the peak intensity. For the first step, to stay as close as possible to the system at hand, this is typically performed by dissolving known concentrations of TEMPO in the respective monomer. In this case, this yielded physically unreasonable values. Therefore it was chosen to use a calibration of TEMPO in toluene which had been measured earlier. A calibration factor of $h_1 = (3.92 \pm 0.03) \cdot 10^{-8}$ was obtained for the toluene calibration. This factor has been used for all temperatures. This of course introduces an error. It seems reasonable to assume that the error appears in the form of a constant factor f in the expression for k_t.

$$k_t = A \cdot e^{\left(-\frac{E_A}{RT}\right)} \cdot f \tag{5.11}$$

When linearising this, the factor f distorts only the pre-exponential factor but not the activation energy:

$$\ln(k_t) = \ln(A) + \ln(f) - \frac{E_A}{RT} \tag{5.12}$$

Consequently, correct activation energies should be obtained from an Arrhenius fit, however the preexponential factors will be wrong and will not be reported consequently.

The rate coefficients can be calculated from the ordinate intercept of the straight lines in fig. 5.13.

$$b = \log\left(\frac{2k_\mathrm{t}^{1,1} \cdot c_\mathrm{R}^0 \cdot t_\mathrm{p}^{\alpha_\mathrm{s}}}{1-\alpha_\mathrm{s}}\right) \tag{5.13}$$

$$k_\mathrm{t}^{1,1} = \frac{10^b \cdot (1-\alpha_\mathrm{s})}{2c_\mathrm{R}^0 \cdot t_\mathrm{p}^{\alpha_\mathrm{s}}} \tag{5.14}$$

For the long-chain analogues, one simply has to replace $k_\mathrm{t}^{1,1}$ by k_t^0 and α_s by α_l and use the intercept of the long-regime fit, naturally. Arrhenius fits of the obtained rate coefficients are shown in fig. 5.17. The uncertainties of each value was calculated using Gaussian propagation of errors on eq. 5.14. The obtained uncertainties are 1-2 orders of magnitude larger than the rate coefficients themselves and are not shown in fig. 5.17 for reasons of visual clarity. However, they have been considered in the fit.

Immediately one notices that the obtained values for $k_\mathrm{t}^{1,1}$ are larger than the diffusion limit which is the limit, when every encounter of two macroradicals leads to termination. This is consequently not possible. As discussed, this can be attributed to the error introduced by the calibration which scales all rate coefficients by a constant factor. One obtains values of $E_\mathrm{A}\left(k_\mathrm{t}^{1,1}\right) = (40 \pm 2)\,\mathrm{kJ\,mol^{-1}}$ and $E_\mathrm{A}\left(k_\mathrm{t}^0\right) = (55 \pm 5)\,\mathrm{kJ\,mol^{-1}}$. This can be compared to the activation energy of the fluidity. As termination is diffusion-controlled, $E_\mathrm{A}\left(k_\mathrm{t}^{1,1}\right) \approx E_\mathrm{A}\left(\eta^{-1}\right)$ should be fulfilled. The activation energy of fluidity was found to be $E_\mathrm{A}\left(\eta^{-1}\right) = (17.5 \pm 0.5)\,\mathrm{kJ\,mol^{-1}}$, approximately half of the expected value. This large deviation suggests that either the error introduced by the calibration or from the α_s value which also is far from the expected value distorts the results significantly. Kattner found for DBI an activation energy of fluidity and $k_\mathrm{t}^{1,1}$ at around $20\,\mathrm{kJ\,mol^{-1}}$.[32,118] Bearing in mind, that DEI is a homologue of DBI, similar values are expected and the activation energy of fluidity determined in this work likely is correct while the result for $k_\mathrm{t}^{1,1}$ is wrong.

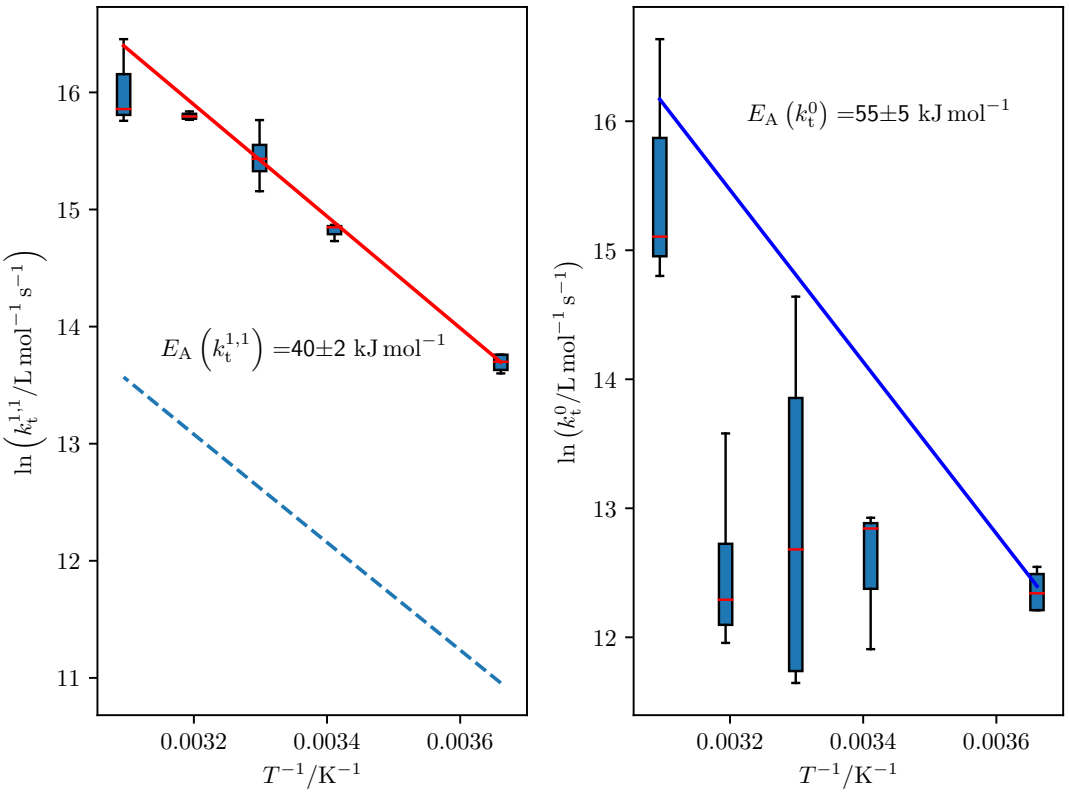

Figure 5.17.: Arrhenius fits for $k_t^{1,1}$ and k_t^0 in a bulk polymerisation of DEI. The dashed line in the left plot corresponds to the diffusion limit.

monomer	$A\left(k_t^{1,1}\right)$ /L mol^{-1} s^{-1}	$E_A\left(k_t^{1,1}\right)$ /kJ mol^{-1}	reference
Sty	$2.0 \cdot 10^{10}$	9±1	[32, 106]
NaMA (5 % in H_2O)	$2.0 \cdot 10^{8}$	8.4 ± 0.2	[32, 107]
NaMA (10 % in H_2O)	$7.2 \cdot 10^{8}$	8.7 ± 0.2	[32, 107]
PnMA	$1.56 \cdot 10^{10}$	12±2	[89, 105]
TMAEA	$(2.6 \pm 0.9) \cdot 10^{8}$	8.3 ± 0.7	[32]
DEI	-	40±2	this work
DBI	$2.4 \cdot 10^{9}$	19.8	[32, 118]

Table 5.11.: Activation energies and pre-exponential factors for the termination rate coefficient of two monomer radicals for several different monomers. The value for DEI determined in this work is likely incorrect.

5.3. Conclusion

The propagation kinetics of DEI and DPI were examined with PLP–SEC as no k_p values have been reported for these monomers. A gap in the homologous series of di-n-alkylitaconates was therefore closed. Furthermore, the propagation step of DEI has also been investigated with quantum chemistry, predicting Arrhenius parameters. The predicted Arrhenius parameters of $A = 2.0 \cdot 10^3 - 1.5 \cdot 10^4\,\mathrm{L\,mol^{-1}\,s^{-1}}$ and $E_A\,(k_p) = 22.3 - 22.7\,\mathrm{kJ\,mol^{-1}}$ are close to the experimental ones which are $A = 1.1 \cdot 10^4\,\mathrm{L\,mol^{-1}\,s^{-1}}$ and $E_A\,(k_p) = 17.5\,\mathrm{kJ\,mol^{-1}}$. An approximately linear relationship between the ester side chain length and k_p was seen. This can be attributed to prestructuring in the bulk monomer. With increasing chain length the attractive forces between the side chains of two different monomer molecules become so strong that they align and thus decrease the distance of the olefinic bonds, reducing k_p.

Next, the termination kinetics were investigated using the SP–PLP–EPR method. Less plausible results were obtained here, especially for the composite model parameters α_s and α_l. Only for one temperature the results met the expectations, for all other temperatures the results are far below physically reasonable values. The crossover-chainlength i_c scatters irregularly with temperature. The termination rate coefficient for two monomer radicals $k_t^{1,1}$ is higher than the diffusion limit which is physically impossible. However this can be attributed to the fact that a calibration for a different system had to be used for this system which distorts the pre-exponential factors but noth the activation energy. The obtained activation energy however is still double of what is expected from fluidity measurements, as the activation energy of fluidity and $k_t^{1,1}$ should be identical.

6. The propagating radical fraction in free-radical copolymerisation

Up to now copolymerisations are mainly characterized by two observables: the copolymer composition F and the overall rate coefficient $\langle k_\mathrm{p} \rangle$. These can be fitted in order to obtain information about the propagation kinetics, more specifically the reactivity ratios (RR) (also known as copolymerisation parameters). This is a practice that is well established in literature.[20,119–121] For fitting the copolymer composition two linearisation methods instead of directly fitting eq. 2.30 exist: The Fineman-Ross method and the Kelen-Tüdos method.[43–46] The latter is an improvement over the Fineman-Ross method and increases the accuracy for very low and very high f by choosing different coordinates.

In the terminal model (TM) (see section 2.5.2) this is a quite successful method. However it was noted that the RR obtained from the copolymer composition differ from those obtained from $\langle k_\mathrm{p} \rangle$. Both are described well by their respective RR but poorly by the RR obtained from the other observable.[20] The TM is thus incapable of describing a copolymerisation completely. Consequently the model was improved to include not only the last unit in the growing polymer chain, but also the second-last. This gives rise to more RR, and this more complex model is called the penultimate model (PUM). This model however has its problems, most prominently that due to the high number of adjustable parameters overfitting occurs easily. An unrealistic high number of data points would be needed to minimise this problem. This work introduces an additional observable, the propagating radical fraction (PRF). This observable describes the percentage of radicals bearing a specific monomer unit at the active chain end during the polymerisation (as opposed

to the composition of monomers in the final polymer which is described by F). It was first described by Heuts *et al.*.[122] A mathematical expression for this is easily derived. Assuming stationary conditions, the rate of appearance and disappearance of radicals with monomer A at the chain-end are equal. Only the cross-propagation steps are relevant for this, as homopropagation steps do not alter the PRF.

$$k_{\mathrm{p}}^{12} \cdot [1^{\cdot}] \cdot [2] = k_{\mathrm{p}}^{21} \cdot [2^{\cdot}] \cdot [1] \tag{6.1}$$

By rearranging and inserting eq. 2.28 the ratio of the propagating radicals can be obtained:

$$\frac{[1^{\cdot}]}{[2^{\cdot}]} = A_{12} = \frac{k_{\mathrm{p}}^{22} \cdot r_1 \cdot f_1}{k_{\mathrm{p}}^{11} \cdot r_2 \cdot f_2} \tag{6.2}$$

In the PUM this reads as:

$$\frac{[1^{\cdot}]}{[2^{\cdot}]} = A_{12} = \frac{\overline{k_{\mathrm{p}}^{22}} \cdot \overline{r_1} \cdot f_1}{\overline{k_{\mathrm{p}}^{11}} \cdot \overline{r_2} \cdot f_2} \tag{6.3}$$

It should be noted that in reference [122] a typo has occured in this formula. From eq. 6.3 the PRF ϕ_1 can be easily calculated as:

$$\phi_1 = \frac{A_{12}}{1 + A_{12}} = \frac{\frac{\overline{k_{\mathrm{p}}^{22}} \cdot \overline{r_1} \cdot f_1}{\overline{k_{\mathrm{p}}^{11}} \cdot \overline{r_2} \cdot f_2}}{1 + \frac{\overline{k_{\mathrm{p}}^{22}} \cdot \overline{r_1} \cdot f_1}{\overline{k_{\mathrm{p}}^{11}} \cdot \overline{r_2} \cdot f_2}} = \frac{\overline{k_{\mathrm{p}}^{22}} \cdot \overline{r_1} \cdot f_1}{\overline{k_{\mathrm{p}}^{22}} \cdot \overline{r_1} \cdot f_1 + \overline{k_{\mathrm{p}}^{11}} \cdot \overline{r_2} \cdot f_2} \tag{6.4}$$

To the best knowledge of the author, measurements of this observable have not been published until 2021, when Vana *et al.* measured 4 data points of the often investigated Sty/MMA-System and used these to refine an existing set of RR by a manual procedure.[19] This approach however has the disadvantage that the used manual procedure is rather laborious and also it can not be ensured that the globally best solution is found instead of a local minimum. Consequently, this approach was improved and replaced by a fully automated fitting procedure.

First, the PRF is measured for the systems styrene-d8 (Sty-d8)/DMA and Sty-d8/DEI and a simple fit is applied according to eq. 6.4 without considering the other observables, $\langle k_{\mathrm{p}} \rangle$ and the copolymer composition. Later on, the newly introduced

PRF will be used in a sophisticated fitting method which incorporates the copolymer composition F, the overall propagation rate coefficient $\langle k_\mathrm{p} \rangle$ as well as the PRF ϕ simultaneously. The RR obtained in this way describe the combination of the three observables best. This is done for the systems Sty/DMA, Sty/DEI and Sty/MMA.

6.1. Determination of the propagating radical fraction

6.1.1. General considerations

The measurement principle is straightforward. First, the EPR spectra of the homopolymerisations are measured and hyperfine coupling constants are obtained. As the EPR spectrum of a copolymerisation consists of the sum of the homopolymerisation spectra, the copolymerisation spectrum can be simply fitted by a weighted sum of the homopolymerisation spectra, where the weights equal the radical composition. This approach requires the EPR spectra of both monomers to be substantially different, otherwise the fit is extremely difficult to perform. Typically this requirement is synonymous with both monomers being from different families as the EPR spectra for monomers of the same family are nearly identical because the side-groups do not influence the spectrum significantly. For the reason of spectra separability Sty-d8 is used over non-deuterated Sty. Due to the smaller gyromagnetic ratio of deuterium compared to protium, the very complex spectrum is collapsed into a broad singlet, making the fit significantly more reliable. This was shown by Riemann.[105] The determination of the spectra weights was performed using the *easyspin*-package in MATLAB. As a general plausibility check, if the k_p of the homopolymerisations are known one can predict whether the curve of ϕ vs f will be above or below a straight line with slope 1 through the origin. The slower propagating radical will be present for longer, hence have a higher PRF.

Table 6.1.: Determined hyperfine coupling constants for Sty-d8 at 293 K.

# and pos. of atoms	a/G
$1D_{\alpha}$	2.1
$2D_{\beta}$	0.2

Table 6.2.: Determined hyperfine coupling constants for DMA at 293 K.

# and pos. of atoms	a/G conformer 1	a/G conformer 2
$1H_{\beta 1}$	15.8	23.5
$1H_{\beta 2}$	6.3	0.2
$3H_{\text{methyl}}$	22.3	22.3

6.1.2. Styrene-d8/Dodecylmethacrylate

First, the system Sty-d8/DMA was investigated because both monomers give strong signals and the spectra differ substantially from each other, allowing easy fitting. The hyperfine coupling constants obtained from the homopolymerisation spectra are shown in table 6.1 and table 6.2. As is typical for methacrylate radicals, DMA has two different conformers which need to be considered as individual species in the determination of the radical fractions.[19]

Using these hyperfine coupling constants, the fitting procedure can be illustrated using experimental spectra. Figure 6.1 shows the simulated spectra of Sty-d8 and DMA alongside two experimental spectra and the respective corresponding simulated spectra. It can clearly be seen that the copolymerisation spectrum is indeed the sum of homopolymerisation spectra so that this fitting procedure is justified.

This methodology was applied to obtain the PRF for a broad range of the feed fraction. The obtained results were fitted to eq. 6.4 or the simplified versions of it, using the TM, the implicit PUM and the explicit PUM in order to test whether

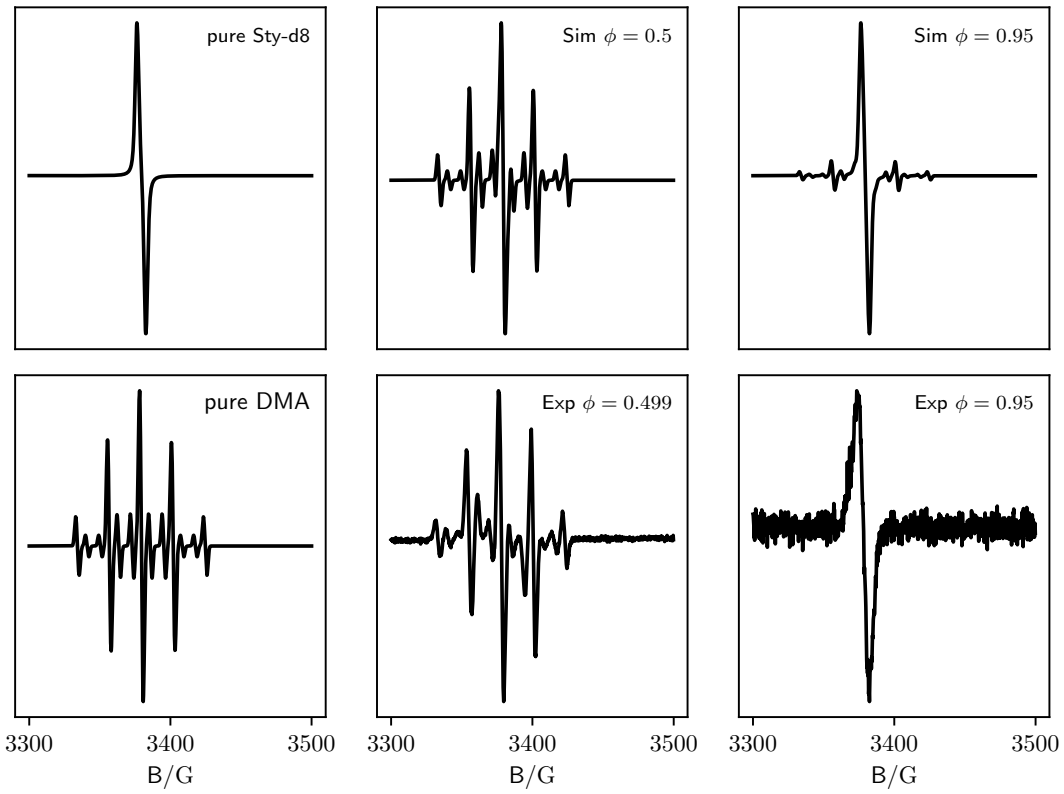

Figure 6.1.: Simulated EPR spectra of Sty-d8 and DMA as well as two experimental spectra with different feed fraction and their respective fits.

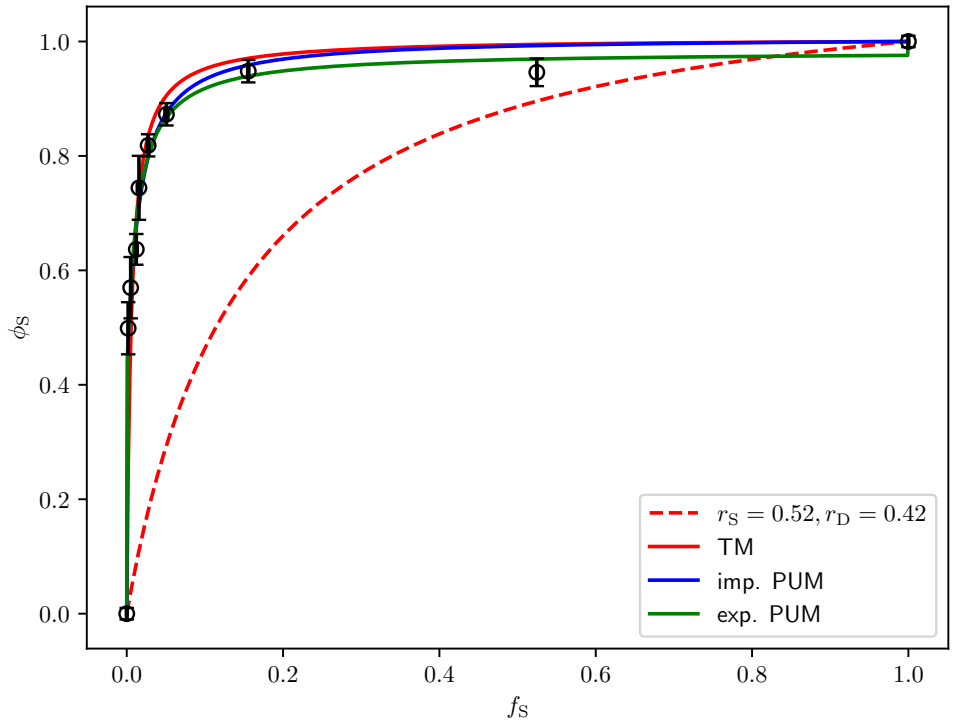

Figure 6.2.: The PRF of Sty-d8 as a function of the feed fraction of Sty-d8 in the copolymerisation with DMA at 293 K. Fits with the TM, implicit PUM and explicit PUM are provided as well as a prediction with the TM using literature values.[121]

sensible results can be obtained from the PRF alone. The homopolymerisation propagation rate coefficients which are needed for the fit are 432.7 L mol^{-1} s^{-1} for DMA and 68.8 L mol^{-1} s^{-1} for Sty.[123,124] All three models yield a reasonable fit curve.

The obtained RR are shown in table 6.3. Typically RR are in the order of 0.1-10. The value for r_S is clearly out of that range. However the fit to the data is quite satisfactory. In fig. 6.2 also the TM prediction with literature values obtained from the copolymer composition is shown. This curve differs significantly from the fitted one, showing again that the TM is capable of describing one observable but incapable of describing multiple observables simultaneously. The PUM was

Table 6.3.: Results of the Sty-d8/DMA PRF fit for the TM, the implicit PUM and the explicit PUM.

	TM	implicit PUM	explicit PUM
r_S	94.31	43.06	45.47
r_M	3.31	0.01	2.18
r'_S	-	-	289 948.0
r'_M	-	-	75 692.1
s_S	-	1.69	4.38
s_M	-	0.000 48	0.14

developed to adress this problem. However, it brings with it different problems, namely overfitting due to too many adjustable parameters. The results from the implicit PUM show a very high value for r_S, too and a very low value for s_M. The explicit PUM also yields a high value for r_S but realistic values for r_M, s_S and s_M. The results for r'_S and r'_M however are several orders of magnitude too large to be believable. The influence of r' on the PRF thus seems to be very small so that extreme values are necessary to have a noteworthy impact. This goes hand in hand with overfitting.

6.1.3. Styrene-d8/Diethylitaconate

As the next step, one of the monomers was exchanged for a monomer from a different family. The EPR spectrum of itaconates is a fairly simple quintett. This allows for easy spectra separation. The already investigated DEI was chosen due to its commercial availability. The hyperfine coupling constants for DEI were already determined earlier (see table 5.8). Also, the k_p of DEI ($8.4\,\mathrm{L\,mol^{-1}\,s^{-1}}$ at 20 °C) is lower than for Sty ($68.8\,\mathrm{L\,mol^{-1}\,s^{-1}}$), thus the data trace of ϕ_S vs f_S should be below the straight line through the origin with a slope of 1.

Contrary to the expectation, the observed data trace is in fact above the aforemen-

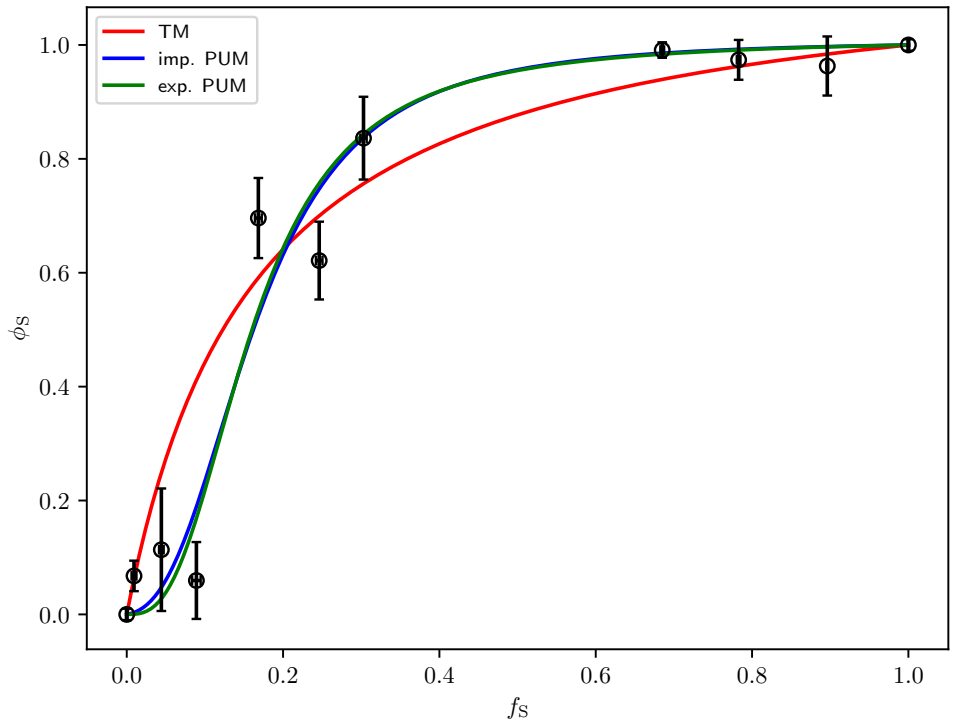

Figure 6.3.: The PRF of Sty-d8 as a function of the feed fraction of Sty-d8 in the copolymerisation with DEI at 293 K. Fits with the TM, implicit PUM and explicit PUM are provided.

Table 6.4.: Results of the Sty-d8/DEI PRF fit for the TM, the implicit PUM and the explicit PUM.

	TM	implicit PUM	explicit PUM
r_S	24.63	1.53	26.78
r_M	0.42	0.04	48.58
r'_S	-	-	3.09
r'_M	-	-	0.000 57
s_S	-	21.63	63.70
s_M	-	9.28	0.0064

tioned straight line. However it is significantly lower than the trace in the case of Sty-d8/DMA. As k_p of Sty-d8 and DEI are in a similar order of magnitude, it might be that the prediction is starting to fail, as it only considers the homopolymerisation k_p^{iii} and now the other reaction steps such as crosspropagation start to take significant effect. The same fitting is performed as for Sty-d8/DMA and the results are shown in table 6.4. The results are also unrealistic. This might be due to the higher uncertainty in the data compared to Sty-d8/DMA.

6.2. New fitting procedure: DRACO

In 1993 Schweer published a paper describing a fit procedure in which both the copolymer composition and $\langle k_p \rangle$ were fitted in a simultaneous fashion, i.e. finding a set of RR (according to the PUM) which describe both observables at the same time.[18] The general idea is that different sets of RR can yield curves that are very similar for one observable, the curves for a different observable will differ more strongly. This can be used to discriminate between the sets of RR. For example the lines for copolymer composition in fig. 6.4 are very similar and both can be considered a decent fit. However using the same RR for $\langle k_p \rangle$, the curves differ more strongly and the blue line now is a better description of the data, thus the

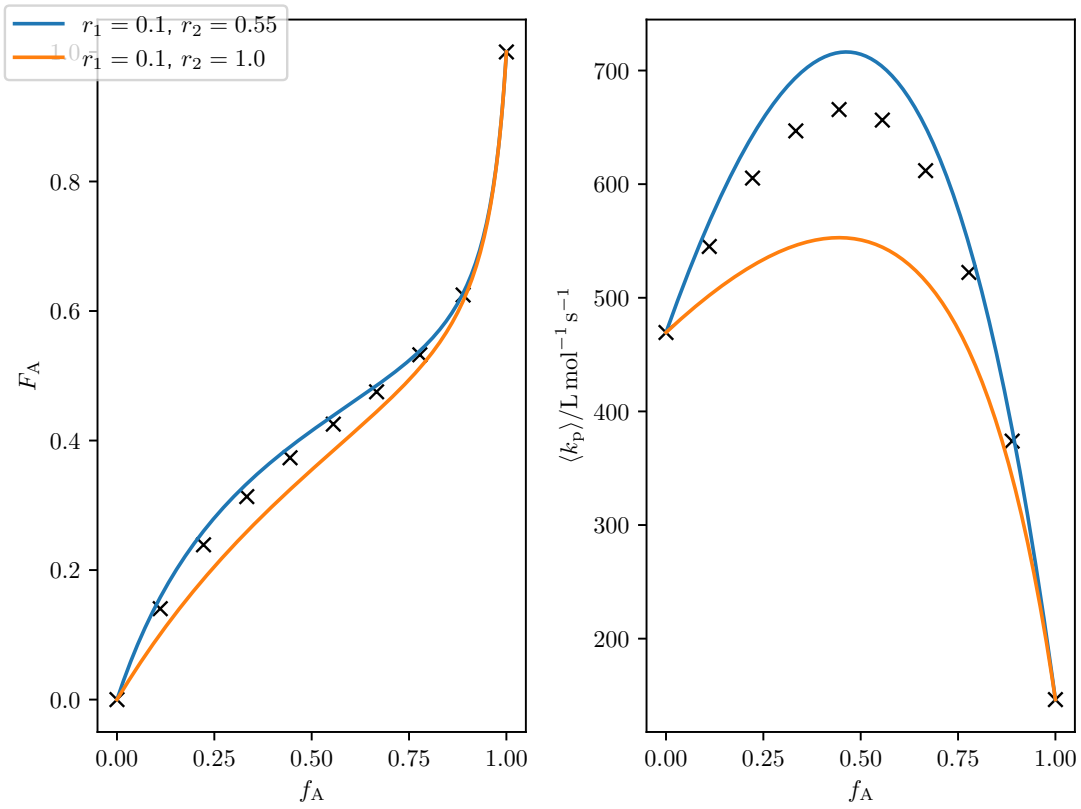

Figure 6.4.: Copolymer composition and $\langle k_p \rangle$ for two different sets of RR and fictional data. While for the copoylmer composition both sets of RR fitr the data decently, for $\langle k_p \rangle$ the blue line is a significantly better fit, thus making the first set of RR the better overall description of the system.

combined deviation of data and model is better for the blue line. This work now aims to define a new fit procedure, similar to that of Schweer but including also the PRF which should give a substantial improvement. As mentioned, overfitting is a serious problem when using the PUM. When the experimental data show only small deviations from the true value (for example due to systematic errors), a completely different set of RR will be obtained. By imposing the condition that the obtained RR also have to describe the other observables well, one has means of mitigating the influence of experimental noise. This approach was used in a new fitting procedure which is called 'determining reactivity ratios with a conjoined scalable fit' or in short DRACO. The name already states that it is scalable, more

observables can be included in the fit procedure with little effort.

The fitting procedure was implemented in *python3* using the *lmfit*-package which provides a flexible interface, allowing for easy imposing of constraints on the fit parameters and switching the fitting algorithm. The equations implemented are the explicit PUM equations for F, $\langle k_\mathrm{p} \rangle$ and ϕ (eqs. 2.38, 2.39 and 6.4). By imposing the constraints $r_1' = r_1 = \overline{r_1}$ and $r_2' = r_2 = \overline{r_2}$ the explicit PUM is simplified to the implicit PUM. If one further constraints $s_1 = s_2 = 1$, the model is simplified to the TM.

As routine fitting packages offer only the possibility to fit a single data set, for this case the objective function which shall be minimised has to be manually defined. Normally this is simply the deviation of the data from the model which can be scaled by the uncertainty of the data, if known. Using the observables F, $\langle k_\mathrm{p} \rangle$ and ϕ, this simple approach would give an extremely high weight to $\langle k_\mathrm{p} \rangle$ because the values of $\langle k_\mathrm{p} \rangle$ (in $\mathrm{L\,mol^{-1}\,s^{-1}}$) are several orders of magnitude larger, depending on the respective comonomers. F and ϕ are both mole fractions and therefore run from 0-1. A method for accounting for this is needed. Two prominent methods exist: standardisation and normalisation.

$$d_\mathrm{std,i} = \frac{d_\mathrm{i} - \overline{d}}{\sigma(d)} \tag{6.5}$$

Standardisation (see eq. 6.5) scales the data with the respective mean and standard deviation of the data set. Whether the data trace is for example very steep has an influence on the data limits which will be obtained after standardisation. Different comonomer systems can have very different curve shapes. Standardisation is therefore not suitable for a general scaling method.

$$d_\mathrm{norm,i} = \frac{d_\mathrm{i} - d_\mathrm{min}}{d_\mathrm{max} - d_\mathrm{min}} \tag{6.6}$$

Normalisation (see eq. 6.6) scales the data in a fashion that the data run from 0-1. F and ϕ already do that, being molar fractions. Consequently normalisation does

not have an influence on them, provided that the experimental data do contain data points for f_1=0 and f_1=1. By definition, when f_1=0 also $F_1 = \phi_1 = 0$ and vice versa, when f_1=1, $F_1 = \phi_1 = 1$. These data points are therefore always given. Normalisation consequently only has an influence on $\langle k_\mathrm{p} \rangle$ and will scale it always from 0-1. For these reasons, normalisation was chosen as data scaling method. The uncertainty of the normalised experimental data was calculated using Gaussian propagation of errors on eq. 6.6. Using normalisation it is possible to simply use the deviation of the normalised data to the normalised model as objective function and ensure equal weighting.

The objective function which was minimised in the fit procedure is shown in eq. 6.7.

$$\#_{\mathrm{o}=1}^{3} \#_{\mathrm{i}} \frac{\left(\frac{d_{\mathrm{n,o,i}} - m_{\mathrm{n,o,i}}}{u_{\mathrm{n,o,i}}}\right)^2}{N_\mathrm{o}} \tag{6.7}$$

The index n refers to normalised data, o refers to the respective observables (F, $\langle k_\mathrm{p} \rangle$ and ϕ) and i is the counting index for the data points. d refers to the experimental data, m to the model function, u is the uncertainty of the experimental data and N is the number of data points for the respective observable. The $\#$ operator means concatenation. In words, the deviation of normalised data and normalised model at each data point is divided by the normalised data uncertainty. This is squared to avoid cancelling of positive and negative contributions. Also it is divided by the number of data points for the respective observable. The data sets for each observable likely have different amounts of data points. Scaling by the number of points ensures that equal weight is given to the observables as a whole instead of equal weight for each data point. This is of course debatable and can be changed in certain cases. The described quantity is calculated for each i, i.e. each data point of one observable and those are stacked together in an array. This corresponds to the inner concatenation. The outer concatenation runs over the three observables o, so that the described quantity is calculated for each of the observables.

The actual fitting algorithm which was used is the Nelder-Mead algorithm modified for high dimensionalities as described by Gao and Han.[125,126] Initial guesses were 1 for all parameters as this is the value for an ideal copolymerisation and has no

assumptions about the investigated system. Depending on the use case this can be modified, for example setting the initial guesses for r_1 and r_2 to the values obtained from the TM would be a sensible approach. The full code is given in appendix A.2.

6.2.1. Testing of DRACO

Before the algorithm was used on any real data, its performance was tested on artificial data. First, some notation needs to be explained. Sample size refers to the number of data points from the artificial data sets which were handed to DRACO. Noise refers to random values that are added to the data points, distorting the data curves, thus reducing the accuracy of the data. Uncertainty on the other refers to the statistical property of precision, which can be interpreted in terms of the standard deviation from multiple measurements. A series of tests was carried out which examine the influence of the sample size, the noise as well as the uncertainties. Also it was tested whether including the PRF brings a benefit in the first place. These tests will be presented in the following sections.

The artificial data sets for the tests were created by choosing a set of reactivity ratios, inserting them into eqs. 2.38, 2.39 and 6.4 and saving each of the obtained curves. The curves were saved with 10 000 data points, i.e. at intervals of $\Delta f_1 = 0.0001$. The reactivity ratios used are those obtained by Schweer for the Sty/MMA system, listed in table 6.5, but any other arbitrary set could have been used.[18] Depending on the test, noise was also added to the data set in order to perturb the curve shapes. This noise was taken from a Gaussian distribution with mean 0 and variance 1. It was scaled by a varying factor. For $\langle k_\mathrm{p} \rangle$ the noise was additionally multiplied by the higher of the homopolymerisation propagation rate constants before the normalisation. The results of the tests will be presented with graphs showing the absolute values of the deviation of the fit results from the true values in table 6.5 for each of the six reactivity ratios on logarithmic axes. The smaller the deviations, the better. A deviation of roughly $1 \cdot 10^{-1}$ is deemed satisfactorily accurate.

r_A	0.498
r_B	0.463
r'_A	0.547
r'_B	0.589
s_A	0.478
s_B	0.256

Table 6.5.: Reactivity ratios for the test data set. These values are the best values from a simultaneous fit of F and $\langle k_\mathrm{p} \rangle$ in the Styrene/MMA system.[18] The index A refers to Styrene and B to MMA.

As in the development process of DRACO the uncertainties were not considered in an earlier stage, the first three tests do not include uncertainties in the data. In terms of the objective function this simply means omitting u from eq. 6.7.

Test 1: Influence of sample size

For this test, the full data set of 10 000 data points and equally spaced subsets of 1000, 100, 10 and 5 were used for a fit.

As visible, the targeted accuracy is already surpassed by three orders of magnitude with only five data points per observable. However these data points contain no noise whatsoever, which is of course unrealistic for any real experiment. Consequently, the next test will test the influence of noise which is added on to the experimental data, to see if this performance still holds up.

Test 2: Influence of noise on data

Now the aforementioned noise will be added to the experimental data. Several data sets were created, each with a different amount of noise. The sample size had to be fixed of course. Sizes of 10, 50 and 10 000 points per observable were chosen, based on the results from test 1. For sake of brevity, only the graph for sample

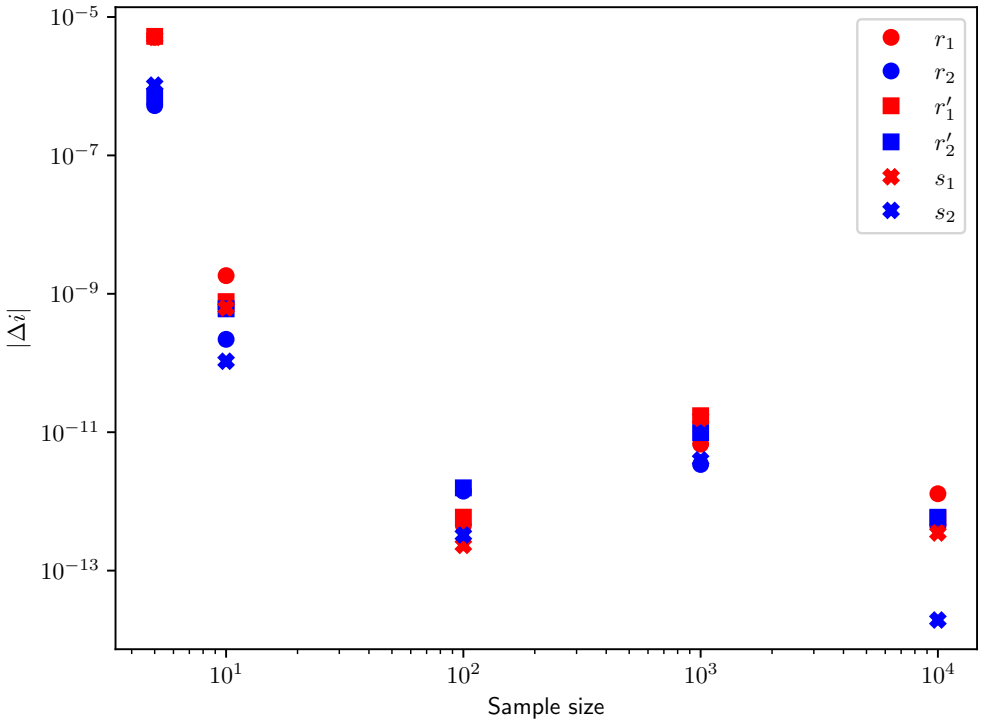

Figure 6.5.: Test 1: Absolute values of the deviation of the obtained RR from the true values in table 6.5 as a function of the sample size. The underlying data are perfectly accurate. The deviation of the results is below 10^{-5} using only 5 data points per observable which is more than satisfactory.

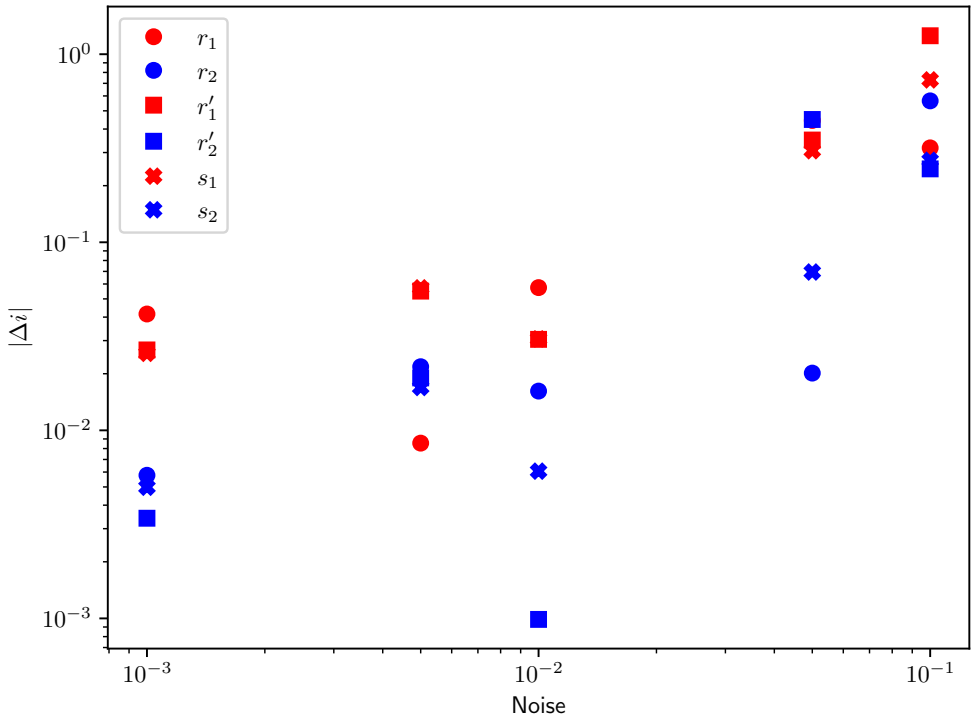

Figure 6.6.: Test 2: Absolute values of the deviation of the obtained RR from the true values in table 6.5 as a function of noise added to the data.

size 10 is shown for this and the subsequent tests. Plots for other sample sizes can be found in the appendix.

It can be seen that on double-log axes an approximately linear relationship between accuracy and noise can be identified. The noise (which approximately corresponds to the inaccuracy of the data) needs to be lower than 1 % in order to obtain reactivity ratios that are within 0.1 of their true values. A deviation of only 1 % is a rather challenging task for experimentators, as likely already the composition drift even at low conversion prevents from reaching this high accuracy not to mention the uncertainties arising from the NMR analysis for the composition, SEC for $\langle k_\mathrm{p} \rangle$ and EPR for the PRF. This already shows that as soon the data are no longer perfectly accurate, the performance significantly drops. High accuracy of the data is crucial for a correct result.

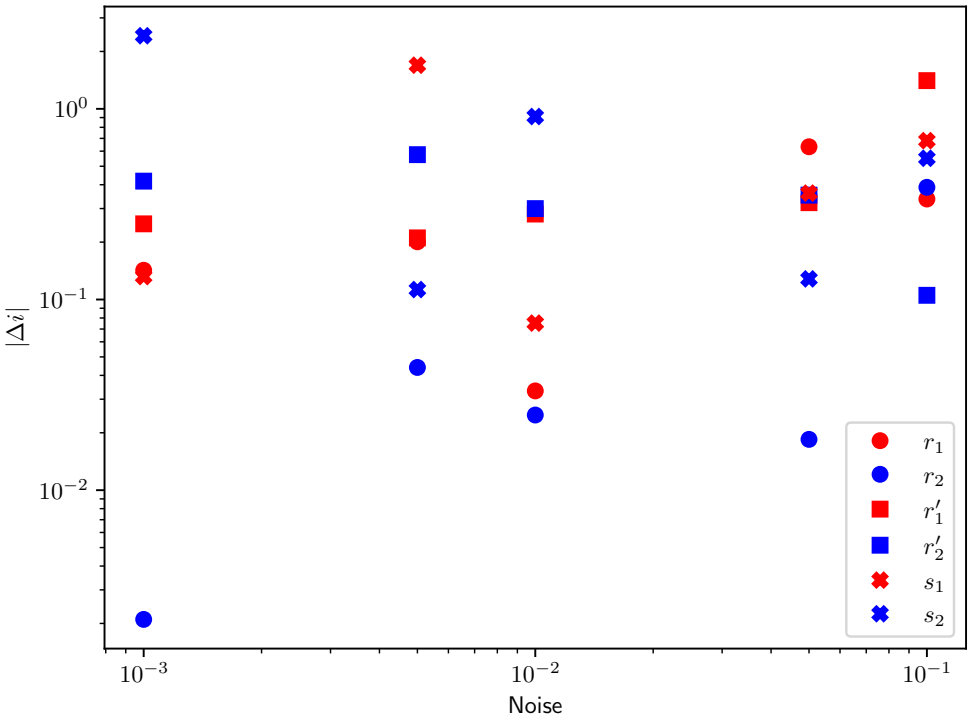

Figure 6.7.: Test 3: Absolute values of the deviation of the obtained RR from the true values in table 6.5 as a function of noise added to the data when not including the PRF in the fit.

Test 3: Benefit of including the PRF

To test whether using more observables in the fit brings a benefit in the first place, the exact same data sets as for test 2 are used, only that the PRF is not included in the fit. This way tests 2 and 3 can be directly compared and the difference is only due to including more observables.

Comparing fig. 6.7 to fig. 6.6 from test 2, it can be seen that the accuracy drops about 1-2 orders of magnitude, clearly showing a great benefit of including the PRF in the fit. It is likely that including even more observables increases the accuracy even further.

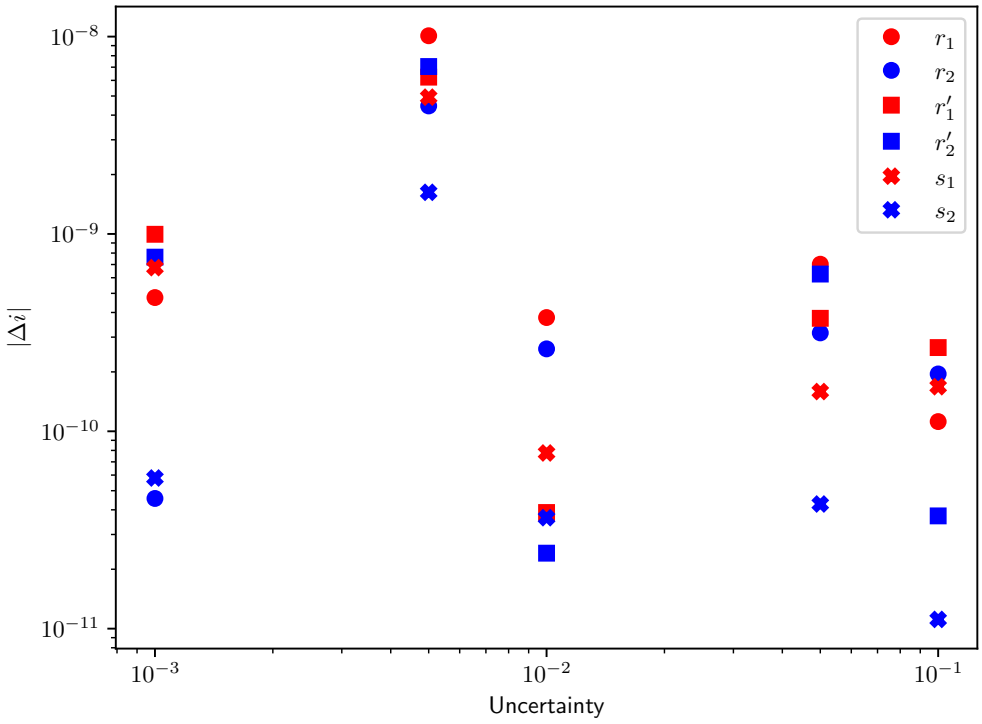

Figure 6.8.: Test 4: Absolute values of the deviation of the obtained RR from the true values in table 6.5 as a function of the uncertainty given to perfectly accurate data.

Test 4: Influence of uncertainty on accurate data

In this test uncertainty in the experimental data is now present. The data set itself is perfectly accurate, i.e. no noise is present. However each data point has an associated uncertainty, which is modelled by the same procedure as for modelling the noise. Again, sample sizes of 10, 50 and 10 000 points were used.

The deviation of the results from the true values are in the order of 10^8-10^{10}, similar to test 1. This indicates that perfectly accurate data will always give the correct result, whether an uncertainty is given or not. Just as test 2, it shows that high accuracy of the data is the most crucial point.

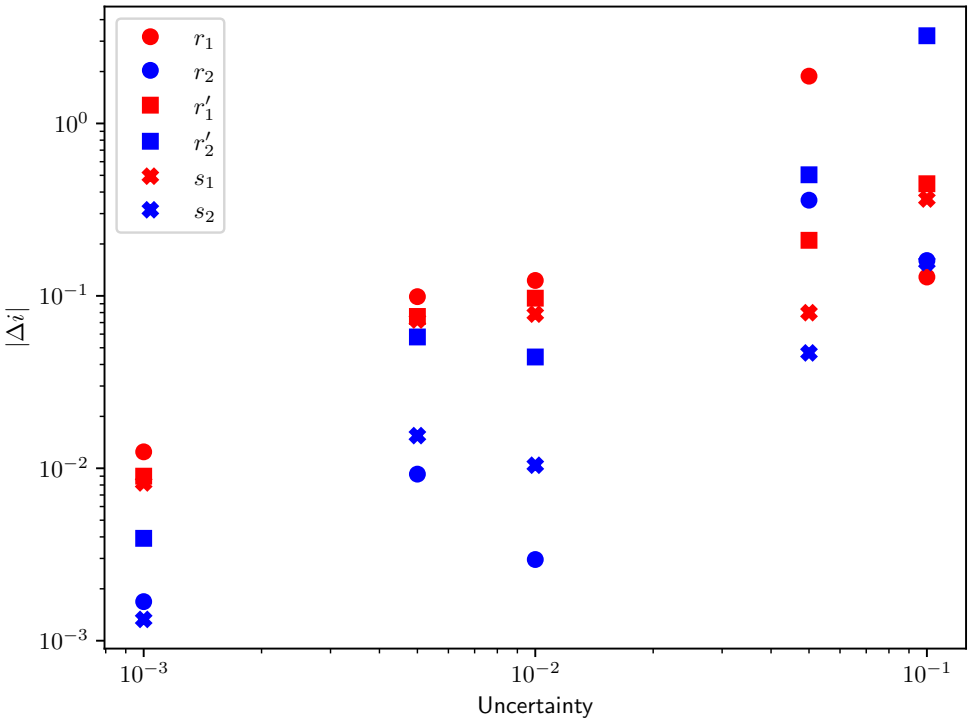

Figure 6.9.: Test 5: Absolute values of the deviation of the obtained RR from the true values in table 6.5 as a function of the uncertainty and noise added to the data.

Test 5: Influence of uncertainty on inaccurate data

This test is very similar to test 4, but now the data itself has some added noise as well as an uncertainty both of which scale with the noise on the abscissa in fig. 6.9.

Comparing test 5 to test 4 one notices immediately that the accuracy of the results drops about 8 orders of magnitude. As the only difference between the two tests is that the data points are no longer accurate, this is the cause for this loss of accuracy. The accuracy of test 5 is roughly equal to that of test 2, indicating that including the uncertainty brings only little benefit.

Summing up, the biggest influence on the accuracy of the RR is the accuracy of the experimental data. In order to obtain RR that are within 0.1 of their true values, the experimental data has to have an accuracy of 99 %, or in other words the data can only deviate from their true values by 1 %. It was also shown that including more observables improves the results by 1-2 orders of magnitude. However only little benefit is gained from using more data points. Only when going to extremely high sample sizes which are not feasible to measure manually, a minor improvement can be seen. This can be seen by comparing the graphs presented here to their counterparts for larger sample sizes, which are given in appendix A.3. The uncertainty of the data points brings only little benefit regarding the accuracy of the results, which can be seen by tests 2 and 5 having similar results. However a huge improvement concerning the confidence ellipsoids can be seen when including the uncertainties. Using Markov-chain Monte Carlo as implemented in the *emcee*-package for *python3* the 95 % confidence ellipsoids were calculated.[127,128] The data set used for this is from test 5 with a noise of 0.001. The confidence ellipsoids were calculated once using the uncertainties and once without the uncertainties.

When not using the uncertainties, *emcee* will automatically estimate them, which is reflected in the 'lnsigma' parameter which can be seen in fig. 6.10.Figure 6.11 shows a clear improvement over fig. 6.10. Using uncertainties is consequently recommended to better explore the parameter space and assess the plausability of the results.

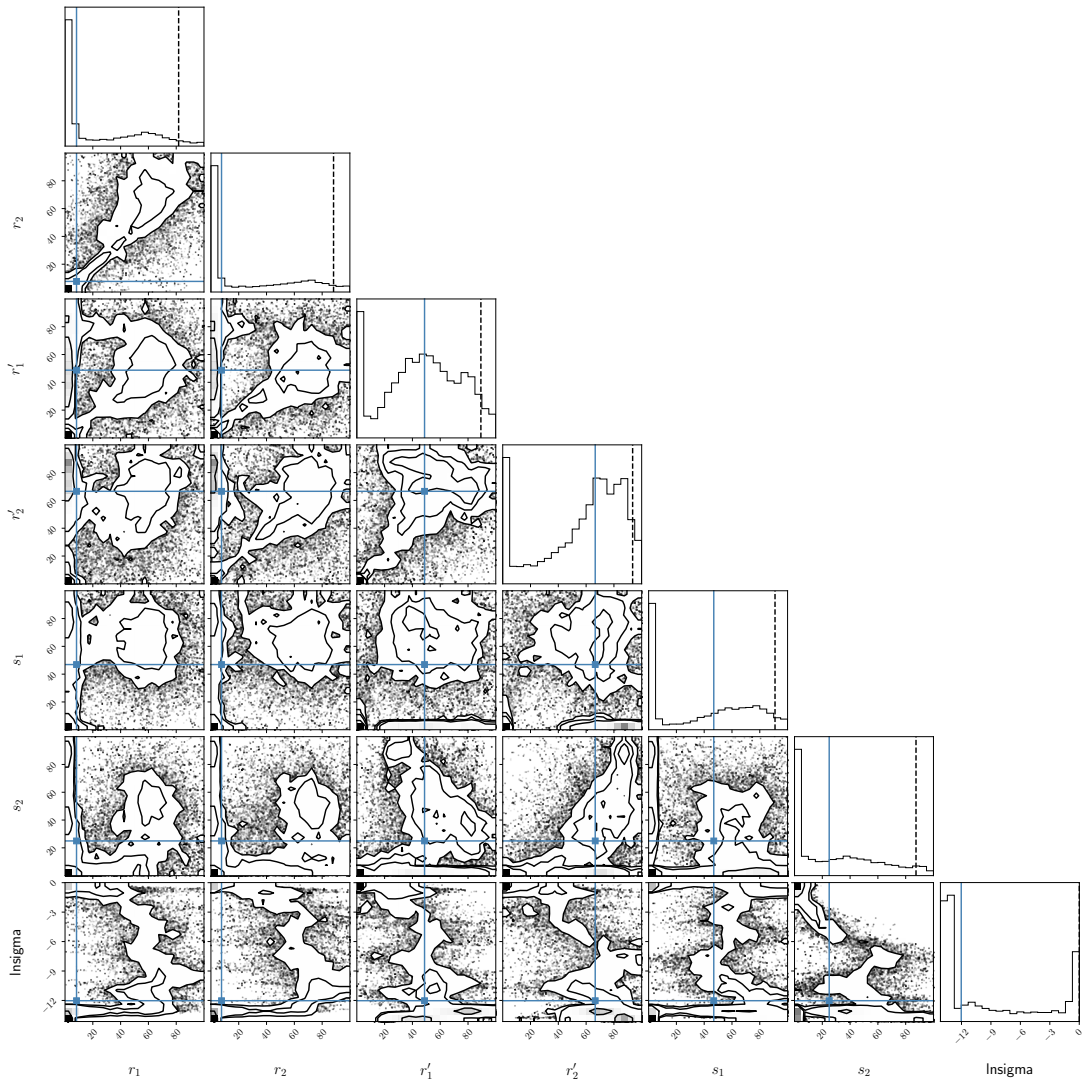

Figure 6.10.: 95 % confidence ellipsoids for the data of test 5 with a noise of 0.001 when the uncertainties are not included in the fit.

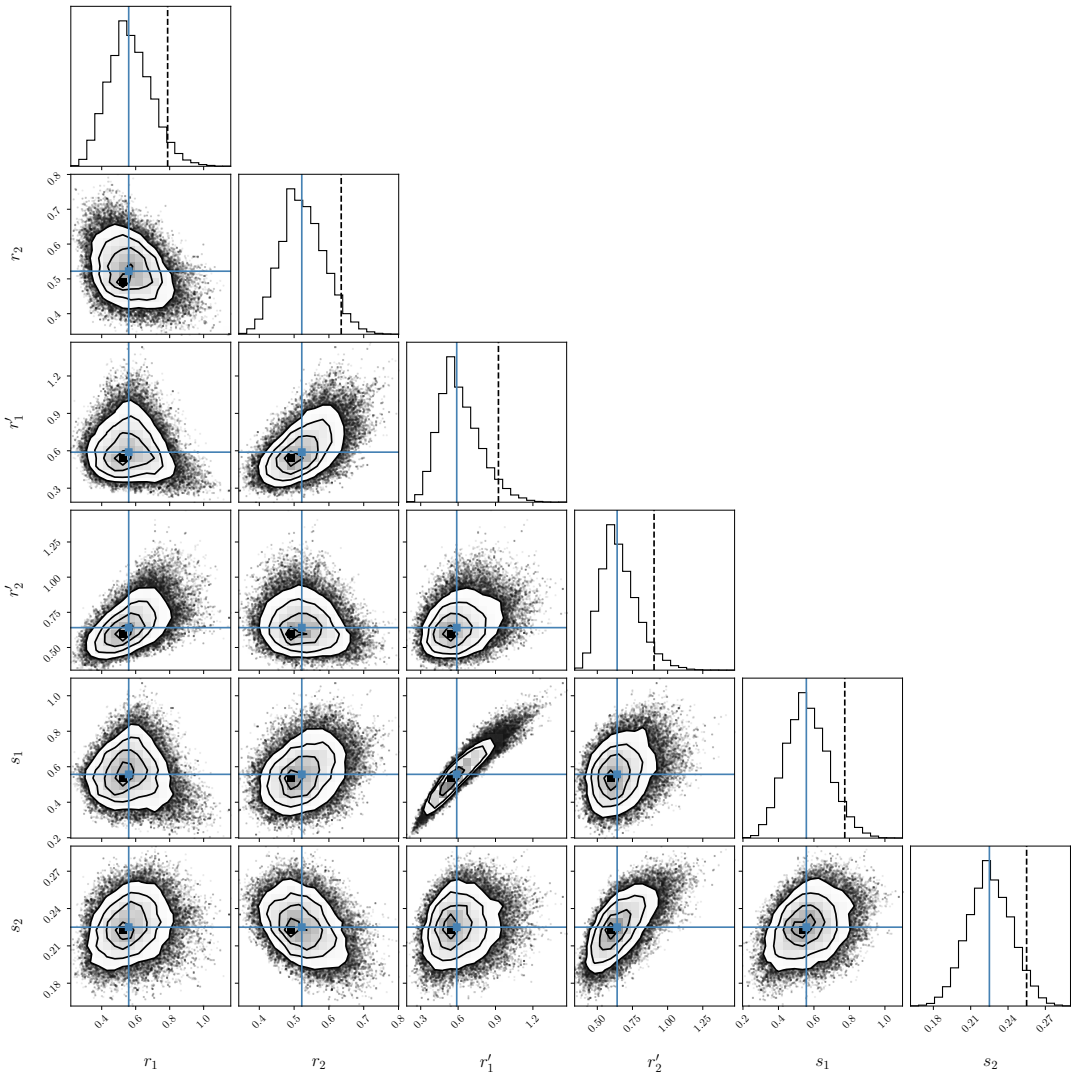

Figure 6.11.: 95 % confidence ellipsoids for the data of test 5 with a noise of 0.001 when the uncertainties are included in the fit.

6.3. The Sty/DMA system

In order to apply DRACO to the Sty/DMA system, first data for the copolymer composition and $\langle k_p \rangle$ needed to be gathered. Literature values were used. Values for $\langle k_p \rangle$ were taken from Davis *et al.* (in toluene, at 298 K).[120] The values for the hompopolymerisations were taken from before (section 6.1.2) and were allowed to vary by 10 %. Values for the copolymer composition were taken from Vidović *et al.* (in toluene at 60 °C) and from Davis *et al.*.[120,121] Different temperatures have very little influence on the copolymer composition and reactivity ratios, thus the data sets were joined as having more data points is considered more beneficial than the introduced error in this case. Both literature sources do not state uncertainties for their data, consequently a relative uncertainty of 5 % was assumed. The upper and lower bounds for the reactivity ratios were changed to 100 and 0.01 because the upper limit was reached during the fit procedure.

DRACO was run using the explicit PUM, implicit PUM and TM, the results are shown in table 6.6. In the explicit PUM, s_B and r'_B are higher than expected, they are at the defined limit of 100. It can therefore be concluded that both parameters have no influence on the fit. In the implicit PUM s_B is at the constrained limit again. Inspecting the confidence ellipsoids in fig. 6.13 (for the explicit PUM), this can also be seen there, as the ellipsoids for s_B and r'_B are significantly broader and diffuser than the other ones, indicating that both RR have little influence on the fit and thus their value is poorly estimated. However it was decided to not change the limits for the parameters again, as a value of 100 is already unrealistic.

As can be seen readily from fig. 6.15 the TM fails again in describing multiple observables simultaneously. For comparison, literature values which are based on the TM are given in table 6.7.

One would expect the values of r_A and r_B in a fit using the PUM to deviate from those obtained using the TM, as the PUM has more parameters. This is the case here. However also the results using the TM (see table 6.6) differ from the literature values. To verify that this is only due to the additional data, DRACO was run using only the copolymer composition data from Vidović *et al.* and the TM. The

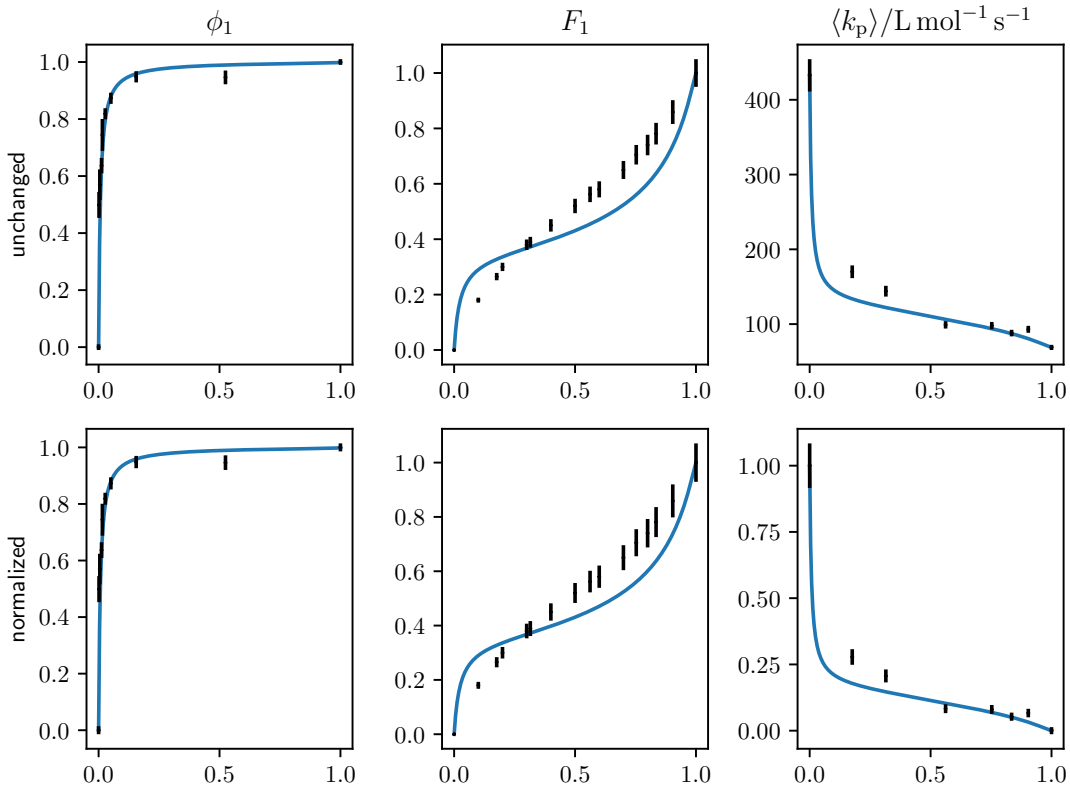

Figure 6.12.: Unchanged and normalized PRF, copolymer composition and $\langle k_p \rangle$ for the Sty/DMA system and their DRACO fit using the explicit PUM.

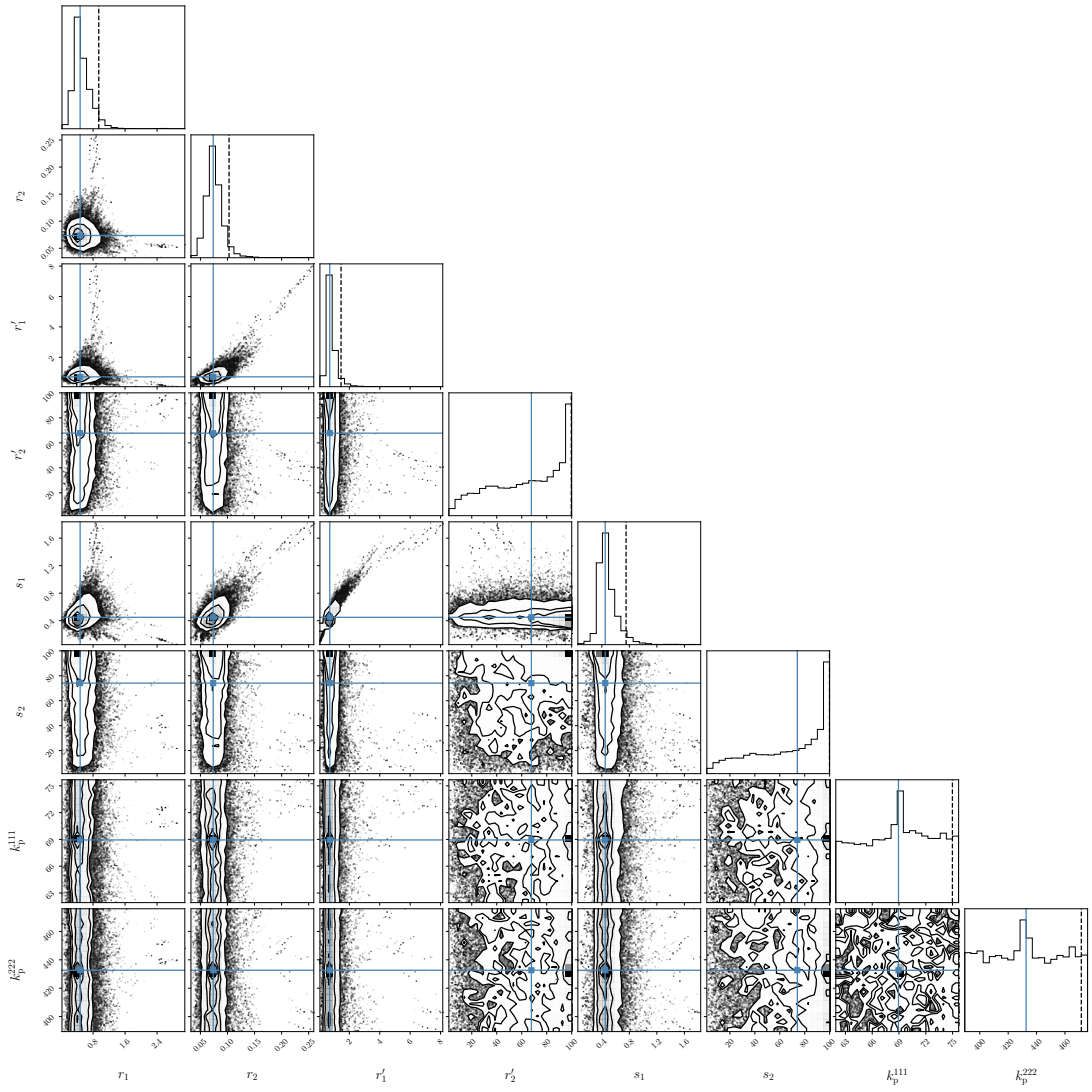

Figure 6.13.: 95 % confidence ellipsoids for the Sty/DMA system using the explicit PUM.

	explicit PUM	implicit PUM	TM
r_A	0.44	0.27	1.52
r_B	0.07	0.16	0.14
r'_A	0.63	$=r_A$	$=r_A$
r'_B	100.0	$=r_B$	$=r_B$
s_A	0.41	0.14	=1
s_B	100.0	100.0	=1
k_p^{AAA}	68.89	68.82	68.80
k_p^{BBB}	432.66	432.82	432.69

Table 6.6.: Obtained reactivity ratios for the Sty/DMA system using DRACO according to the explicit PUM, implicit PUM and TM. The index A refers to Sty and B to DMA. Uncertainties could not be estimated by DRACO.

r_A	0.57	Otsu[129]
r_B	0.45	
r_A	0.52	Vidović[121]
r_B	0.42	

Table 6.7.: Reactivity ratios for the Sty/DMA system found in the literature. Both sets rely on the terminal model.

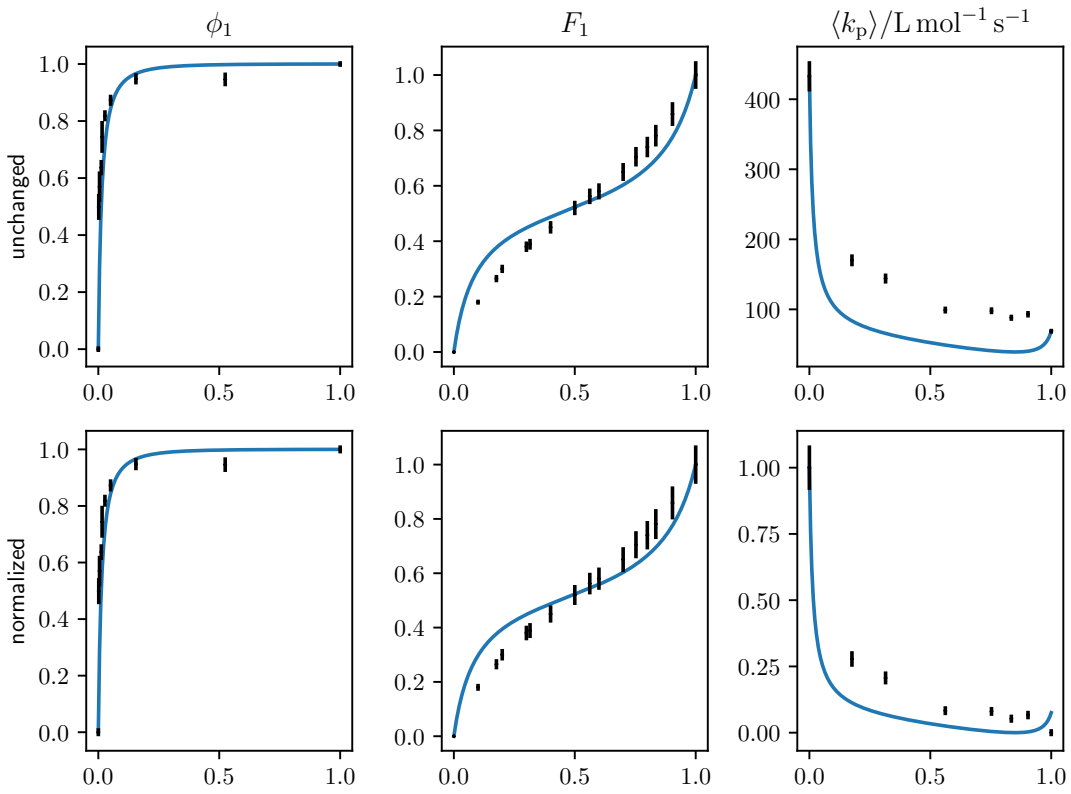

Figure 6.14.: Unchanged and normalized PRF, copolymer composition and $\langle k_p \rangle$ for the Sty/DMA system and their DRACO fit using the implicit PUM.

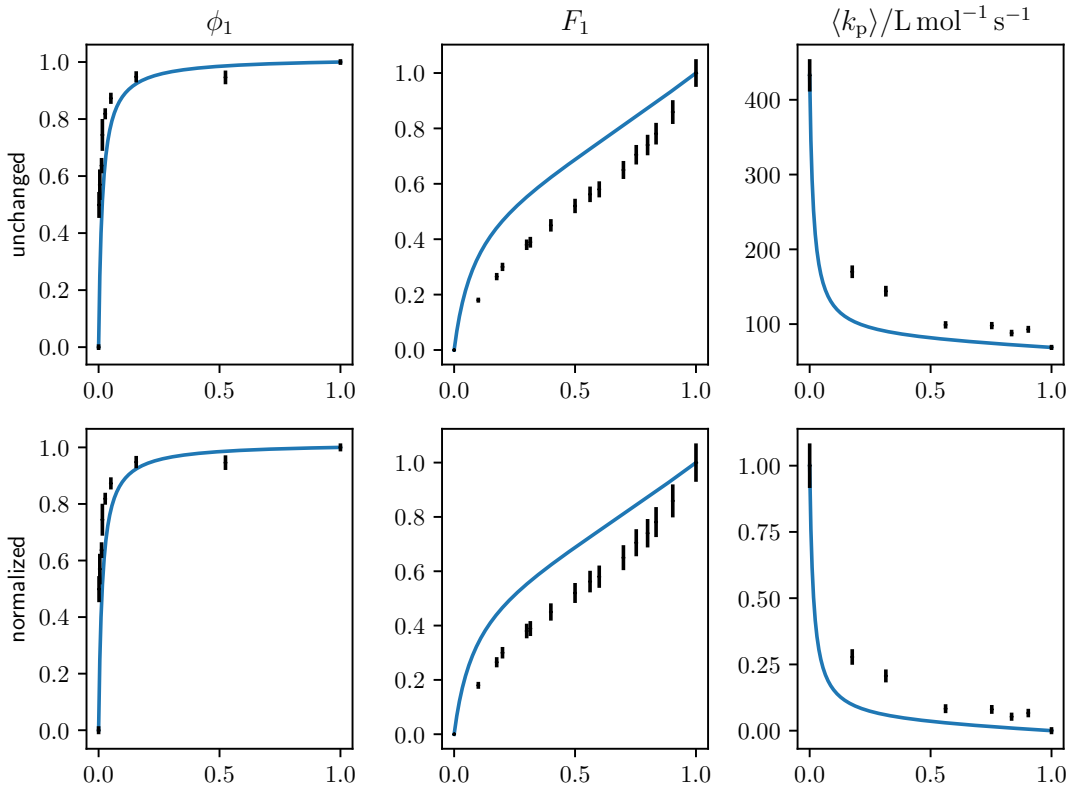

Figure 6.15.: Unchanged and normalized PRF, copolymer composition and $\langle k_p \rangle$ for the Sty/DMA system and their DRACO fit using the TM.

results were perfectly reproduced. Consequently the difference of the results has to stem from the additional data. It is debatable whether the values obtained in this work are an improvement over the literature-known values, since no objectively best values exist. In fact it is still a point of discussion what is considered 'best' values. Some authors argue that for every observable a separate set of RR should be given in order to ensure that each observable is described as precise as possible. Other authors argue that if the model is supposed to describe both observables, one set of RR has to describe them even though the precision for each individual observable is lower than in the first approach. In this work, the latter reasoning is considered more adequate. Consequently the values obtained in this work are considered the current best values. When comparing them to literature values one has to take care to use the same model basis and assumptions/approximations as the PUM and the TM produce significantly different RR for the same data.

6.4. The Sty/DEI system

The same type of analysis was done for the combination of Sty with the previously investigated DEI. However, for $\langle k_\mathrm{p} \rangle$ only data for Sty/DMI (20 °C, bulk) was found in the literature which was used instead.[130] This is of course introducing an error which was considered tolerable. Data for the copolymer composition were taken from Sato *et al.* (50 °C, in benzene).[131] The different temperature and solvent is considered to have a very minor influence on the RR.

As can be seen from the results in table 6.8, no sensible results were obtained. Using the explicit PUM, r'_B is at the lower limit and s_B is very high. For the implicit PUM, s_B even is at the upper limit and r_A is very high. In the TM fit, r_A is at the upper limit. These results are unplausible. A likely explanation is that using the $\langle k_\mathrm{p} \rangle$ for Sty/DMI instead of Sty/DEI introduces a deviation significantly larger than assumed. Measuring $\langle k_\mathrm{p} \rangle$ for the Sty/DEI system and using these values should bring a significant improvement.

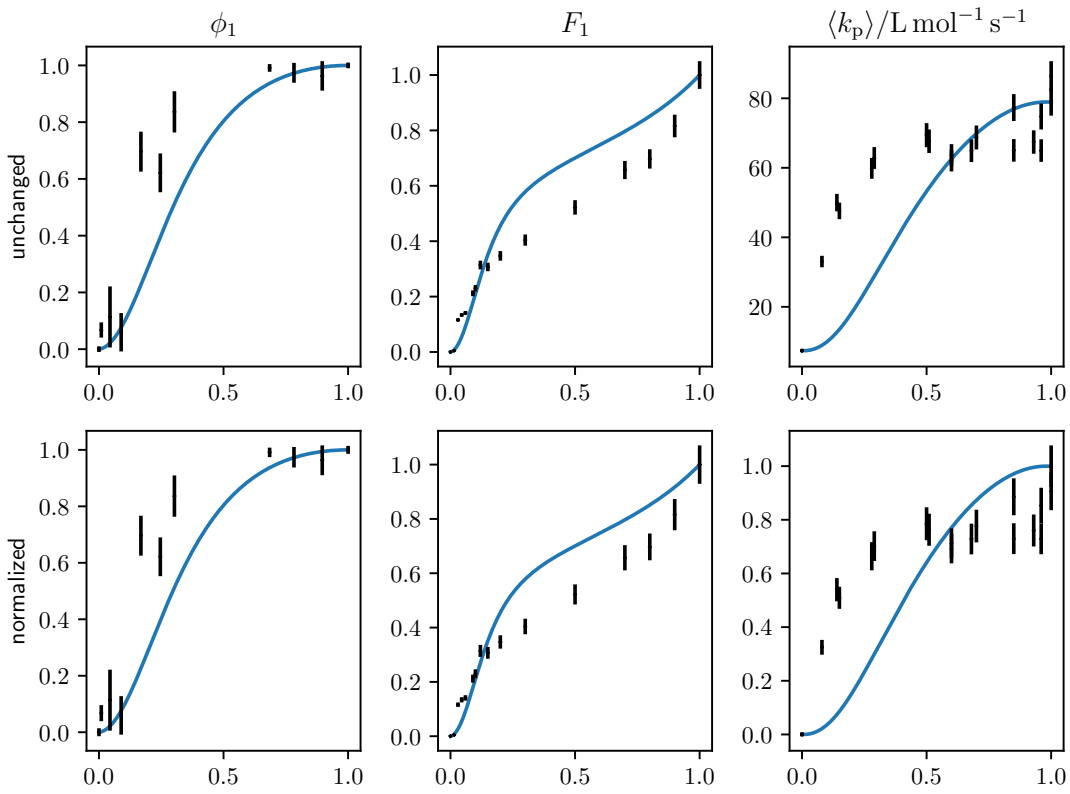

Figure 6.16.: Unchanged and normalized PRF, copolymer composition and $\langle k_p \rangle$ for the Sty/DEI system and their DRACO fit using the explicit PUM.

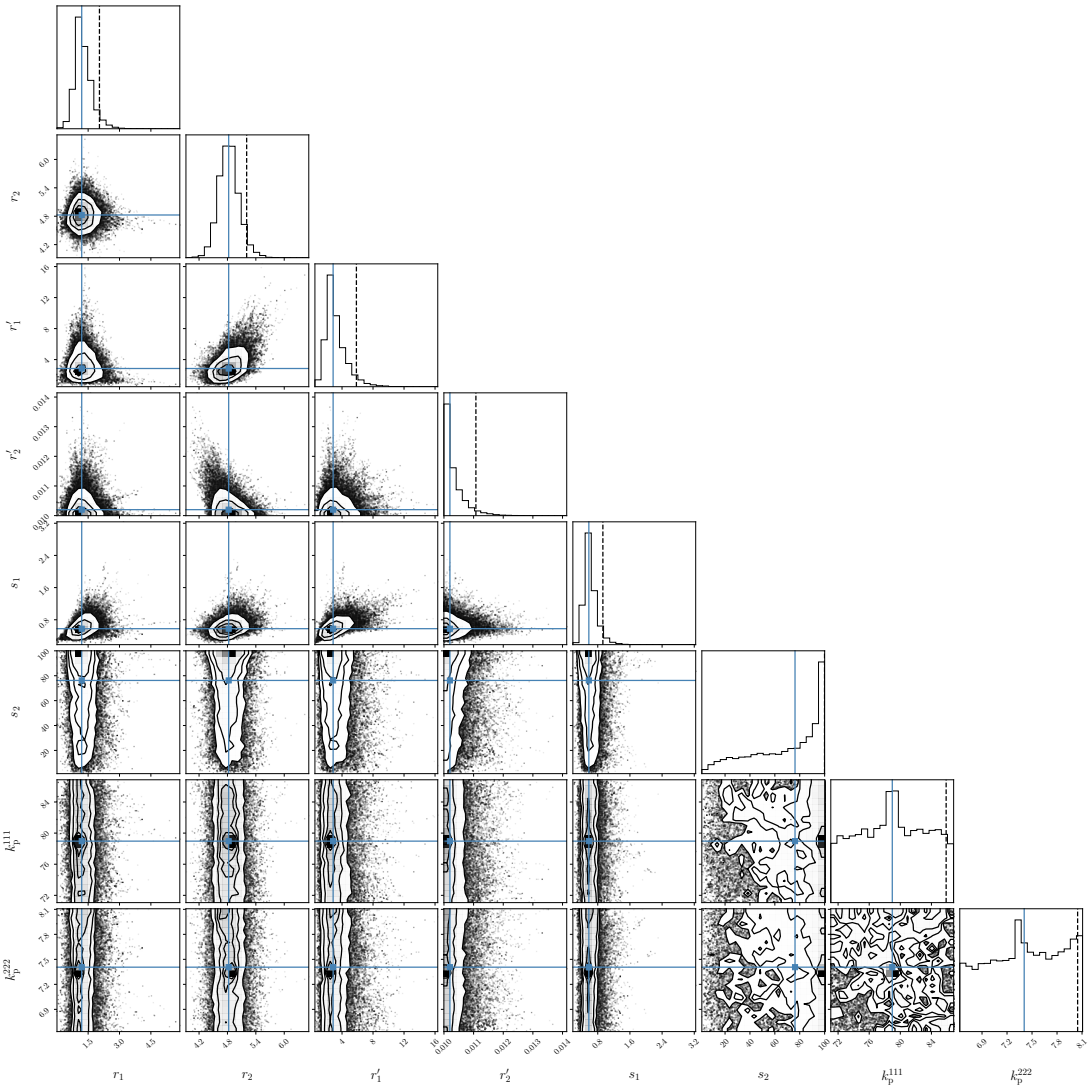

Figure 6.17.: 95 % confidence ellipsoids for the Sty/DEI system using the explicit PUM.

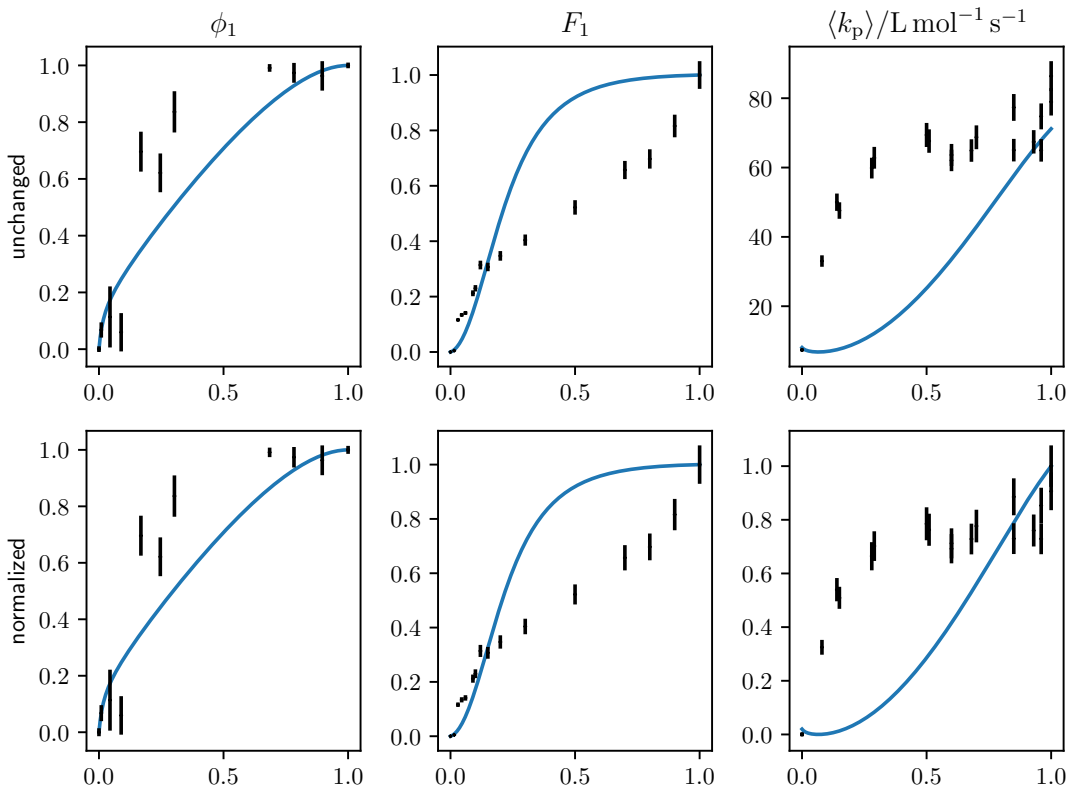

Figure 6.18.: Unchanged and normalized PRF, copolymer composition and $\langle k_p \rangle$ for the Sty/DEI system and their DRACO fit using the implicit PUM.

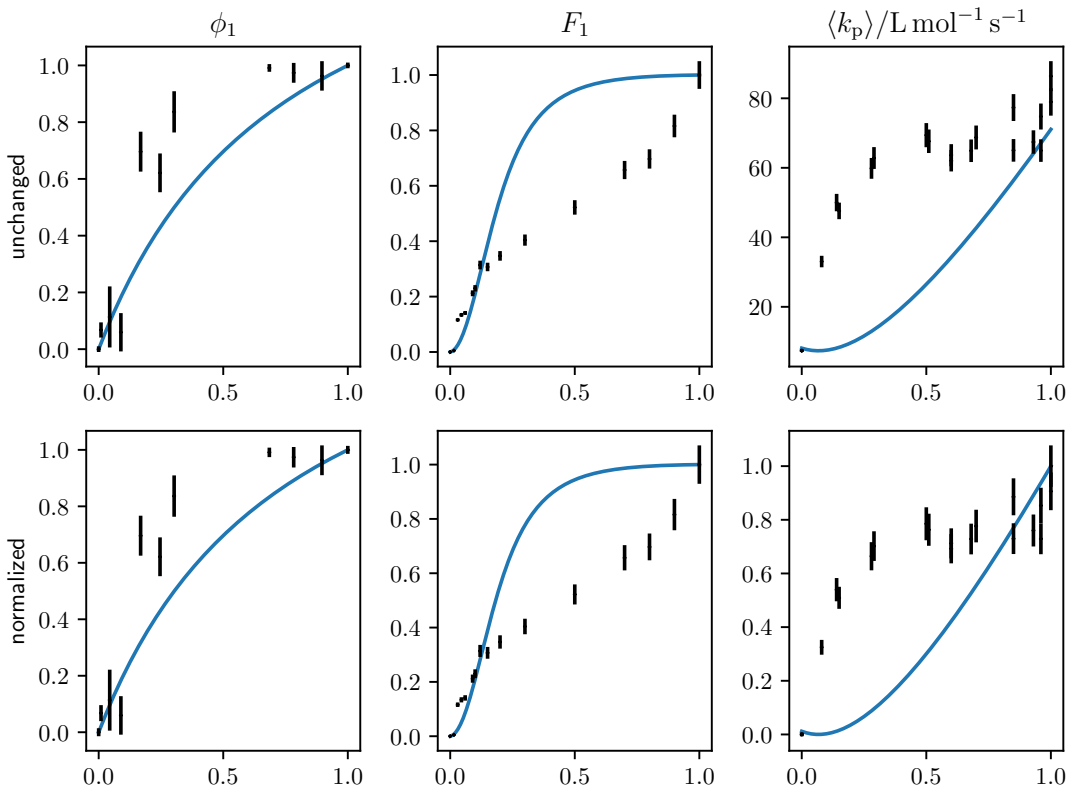

Figure 6.19.: Unchanged and normalized PRF, copolymer composition and $\langle k_p \rangle$ for the Sty/DEI system and their DRACO fit using the TM.

	explicit PUM			implicit PUM			TM		
r_A	1.05	±	0.14	46.43	±	20.44	100.0	±	0.2
r_B	4.84	±	0.37	3.17	±	0.85	4.97	±	0.52
r'_A	2.54	±	1.00		$=r_A$			$=r_A$	
r'_B	0.01	±	0.00		$=r_B$			$=r_B$	
s_A	0.53	±	0.07	0.16	±	0.25		$=1$	
s_B	76.65	±	76.84	100.0	±	0.8		$=1$	
k_p^{AAA}	78.90	±	64.83	71.18	±	1.74	71.06	±	0.01
k_p^{BBB}	7.38	±	6.65	8.07	±	0.33	8.11	±	0.00

Table 6.8.: Obtained reactivity ratios for the Sty/DEI system using DRACO according to the explicit PUM, implicit PUM and TM. The index A refers to Sty and B to DEI.

6.5. The Sty/MMA system

The Sty/MMA system is one of the most studied copolymerisation systems. The failure of the TM was shown using this system by Fukuda *et al.* in 1985.[20] MMA itself is widely used in commercial polymer products, consequently the hompolymerisation kinetics are well examined.[109,132–134] A number of publications have been investigating the copolmyerisation kinetics.[19,119,135,136] Data for the copolymer composition were taken from the historical paper by Fukuda (40 °C, bulk).[20] Data for $\langle k_p \rangle$ were taken from Cootes PhD thesis (37.6 °C, bulk).[136] The PRF was previously determined by Vana *et al.* (333 K, bulk).[19] This data set only contained 4 data points except the points at $f_A = 0$ and $f_A = 1$ which are required to run through 0 and 1 respectively. More data points were measured in this work using the same method, but at 313 K, to ensure a better match with the literature data for copolymer composition and $\langle k_p \rangle$. Also, Heuts *et al.* determined the PRF using chain transfer reactions.[135] These data were not included in the data for the fit as they were determined with a different method, however the results using EPR are in agreement with these data.

Table 6.9.: Determined PRF for the Sty/MMA system in bulk at 313 K. Data from reference [19] (bulk, 333 K, marked in green) were joined with data from this work. The values for $f_S = 0$ and $f_S = 1$ were given a very small uncertainty to ensure that the fitted curve does run through these points which is required for physical reasons.

f_S	ϕ_S	$\Delta\phi_S$
0.0	0.0	$1 \cdot 10^{-7}$
0.045	0.63	0.08
0.076	0.62	0.13
0.118	0.74	0.04
0.125	0.57	0.08
0.239	0.91	0.04
0.349	0.96	0.04
0.467	0.95	0.04
1.0	1.0	$1 \cdot 10^{-7}$

	explicit PUM			implicit PUM			TM		
r_A	0.59	±	0.25	0.40	±	0.08	1.45	±	0.07
r_B	0.46	±	0.03	0.46	±	0.02	0.46	±	0.02
r'_A	1.32	±	0.34		$=r_A$			$=r_A$	
r'_B	1.35	±	0.59		$=r_B$			$=r_B$	
s_A	0.64	±	0.15	0.23	±	0.03		$=1$	
s_B	88.29	±	95.46	9.02	±	20.46		$=1$	
k_p^{AAA}	103.95	±	0.07	104.16	±	1.43	104.13	±	0.74
k_p^{BBB}	456.87	±	44.34	441.03	±	62.91	499.02	±	2.94

Table 6.10.: Obtained reactivity ratios for the Sty/MMA system using DRACO according to the explicit PUM, implicit PUM and TM. The index A refers to Sty and B to MMA.

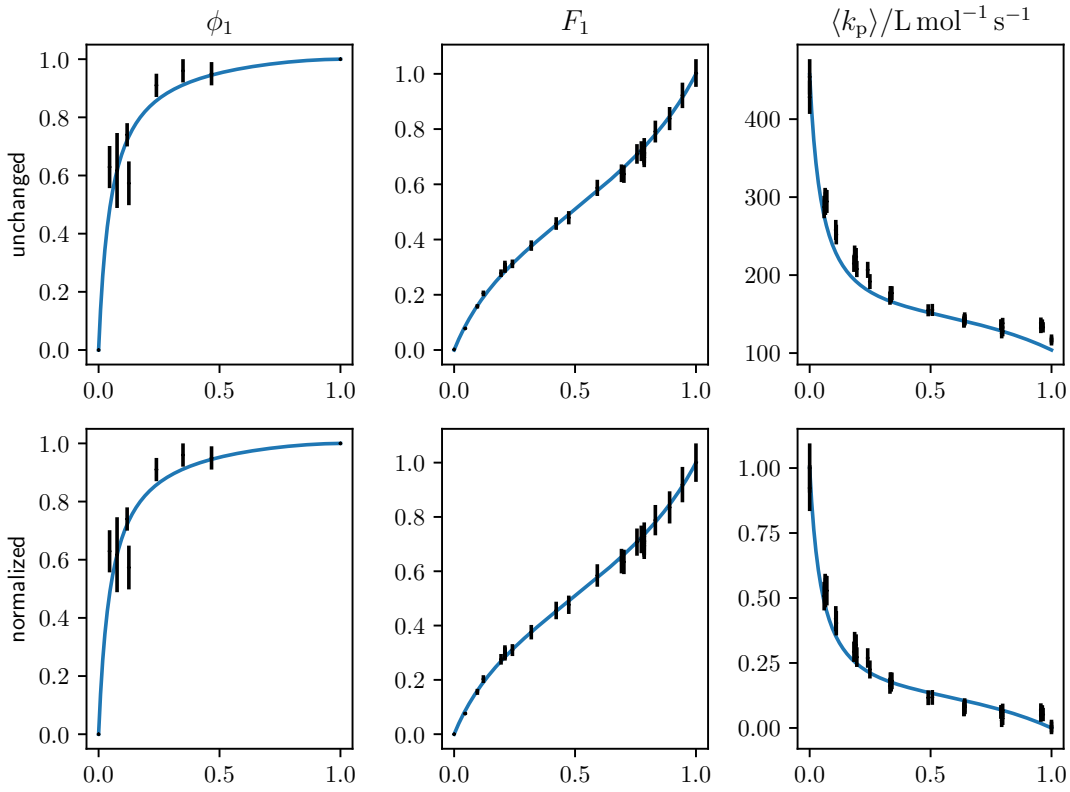

Figure 6.20.: Unchanged and normalized PRF, copolymer composition and $\langle k_p \rangle$ for the Sty/MMA system and their DRACO fit using the explicit PUM.

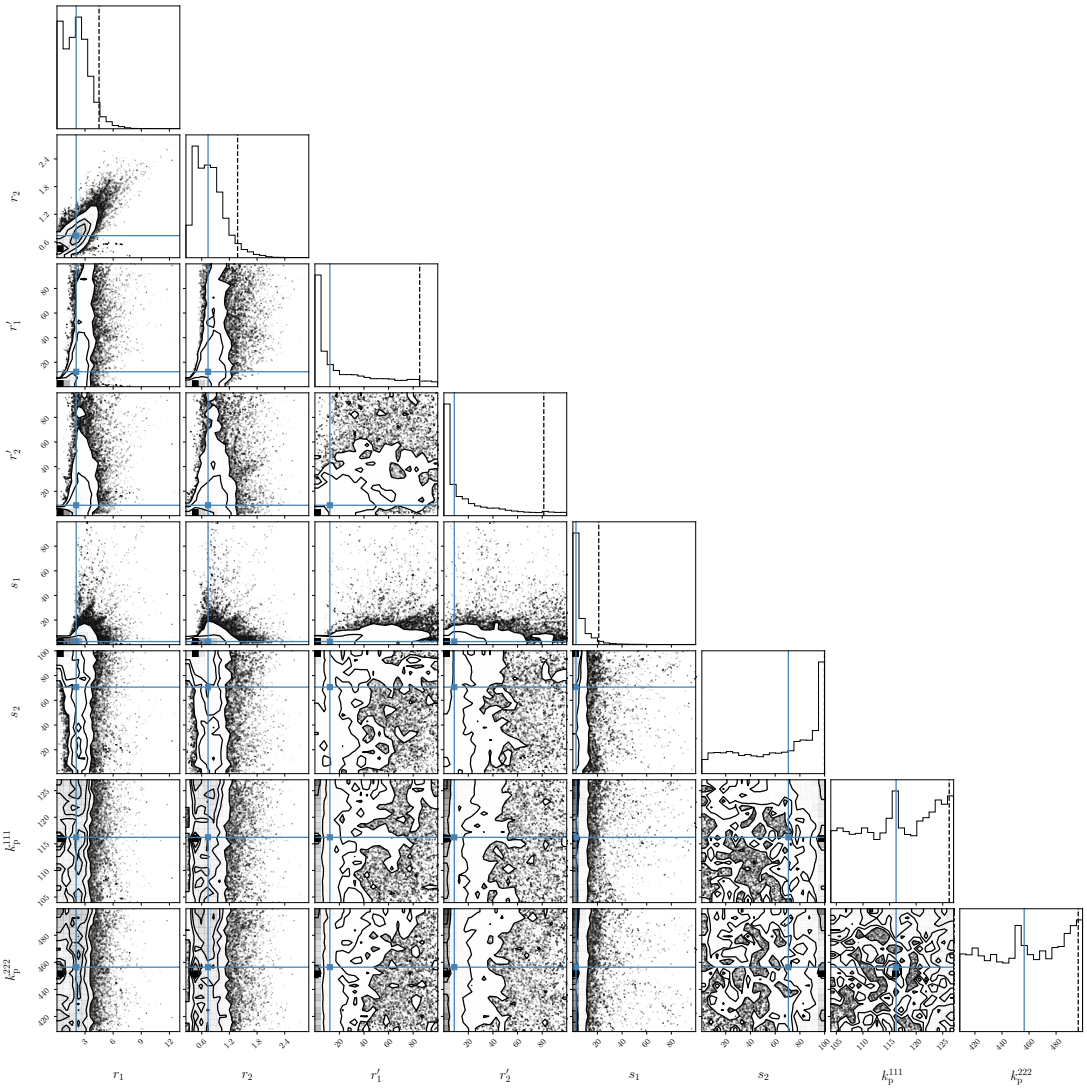

Figure 6.21.: 95 % confidence ellipsoids for the Sty/MMA system using the explicit PUM.

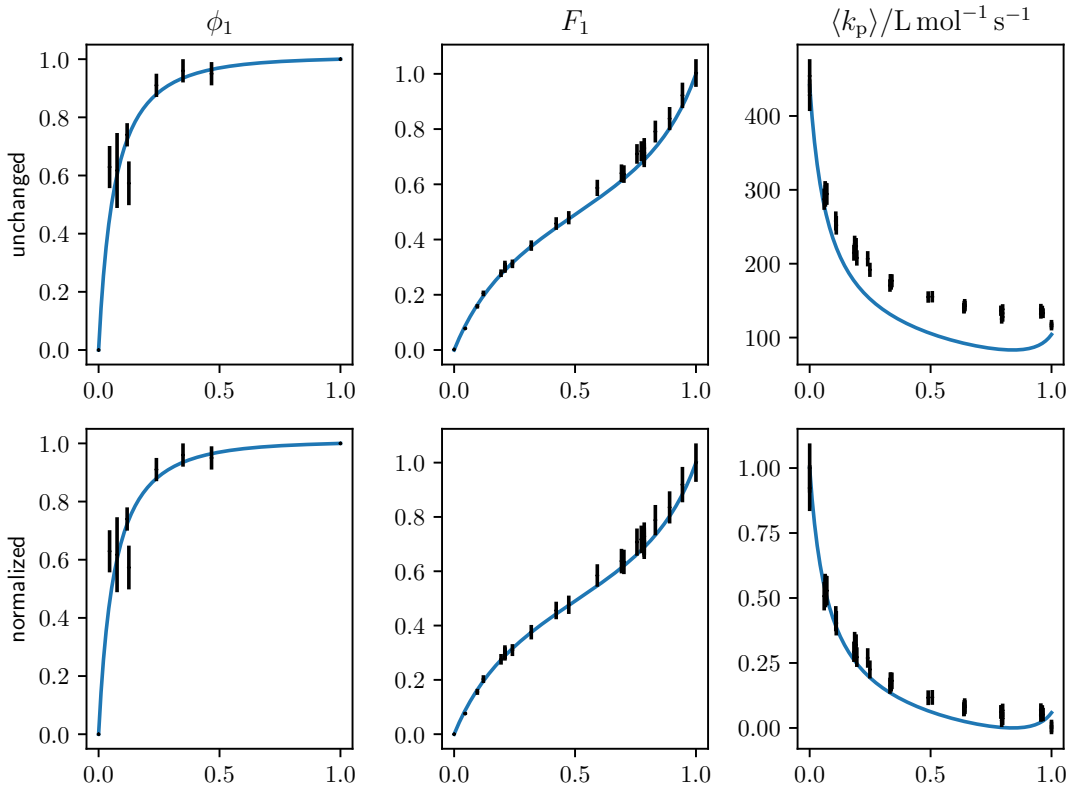

Figure 6.22.: Unchanged and normalized PRF, copolymer composition and $\langle k_p \rangle$ for the Sty/MMA system and their DRACO fit using the implicit PUM.

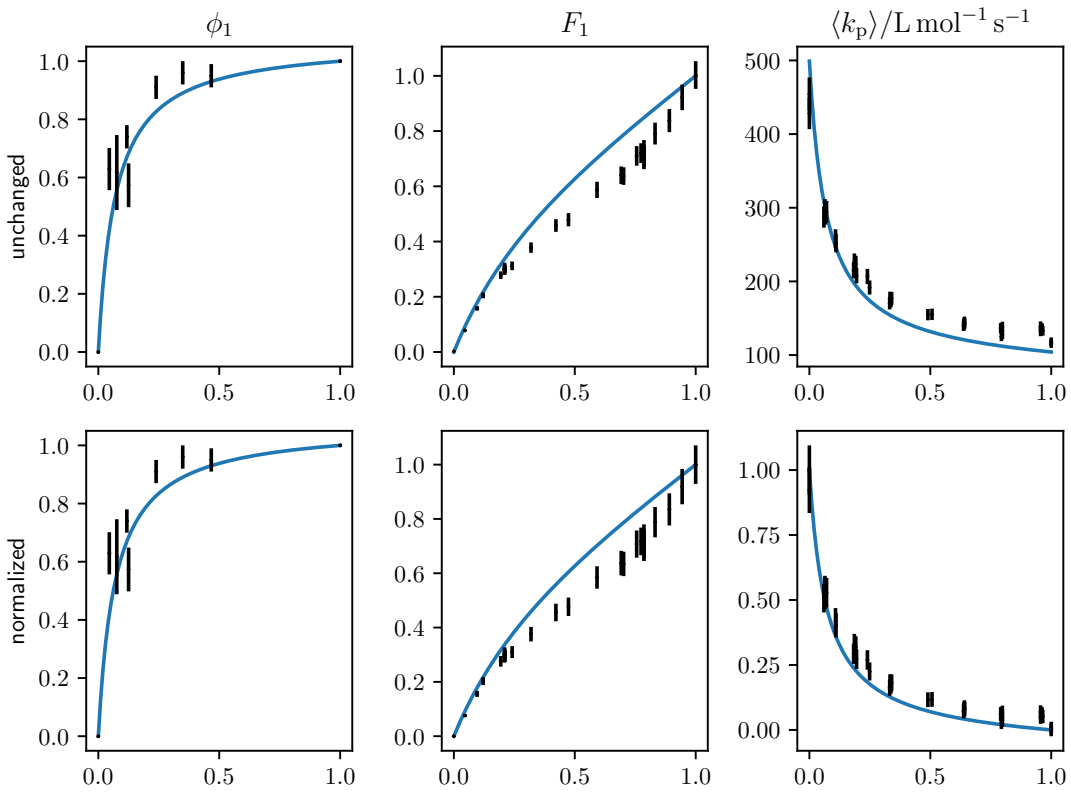

Figure 6.23.: Unchanged and normalized PRF, copolymer composition and $\langle k_p \rangle$ for the Sty/MMA system and their DRACO fit using the TM.

Table 6.10 shows the results using DRACO for the explicit PUM, implicit PUM and TM. Inspecting the results for all models, the result for k_p^{AAA} is at the lower limit (k_p homopolymerisation values were allowed to vary by 10 % from their literature values which were taken from the $\langle k_p \rangle$ data set). Furthermore, in the TM k_p^{BBB} is at the upper bound. Also in the explicit PUM s_B is very high and has a high uncertainty, indicating that s_B has very little influence on the fit. It was tested whether increasing the bounds on that parameter produces more sensible results which was not the case. This high value of s_B has been observed for all three systems under investigation, which suggests that this is a systematic problem. A possible explanation is that for the PRF data Sty-d8 was used instead of styrene-h8 (Sty-h8), which both have different k_p. At 313 K, k_p for Sty-h8 is 115.5 L mol^{-1} s^{-1} while for Sty-d8 it is 200.97 L mol^{-1} s^{-1}.[136,137] Another version of DRACO was constructed in which the PRF is fitted with the k_p value of Sty-d8 instead of Sty-h8. This however did not bring an improvement regarding s_B or the general quality of the fit.

Again, fig. 6.23 shows that the TM is incapable of describing multiple observables simultaneously. In contrast to the results from Schweer, the fits for the TM and explicit PUM do no longer match on the graphical scale.[18] Especially for the copolymer composition significant deviations can be seen. This might be due to the fact that now three observables are fitted and thus the TM has even more difficulties in describing all observables simultaneously. It should be noted that Schweer did not mention any form of data normalisation, however it can be assumed that it was performed because otherwise the data analysis shown in his work would not have worked.

6.6. Conclusion

A method to determine the propagating radical fraction using EPR spectroscopy in a copolymerisation has been presented and measurements for the Sty/DMA, Sty/DEI and Sty/MMA system have been performed. Fitting these results directly with eq. 6.4 yields unreasonable values for the RR, however this might possibly be

due to fitting to an unsuitable form of the governing equation. Based on the work of Schweer and Riemann a new fitting method was developed which performs a simultaneous fit on the copolymer composition, the overall propagation rate coefficient $\langle k_\mathrm{p} \rangle$ and the PRF based on the Nelder-Mead algorithm.[18,19,125,126] The model can be chosen to be either the explicit penultimate model, implicit penultimate model or terminal model. Because the respective equations of the explicit PUM simplify to the implicit PUM or TM by choosing appropriate constraints this change of model is very easy. This new method was named 'determining reactivity ratios with a conjoined scalable fit' (DRACO). Several tests on artificial data were performed, showing that the accuracy of the data is crucial for a correct result while a high uncertainty does not influence the fit notably. It was also shown that including more observables improves the accuracy of the results. It would be beneficial to include even more observables which is easily doable using DRACO. For example, Alfrey and Goldfinger derived expressions for the sequence distribution and the polymerisation degree which can be incorporated.[42] Especially the polymerisation degree is easy to determine with size exclusion chromatography. DRACO was then used to determine RR for the previously investigated systems. For Sty/DEI poor fits were obtained, likely due to an inaccurate data basis. For the Sty/MMA system, which is the most investigated one, both k_p values were at the variation limit of 10 %, limiting the meaningfulness of the results. However the obtained RR are in a plausible range and thus are considered the current best values. They are: $r_\mathrm{A} = 0.59$, $r_\mathrm{B} = 0.46$, $r'_\mathrm{A} = 1.32$, $r'_\mathrm{B} = 1.35$ and $s_\mathrm{A} = 0.64$, where A denotes Sty and B MMA. A plausible value for s_B can not be given. It seems that s_B has nearly no influence on the fit whatsoever.

7. Conclusion and outlook

In the course of this work, the propagation kinetics of DEI and DPI were investigated and with that a significant gap in the homologue series of di-n-alkylitaconates was closed. It was found that k_p decreases approximately linearly with the length of the side chain. This was explained by prestructuring in the bulk monomer. The side chains of neighboring molecules align which leads to a greater distance of the olefinic bonds of those molecules, hindering the propagation. In solution this effect should thus be greatly reduced or completely eliminated. This is a worthwhile investigation which can be easily done with PLP–SEC.

For the termination kinetics of DEI, less sensible results were obtained. The composite-model parameters α_s and α_l were significantly lower than expected and showing significant scatter. The crossover chainlength i_c also scatters strongly but is in a plausible range of values. Absolute termination rate coefficients $k_\mathrm{t}^{1,1}$ and k_t^{0} could not be determined as an exact calibration was not possible, however the activation energies could still be obtained. They were however too high by a factor of 2, roughly as can be seen from the activation energy of fluidity. When one of the observables is determined incorrectly, it is plausible that the other ones are wrong as well because α_s and α_l are determined from the slopes of a linear fit and $k_\mathrm{t}^{1,1}$ and k_t^{0} are determined from the intercept with the ordinate (and the respective α value, which are of course correlated. It can therefore not be definitely concluded whether the calibration or the incorrect α values or both are responsible for the incorrect results for the termination rate coefficients. While best practices were used to keep oxygen out of the sample, it can not be definitely excluded that an oxygen contamination disturbed the kinetics. Furthermore, it was shown that if the peak intensity of the SP–PLP–EPR measurement is set too low in the data evaluation

procedure, all results have lower values. This is also a possible explanation for the unplausible results. Further investigation and perhaps new samples should be prepared and new measurements should be performed.

In the second part of this work, the propagating radical fraction (PRF) ϕ which has been described only a few times and measured even less was measured for three copolymerisation systems,Sty/DMA, Sty/DEI and Sty/MMA. By fitting, the reactivity ratios (RR) were obtained but the results were physically unrealistic. This might be due to the fact that the fit was performed on an unfavourable form of the equation (eq. 6.4), which has a singularity. Naturally, this can influence a fit procedure negatively. This analysis should best be redone using the simplified form which does not have this shortfall.

The PRF was then incorporated into a new data evaluation procedure, called 'determining reactivity ratios with a conjoined scalable fit (DRACO)'. It is based on the pioneering work by Schweer.[18] This method uses data for more than one observable such as copolymer composition, the overall propagation rate coefficient $\langle k_\mathrm{p} \rangle$ and the PRF but it can easily be expanded to include more observables. A simultaneous fit is performed on the combined data basis. The model to be fitted can be either explicit PUM, implicit PUM or TM. Optionally, the propagation rate coefficients of the homopolymerisations which appear in the equations for $\langle k_\mathrm{p} \rangle$ and ϕ can also be fitted. Constraints and approximations can be introduced with minimal effort. If the need arises, also other models can be implemented in the program, which however requires rewriting the underlying equations. The DRACO approach was used for the three copolymerisation systems and new best values for the RR were obtained. However, an important question is what is considered the best values. One might argue that fitting each observable separately gives a more accurate fit, albeit each observable then yields a corresponding set of RR. This approach however has no benefit over simly using a generic high-order polynom as the resulting values have no physical meaning. The DRACO approach ensures that the obtained RR are physically relevant properties and thus should be preferred. DRACO is far from complete, though. It is encouraged to add more observables, further increasing the accuracy of the results. Alfrey and Goldfinger derived equations for sequence distributions and polymerisation degree already.[42]

The latter however comes with the disadvantage that initiation and termination rate coefficients are required as well which introduces additional sources of error. On the other hand they are very easy to measure by size-exclusion chromatography. Sequence distributions are harder to determine experimentally but would prove a valuable addition to DRACO.

Bibliography

[1] L. Baekeland, 'Bakelit, Ein Neues Synthetisches Harz', *Chemiker-Zeitung* **1909**, *35*, 317326347358.

[2] H. Staudinger, 'Über Polymerisation', *Berichte der deutschen chemischen Gesellschaft (A and B Series)* **1920**, *53*, 1073–1085.

[3] Plastics Europe AISBL, European Association of Plastics Recycling and Recovery Organisations, Plastics – the Facts 2022, **2022**.

[4] M. G. Steiger, M. L. Blumhoff, D. Mattanovich, M. Sauer, 'Biochemistry of Microbial Itaconic Acid Production', *Frontiers in Microbiology* **2013**, *4*.

[5] Th. Willke, K.-D. Vorlop, 'Biotechnological Production of Itaconic Acid', *Applied Microbiology and Biotechnology* **2001**, *56*, 289–295.

[6] M. Okabe, D. Lies, S. Kanamasa, E. Y. Park, 'Biotechnological Production of Itaconic Acid and Its Biosynthesis in Aspergillus Terreus', *Applied Microbiology and Biotechnology* **2009**, *84*, 597–606.

[7] K. Yahiro, S. Shibata, S.-R. Jia, Y. Park, M. Okabe, 'Efficient Itaconic Acid Production from Raw Corn Starch', *Journal of Fermentation and Bioengineering* **1997**, *84*, 375–377.

[8] G. Tevž, M. Benčina, M. Legiša, 'Enhancing Itaconic Acid Production by Aspergillus Terreus', *Applied Microbiology and Biotechnology* **2010**, *87*, 1657–1664.

[9] A. A. El-Imam, C. Du, 'Fermentative Itaconic Acid Production', *Journal of Biodiversity Bioprospecting and Development* **2014**, *1*, 1–8.

[10] M. Zhao, X. Lu, H. Zong, J. Li, B. Zhuge, 'Itaconic Acid Production in Microorganisms', *Biotechnology Letters* **2018**, *40*, 455–464.

[11] N. Wierckx, G. Agrimi, P. S. Lübeck, M. G. Steiger, N. P. Mira, P. J. Punt, 'Metabolic Specialization in Itaconic Acid Production: A Tale of Two Fungi', *Current Opinion in Biotechnology* **2020**, *62*, 153–159.

[12] R. Bafana, R. A. Pandey, 'New Approaches for Itaconic Acid Production: Bottlenecks and Possible Remedies', *Critical Reviews in Biotechnology* **2018**, *38*, 68–82.

[13] V. V. Panic, S. I. Seslija, I. G. Popovic, V. D. Spasojevic, A. R. Popovic, V. B. Nikolic, P. M. Spasojevic, 'Simple One-Pot Synthesis of Fully Biobased Unsaturated Polyester Resins Based on Itaconic Acid', *Biomacromolecules* **2017**, *18*, 3881–3891.

[14] Z. Dai, Z. Yang, Z. Chen, Z. Zhao, Y. Lou, Y. Zhang, T. Liu, F. Fu, Y. Fu, X. Liu, 'Fully Biobased Composites of an Itaconic Acid Derived Unsaturated Polyester Reinforced with Cotton Fabrics', *ACS Sustainable Chemistry & Engineering* **2018**, *6*, 15056–15063.

[15] O. F. Olaj, I. Bitai, F. Hinkelmann, 'The Laser-Flash-Initiated Polymerization as a Tool of Evaluating (Individual) Kinetic Constants of Free-Radical Polymerization, 2. The Direct Determination of the Rate of Constant of Chain Propagation', *Die Makromolekulare Chemie* **1987**, *188*, 1689–1702.

[16] M. Buback, M. Egorov, T. Junkers, E. Panchenko, 'Free-Radical Termination Kinetics Studied Using a Novel SP-PLP-ESR Technique', *Macromolecular Rapid Communications* **2004**, *25*, 1004–1009.

[17] G. B. Smith, G. T. Russell, J. P. Heuts, 'Termination in Dilute-Solution Free-Radical Polymerization: A Composite Model', *Macromolecular Theory and Simulations* **2003**, *12*, 299–314.

[18] J. Schweer, 'Penultimate Model Description of the Propagation Kinetics for the Free Radical Copolymerization of Styrene and Methyl Methacrylate', *Die Makromolekulare Chemie Theory and Simulations* **1993**, *2*, 485–502.

[19] L. Riemann, S. Brandt, P. Vana, 'Refining Reactivity Ratios in the Copolymerization of Styrene and Methyl Methacrylate by EasySpin/MATLAB Simulations and Electron Paramagnetic Resonance Spectroscopy', *Macromolecular Theory and Simulations* **2021**, *30*, 2100048.

[20] T. Fukuda, Y. D. Ma, H. Inagaki, 'Free-Radical Copolymerization. 3. Determination of Rate Constants of Propagation and Termination for Styrene/Methyl Methacrylate System. A Critical Test of Terminal-Model Kinetics', *Macromolecules* **1985**, *18*, 17–26.

[21] *Handbook of Radical Polymerization*, (Eds.: K. Matyjaszewski, T. P. Davis), Wiley-Interscience, Hoboken, **2002**, 920 pp.

[22] G. T. Russell in *Encyclopedia of Polymer Science and Technology*, (Ed.: H. F. Mark), Wiley, **2010**.

[23] D. S. Achilias, 'A Review of Modeling of Diffusion Controlled Polymerization Reactions', *Macromolecular Theory and Simulations* **2007**, *16*, 319–347.

[24] H.-H. Schuh, H. Fischer, 'The kinetics of the bimolecular sel-reaction of t-butyl radicals in solution. I. Termination rates', *Helvetica Chimica Acta* **1978**, *61*, 2130–2164.

[25] H. Fischer, 'ESR of Transient Free Radicals during Liquid Phase Polymerization: III. On the ESR-spectra of Polymerization Radicals of Methacryl-derivatives', *Journal of Polymer Science Part B: Polymer Letters* **1964**, *2*, 529–532.

[26] H. Fischer, H. Paul, 'Rate Constants for Some Prototype Radical Reactions in Liquids by Kinetic Electron Spin Resonance', *Accounts of Chemical Research* **1987**, *20*, 200–206.

[27] A. Einstein, 'Über die von der molekularkinetischen Theorie der Wärme geforderte Bewegung von in ruhenden Flüssigkeiten suspendierten Teilchen', *Annalen der Physik* **1905**, *322*, 549–560.

[28] M. V. Smoluchowski, 'Versuch Einer Mathematischen Theorie Der Koagulationskinetik Kolloider Lösungen', *Zeitschrift für Physikalische Chemie* **1918**, *92U*, 129–168.

[29] M. Buback, 'Free-Radical Polymerization up to High Conversion. A General Kinetic Treatment', *Die Makromolekulare Chemie* **1990**, *191*, 1575–1587.

[30] S. W. Benson, A. M. North, 'The Kinetics of Free Radical Polymerization under Conditions of Diffusion-controlled Termination', *Journal of the American Chemical Society* **1962**, *84*, 935–940.

[31] H. Kattner, M. Buback, 'Chain-Length-Dependent Termination of Vinyl Acetate and Vinyl Pivalate Bulk Homopolymerizations Studied by SP-PLP-EPR', *Macromolecular Chemistry and Physics* **2014**, *215*, 1180–1191.

[32] H. Kattner, 'Radical Polymerization Kinetics of Non-Ionized and Fully-Ionized Monomers Studied by Pulsed-Laser EPR', Georg-August-Universität, Göttingen, **2016**

[33] J. Barth, M. Buback, G. T. Russell, S. Smolne, 'Chain-Length-Dependent Termination in Radical Polymerization of Acrylates', *Macromolecular Chemistry and Physics* **2011**, *212*, 1366–1378.

[34] J. G. Kirkwood, J. Riseman, 'The Intrinsic Viscosities and Diffusion Constants of Flexible Macromolecules in Solution', *The Journal of Chemical Physics* **1948**, *16*, 565–573.

[35] G. Johnston-Hall, M. J. Monteiro, 'Bimolecular Radical Termination: New Perspectives and Insights', *Journal of Polymer Science Part A: Polymer Chemistry* **2008**, *46*, 3155–3173.

[36] B. Friedman, B. O'Shaughnessy, 'Kinetics of Intermolecular Reactions in Dilute Polymer Solutions and Unentangled Melts', *Macromolecules* **1993**, *26*, 5726–5739.

[37] A. R. Khokhlov, 'Influence of Excluded Volume Effect on the Rates of Chemically Controlled Polymer-polymer Reactions', *Die Makromolekulare Chemie Rapid Communications* **1981**, *2*, 633–636.

[38] O. F. Olaj, G. Zifferer, 'Termination Processes in Free Radical Polymerization. 9. Derivation of Universal Relationships between Kinetic Quantities for Arbitrary Chain Length Dependence of the Termination Constant', *Macromolecules* **1987**, *20*, 850–861.

[39] G. Moad, D. H. Solomon, *The Chemistry of Radical Polymerization*, 2nd fully rev. ed, Elsevier, Amsterdam ; Boston, **2006**, 639 pp.

[40] G. T. Russell, 'The Kinetics of Free-Radical Polymerization: Fundamental Aspects', *Australian Journal of Chemistry* **2002**, *55*, 399.

[41] F. R. Mayo, F. M. Lewis, 'Copolymerization. I. A Basis for Comparing the Behavior of Monomers in Copolymerization; The Copolymerization of Styrene and Methyl Methacrylate', *Journal of the American Chemical Society* **1944**, *66*, 1594–1601.

[42] T. Alfrey, G. Goldfinger, 'The Mechanism of Copolymerization', *The Journal of Chemical Physics* **1944**, *12*, 205–209.

[43] M. Fineman, S. D. Ross, 'Linear Method for Determining Monomer Reactivity Ratios in Copolymerization', *Journal of Polymer Science* **1950**, *5*, 259–262.

[44] T. Kelen, F. Tüdős, 'A New Improved Linear Graphical Method for Determing Copolymerization Reactivity Ratios', *Reaction Kinetics and Catalysis Letters* **1974**, *1*, 487–492.

[45] T. Kelen, F. Tüdös, 'Analysis of the Linear Methods for Determining Copolymerization Reactivity Ratios. I. A New Improved Linear Graphic Method', *Journal of Macromolecular Science: Part A - Chemistry* **1975**, *9*, 1–27.

[46] T. Kelen, F. Tüdös, B. Turcsanyi, 'Confidence Intervals for Copolymerization Reactivity Ratios Determined by the Kelen-Tüdös Method', *Polymer Bulletin* **1980**, *2*, 71–76.

[47] E. Merz, T. Alfrey, G. Goldfinger, 'Intramolecular Reactions in Vinyl Polymers as a Means of Investigation of the Propagation Step', *Journal of Polymer Science* **1946**, *1*, 75–82.

[48] T. Fukuda, Y.-D. Ma, H. Inagaki, 'Free-Radical Copolymerization, 6. New Interpretation for the Propagation Rate versus Composition Curve', *Die Makromolekulare Chemie Rapid Communications* **1987**, *8*, 495–499.

[49] C. Barner-Kowollik, M. L. Coote, T. P. Davis, K. Matyjaszewski, P. Vana in *Encyclopedia of Polymer Science and Technology*, (Ed.: H. F. Mark), Wiley, **2004**.

[50] C. Walling, 'Copolymerization. XIII. 1 Over-all Rates in Copolymerization. Polar Effects in Chain Initiation and Termination', *Journal of the American Chemical Society* **1949**, *71*, 1930–1935.

[51] J. N. Atherton, A. M. North, 'Diffusion-Controlled Termination in Free Radical Copolymerization', *Transactions of the Faraday Society* **1962**, *58*, 2049.

[52] K. Ito, K. F. O'Driscoll, 'The Termination Reaction in Free Radical Copolymerization. I. Methyl Methacrylate and Butyl- or Dodecyl Methacrylate', *Journal of Polymer Science: Polymer Chemistry Edition* **1979**, *17*, 3913–3921.

[53] O. F. Olaj, M. Zoder, P. Vana, G. Zifferer, 'Chain Length Dependent Termination in Free Radical Copolymerization. 1. The Copolymerization System Styrene−Methyl Methacrylate in Bulk at 25 °C', *Macromolecules* **2004**, *37*, 1544–1550.

[54] A. Kornherr, O. F. Olaj, I. Schnöll-Bitai, G. Zifferer, 'A Method of Improving the Theoretical Basis of Kp Determination from PLP-SEC Measurements', *Macromolecular Theory and Simulations* **2003**, *12*, 332–338.

[55] A. Kornherr, O. F. Olaj, I. Schnöll-Bitai, G. Zifferer, 'Improving Kp Data Originating from PLP Number Distributions', *Macromolecular Theory and Simulations* **2006**, *15*, 215–225.

[56] P. Pracht, F. Bohle, S. Grimme, 'Automated Exploration of the Low-Energy Chemical Space with Fast Quantum Chemical Methods', *Physical Chemistry Chemical Physics* **2020**, *22*, 7169–7192.

[57] J. Veličković, S. Vasović, 'KUHN-MARK-HOUWINK-SAKURADA Relations and Unperturbed Dimensions of Poly(Di-n-Alkyl Itaconates)', *Die Makromolekulare Chemie* **1972**, *153*, 207–218.

[58] Y. Luo, H. Gu, 'A General Strategy for Nano-Encapsulation via Interfacially Confined Living/Controlled Radical Miniemulsion Polymerization', *Macromolecular Rapid Communications* **2006**, *27*, 21–25.

[59] B. Klumperman, 'Styrene/Maleic Anhydride Macro-RAFT-Mediated Encapsulation', *Macromolecular Chemistry and Physics* **2006**, *207*, 861–863.

[60] S. M. Henry, M. E. H. El-Sayed, C. M. Pirie, A. S. Hoffman, P. S. Stayton, 'pH-Responsive Poly(Styrene-Alt-Maleic Anhydride) Alkylamide Copolymers for Intracellular Drug Delivery', *Biomacromolecules* **2006**, *7*, 2407–2414.

[61] Y. Luo, H. Gu, 'Nanoencapsulation via Interfacially Confined Reversible Addition Fragmentation Transfer (RAFT) Miniemulsion Polymerization', *Polymer* **2007**, *48*, 3262–3272.

[62] V. B. Rodriguez, S. M. Henry, A. S. Hoffman, P. S. Stayton, X. Li, S. H. Pun, 'Encapsulation and Stabilization of Indocyanine Green within Poly(Styrene-Alt-Maleic Anhydride) Block-Poly(Styrene) Micelles for near-Infrared Imaging', *Journal of Biomedical Optics* **2008**, *13*, 014025.

[63] Y. Yu, Q. Zhang, Z. Wang, X. Zhan, R. He, W. Zhang, F. Chen, 'Synthesis of Surface-Functionalized Poly(Styrene-Co-Butadiene) Nanoparticles via Controlled/Living Radical Mini-emulsion Copolymerization Stabilized by Ammonolyzed Poly(Styrene-Alt-Maleic Anhydride) (SMA) RAFT Agent', *Journal of Macromolecular Science Part A* **2012**, *49*, 60–66.

[64] S. Zhang, Y. Wu, B. He, K. Luo, Z. Gu, 'Biodegradable Polymeric Nanoparticles Based on Amphiphilic Principle: Construction and Application in Drug Delivery', *Science China Chemistry* **2014**, *57*, 461–475.

[65] J. M. Dörr, S. Scheidelaar, M. C. Koorengevel, J. J. Dominguez, M. Schäfer, C. A. van Walree, J. A. Killian, 'The Styrene–Maleic Acid Copolymer: A Versatile Tool in Membrane Research', *European Biophysics Journal* **2016**, *45*, 3–21.

[66] H. Zweifel, J. Löliger, T. Völker, 'Zur Kenntnis Der Anionischen Polymerisation von Maleinsäureanhydrid', *Die Makromolekulare Chemie* **1972**, *153*, 125–137.

[67] H. Zweifel, T. Völker, 'On the Mechanism of Anionic Polymerization of Maleic Anhydride', *Die Makromolekulare Chemie* **1973**, *170*, 141–153.

[68] V. Barone, M. Cossi, 'Quantum Calculation of Molecular Energies and Energy Gradients in Solution by a Conductor Solvent Model', *The Journal of Physical Chemistry A* **1998**, *102*, 1995–2001.

[69] E. Tsuchida, T. Tomono, 'Discussion on the Mechanism of Alternating Copolymerization of Styrene and Maleic Anhydride', *Die Makromolekulare Chemie* **1971**, *141*, 265–298.

[70] J. Bartoň, I. Capek, J. Tiňo, 'Effect of UV Light on the System Styrene/Maleic Anhydride at −196°C', *Die Makromolekulare Chemie* **1980**, *181*, 255–260.

[71] M. Rätzsch, G. Schicht, M. Arnold, J. Barton, I. Capek, 'Photopolymerization of Styrene with Maleic Anhydride', *Chem. Zvesti* **1984**, *38*, 823–838.

[72] D. J. T. Hill, J. H. O'Donnell, P. W. O'Sullivan, 'Analysis of the Mechanism of Copolymerization of Styrene and Maleic Anhydride', *Macromolecules* **1985**, *18*, 9–17.

[73] V. Barone in D. P. Chong, *Recent Advances in Computational Chemistry*, *Vol. 1*, WORLD SCIENTIFIC, **1995**, pp. 287–334.

[74] L. H. Yee, M. L. Coote, R. P. Chaplin, T. P. Davis, 'Determination of Propagation Rate Coefficients for an α-Substituted Acrylic Ester: Pulsed Laser Polymerization of Dimethyl Itaconate', *Journal of Polymer Science Part A: Polymer Chemistry* **2000**, *38*, 2192–2200.

[75] Z. Szablan, M. H. Stenzel, T. P. Davis, L. Barner, C. Barner-Kowollik, 'Depropagation Kinetics of Sterically Demanding Monomers: A Pulsed Laser Size Exclusion Chromatography Study', *Macromolecules* **2005**, *38*, 5944–5954.

[76] P. Vana, L. H. Yee, T. P. Davis, 'Multipulse Initiation in Pulsed Laser and Quenched Instationary Polymerization: Determination of the Propagation and Termination Rate Coefficients for Dicyclohexyl Itaconate Polymerization', *Macromolecules* **2002**, *35*, 3008–3016.

[77] T. Sato, S. Inui, H. Tanaka, T. Ota, M. Kamachi, K. Tanaka, 'Kinetic and ESR Studies on the Radical Polymerization of Di-n-butyl Itaconate in Benzene', *Journal of Polymer Science Part A: Polymer Chemistry* **1987**, *25*, 637–652.

[78] T. Sato, Y. Takahashi, M. Seno, H. Nakamura, H. Tanaka, T. Ota, 'Effect of Alkyl Groups on the Rate Constants of Propagation and Termination in the Radical Polymerization of Dialkyl Itaconates', *Die Makromolekulare Chemie* **1991**, *192*, 2909–2914.

[79] T. Otsu, K. Yamagishi, M. Yoshioka, 'Determination of Absolute Rate Constants for Radical Polymerization of Dialkyl Itaconates with Various Ester Groups by Electron Spin Resonance Spectroscopy', *Macromolecules* **1992**, *25*, 2713–2716.

[80] T. Otsu, K. Yamagishi, A. Matsumoto, M. Yoshioka, H. Watanabe, 'Effect of α- and β-Ester Alkyl Groups on the Propagation and Termination Rate Constants for Radical Polymerization of Dialkyl Itaconates', *Macromolecules* **1993**, *26*, 3026–3029.

[81] T. Sato, Y. Hirose, M. Seno, H. Tanaka, N. Uchiumi, M. Matsumoto, 'Kinetic and ESR Studies on Radical Polymerization. Radical Polymerization of Diisopropyl Itaconate', *European Polymer Journal* **1994**, *30*, 347–352.

[82] M. Buback, M. Egorov, T. Junkers, E. Panchenko, 'Termination Kinetics of Dibutyl Itaconate Free-Radical Polymerization Studied via the SP-PLP-ESR Technique', *Macromolecular Chemistry and Physics* **2005**, *206*, 333–341.

[83] E. Meyer, T. Weege, P. Vana, 'Free-Radical Propagation Rate Coefficients of Diethyl Itaconate and Di-n-Propyl Itaconate Obtained via PLP–SEC', *Polymers* **2023**, *15*, 1345.

[84] F. Neese, 'The ORCA Program System', *WIREs Computational Molecular Science* **2012**, *2*, 73–78.

[85] F. Neese, 'Software Update: The ORCA Program System, Version 4.0', *WIREs Computational Molecular Science* **2018**, *8*.

[86] M. L. Coote in *Encyclopedia of Polymer Science and Technology*, (Ed.: John Wiley & Sons, Inc.), John Wiley & Sons, Inc., Hoboken, NJ, USA, **2006**.

[87] A. P. Scott, L. Radom, 'Harmonic Vibrational Frequencies: An Evaluation of Hartree−Fock, Møller−Plesset, Quadratic Configuration Interaction, Density Functional Theory, and Semiempirical Scale Factors', *The Journal of Physical Chemistry* **1996**, *100*, 16502–16513.

[88] M. K. Kesharwani, B. Brauer, J. M. L. Martin, 'Frequency and Zero-Point Vibrational Energy Scale Factors for Double-Hybrid Density Functionals (and Other Selected Methods): Can Anharmonic Force Fields Be Avoided?', *The Journal of Physical Chemistry A* **2015**, *119*, 1701–1714.

[89] A. Nitschke, L. Riemann, L. Kollenbach, V. Braun, M. Buback, P. Vana, 'Investigation into the Kinetics of n-Pentyl Methacrylate Radical Polymerization', *Macromolecular Chemistry and Physics* **2020**, *221*, 1900345.

[90] M. Buback, A. Kuelpmann, 'A Suitable Photoinitiator for Pulsed Laser-Induced Free-Radical Polymerization', *Macromolecular Chemistry and Physics* **2003**, *204*, 632–637.

[91] O. F. Olaj, P. Vana, M. Zoder, A. Kornherr, G. Zifferer, 'Is the Rate Constant of Chain Propagation Kp in Radical Polymerization Really Chain-Length Independent?', *Macromolecular Rapid Communications* **2000**, *21*, 913–920.

[92] O. F. Olaj, P. Vana, M. Zoder, 'Chain Length Dependent Propagation Rate Coefficient Kp in Pulsed-Laser Polymerization: Variation with Temperature in the Bulk Polymerization of Styrene and Methyl Methacrylate', *Macromolecules* **2002**, *35*, 1208–1214.

[93] O. F. Olaj, M. Zoder, P. Vana, A. Kornherr, I. Schnöll-Bitai, G. Zifferer, 'Chain Length Dependence of Chain Propagation Revisited', *Macromolecules* **2005**, *38*, 1944–1948.

[94] A. N. Nikitin, E. Dušička, I. Lacík, R. A. Hutchinson, 'Chain-Length Dependence of the Propagation Rate Coefficient for Methyl Acrylate Polymerization at 25 °C Investigated by the PLP-SEC Method', *Polymer Chemistry* **2022**, *13*, 3053–3062.

[95] A. A. Gridnev, S. D. Ittel, 'Dependence of Free-Radical Propagation Rate Constants on the Degree of Polymerization', *Macromolecules* **1996**, *29*, 5864–5874.

[96] J. P. Heuts, G. T. Russell, 'The Nature of the Chain-Length Dependence of the Propagation Rate Coefficient and Its Effect on the Kinetics of Free-Radical Polymerization. 1. Small-molecule Studies', *European Polymer Journal* **2006**, *42*, 3–20.

[97] R. X. E. Willemse, B. B. P. Staal, A. M. Van Herk, S. C. J. Pierik, B. Klumperman, 'Application of Matrix-Assisted Laser Desorption Ionization Time-of-Flight Mass Spectrometry in Pulsed Laser Polymerization. Chain-Length-Dependent Propagation Rate Coefficients at High Molecular Weight: An Artifact Caused by Band Broadening in Size Exclusion Chromatography?', *Macromolecules* **2003**, *36*, 9797–9803.

[98] S. Beuermann, 'Requirements Associated with Studies into a Chain-Length Dependence of Propagation Rate Coefficients via PLP−SEC Experiments', *Macromolecules* **2002**, *35*, 9300–9305.

[99] A. P. Haehnel, M. Schneider-Baumann, K. U. Hiltebrandt, A. M. Misske, C. Barner-Kowollik, 'Global Trends for Kp? Expanding the Frontier of Ester Side Chain Topography in Acrylates and Methacrylates', *Macromolecules* **2013**, *46*, 15–28.

[100] A. P. Haehnel, M. Schneider-Baumann, L. Arens, A. M. Misske, F. Fleischhaker, C. Barner-Kowollik, 'Global Trends for Kp? The Influence of Ester Side Chain Topography in Alkyl (Meth)Acrylates − Completing the Data Base', *Macromolecules* **2014**, *47*, 3483–3496.

[101] S. Beuermann, M. Buback, 'Rate Coefficients of Free-Radical Polymerization Deduced from Pulsed Laser Experiments', *Progress in Polymer Science* **2002**, *27*, 191–254.

[102] T. Sato, K. Morino, H. Tanaka, T. Ota, 'ESR Determination of Rate Constants for the Radical Polymerization of Methyl Phenethyl Itaconate', *Die Makromolekulare Chemie* **1987**, *188*, 2951–2961.

[103] T. Sato, K. Takahashi, H. Tanaka, T. Ota, K. Kato, 'An ESR Study on the Radical Copolymerization of N-cyclohexylmaleimide and Di-n-Butyl Itaconate in Benzene', *Macromolecules* **1991**, *24*, 2330–2333.

[104] T. Hirano, K. Furuya, M. Seno, T. Sato, '13C NMR and Electron Spin Resonance Analyses of the Radical Polymerization of Diisopropyl Itaconate', *Journal of Polymer Science Part A: Polymer Chemistry* **2002**, *40*, 4513–4522.

[105] L. Riemann, 'Termination Kinetics of Radical Homo- and Copolymerizations Studied via Time-Resolved EPR Spectroscopy', Georg-August-Universität, Göttingen, **2021**

[106] H. Kattner, M. Buback, 'Chain-Length-Dependent Termination of Styrene Bulk Homopolymerization Studied by SP−PLP−EPR', *Macromolecules* **2015**, *48*, 309–315.

[107] H. Kattner, P. Drawe, M. Buback, 'Chain-Length-Dependent Termination of Sodium Methacrylate Polymerization in Aqueous Solution Studied by SP-PLP-EPR', *Macromolecules* **2017**, *50*, 1386–1393.

[108] J. Barth, M. Buback, 'SP-PLP-EPR-A Novel Method for Detailed Studies into the Termination Kinetics of Radical Polymerization', *Macromolecular Reaction Engineering* **2010**, *4*, 288–301.

[109] J. Barth, M. Buback, 'SP-PLP-EPR Investigations into the Chain-Length-Dependent Termination of Methyl Methacrylate Bulk Polymerization', *Macromolecular Rapid Communications* **2009**, *30*, 1805–1811.

[110] G. Johnston-Hall, A. Theis, M. J. Monteiro, T. P. Davis, M. H. Stenzel, C. Barner-Kowollik, 'Accessing Chain Length Dependent Termination Rate Coefficients of Methyl Methacrylate (MMA) via the Reversible Addition Fragmentation Chain Transfer (RAFT) Process', *Macromolecular Chemistry and Physics* **2005**, *206*, 2047–2053.

[111] G. Johnston-Hall, M. H. Stenzel, T. P. Davis, C. Barner-Kowollik, M. J. Monteiro, 'Chain Length Dependent Termination Rate Coefficients of Methyl Methacrylate (MMA) in the Gel Regime: Accessing $Kt^{i,i}$ Using Reversible

Addition-Fragmentation Chain Transfer (RAFT) Polymerization', *Macromolecules* **2007**, *40*, 2730–2736.

[112] J. Barth, M. Buback, P. Hesse, T. Sergeeva, 'Chain-Length-Dependent Termination in n -Butyl Methacrylate and Tert -Butyl Methacrylate Bulk Homopolymerizations Studied via SP-PLP-ESR', *Macromolecules* **2009**, *42*, 481–488.

[113] N. Sörensen, 'Kinetics and Mechanism of Cu-Catalyzed Atom Transfer Radical Polymerization', Georg-August-University Göttingen, **2015**

[114] G. Johnston-Hall, M. J. Monteiro, 'Diffusion Controlled Termination of Linear Polystyrene Radicals in Linear, 4-Arm, and 6-Arm Star Polymer Matrices in Dilute, Semidilute, and Concentrated Solution Conditions', *Macromolecules* **2008**, *41*, 727–736.

[115] A. Theis, T. P. Davis, M. H. Stenzel, C. Barner-Kowollik, 'Probing the Reaction Kinetics of Vinyl Acetate Free Radical Polymerization via Living Free Radical Polymerization (MADIX)', *Polymer* **2006**, *47*, 999–1010.

[116] A. Theis, T. P. Davis, M. H. Stenzel, C. Barner-Kowollik, 'Mapping Chain Length and Conversion Dependent Termination Rate Coefficients in Methyl Acrylate Free Radical Polymerization', *Macromolecules* **2005**, *38*, 10323–10327.

[117] M. Buback, P. Hesse, T. Junkers, T. Theis, P. Vana, 'Chain-Length-Dependent Termination in Acrylate Radical Polymerization Studied via Pulsed-Laser-Initiated RAFT Polymerization', *Australian Journal of Chemistry* **2007**, *60*, 779.

[118] H. Kattner, M. Buback, 'Propagation and Chain-Length-Dependent Termination Rate Coefficients Deduced from a Single SP–PLP–EPR Experiment', *Macromolecules* **2016**, *49*, 3716–3722.

[119] M. L. Coote, L. P. M. Johnston, T. P. Davis, 'Copolymerization Propagation Kinetics of Styrene and Methyl Methacrylate-Revisited. 2. Kinetic Analysis', *Macromolecules* **1997**, *30*, 8191–8204.

[120] T. P. Davis, K. F. O'Driscoll, M. C. Piton, M. A. Winnik, 'Copolymerization Propagation Kinetics of Styrene with Alkyl Methacrylates', *Macromolecules* **1990**, *23*, 2113–2119.

[121] E. Vidović, K. Sarić, Z. Janović, 'Copolymerization of Styrene with Dodecyl Methacrylate and Octadecyl Methacrylate', *Croatica chemica acta* **2002**, *75*, 769–782.

[122] J. P. A. Heuts, M. L. Coote, T. P. Davis, L. P. M. Johnston in *Controlled Radical Polymerization*, (Ed.: K. Matyjaszewski), ACS Symposium Series, American Chemical Society, Washington, DC, **1998**.

[123] M. Buback, R. G. Gilbert, R. A. Hutchinson, B. Klumperman, F.-D. Kuchta, B. G. Manders, K. F. O'Driscoll, G. T. Russell, J. Schweer, 'Critically Evaluated Rate Coefficients for Free-Radical Polymerization, 1. Propagation Rate Coefficient for Styrene', *Macromolecular Chemistry and Physics* **1995**, *196*, 3267–3280.

[124] M. Buback, U. Geers, C. H. Kurz, J. Heyne, 'Propagation Rate Coefficients in Free-Radical Homopolymerizations of Butyl Methacrylate and Dodecyl Methacrylate', *Macromolecular Chemistry and Physics* **1997**, *198*, 3451–3464.

[125] J. A. Nelder, R. Mead, 'A Simplex Method for Function Minimization', *The Computer Journal* **1965**, *7*, 308–313.

[126] F. Gao, L. Han, 'Implementing the Nelder-Mead Simplex Algorithm with Adaptive Parameters', *Computational Optimization and Applications* **2012**, *51*, 259–277.

[127] D. Foreman-Mackey, D. W. Hogg, D. Lang, J. Goodman, 'Emcee : The MCMC Hammer', *Publications of the Astronomical Society of the Pacific* **2013**, *125*, 306–312.

[128] J. Goodman, J. Weare, 'Ensemble Samplers with Affine Invariance', *Communications in Applied Mathematics and Computational Science* **2010**, *5*, 65–80.

[129] T. Otsu, T. Ito, M. Imoto, 'The Reactivities of Alkyl Methacrylates in Their Radical Polymerizations', *Journal of Polymer Science Part B: Polymer Letters* **1965**, *3*, 113–117.

[130] L. H. Yee, J. P. A. Heuts, T. P. Davis, 'Copolymerization Propagation Kinetics of Dimethyl Itaconate and Styrene: Strong Entropic Contributions to the Penultimate Unit Effect', *Macromolecules* **2001**, *34*, 3581–3586.

[131] H. Nakamura, M. Seno, H. Tanaka, T. Sato, 'Kinetic and ESR Studies on the Radical Polymerization. Radical-initiated Copolymerization of the Diethyl Itaconate- SnCl4 Complex and Styrene', *Die Makromolekulare Chemie* **1993**, *194*, 1773–1783.

[132] S. Beuermann, M. Buback, T. P. Davis, R. G. Gilbert, R. A. Hutchinson, O. F. Olaj, G. T. Russell, J. Schweer, A. M. van Herk, 'Critically Evaluated Rate Coefficients for Free-Radical Polymerization, 2. Propagation Rate Coefficients for Methyl Methacrylate', *Macromolecular Chemistry and Physics* **1997**, *198*, 1545–1560.

[133] M. Buback, C. Kowollik, 'Termination Kinetics of Methyl Methacrylate Free-Radical Polymerization Studied by Time-Resolved Pulsed Laser Experiments', *Macromolecules* **1998**, *31*, 3211–3215.

[134] O. F. Olaj, P. Vana, 'Chain-Length Dependent Termination in Pulsed-Laser Polymerization, 6. The Evaluation of the Rate Coefficient of Bimolecular Terminationkt for the Reference System Methyl Methacrylate in Bulk at 25°C', *Macromolecular Rapid Communications* **1998**, *19*, 533–538.

[135] J. P. A. Heuts, D. Kukulj, D. J. Forster, T. P. Davis, 'Copolymerization of Styrene and Methyl Methacrylate in the Presence of a Catalytic Chain Transfer Agent', *Macromolecules* **1998**, *31*, 2894–2905.

[136] M. L. Coote, 'The Origin of the Penultimate Unit Effect in Free-Radical Copolymerization', UNSW Sydney, **1999**

[137] G. Clouet, P. Chaffanjon, 'Rate Constants in the Free-Radical Polymerization of Perdeuterated Styrene', *Journal of Macromolecular Science: Part A - Chemistry* **1990**, *27*, 193–212.

A. Appendix

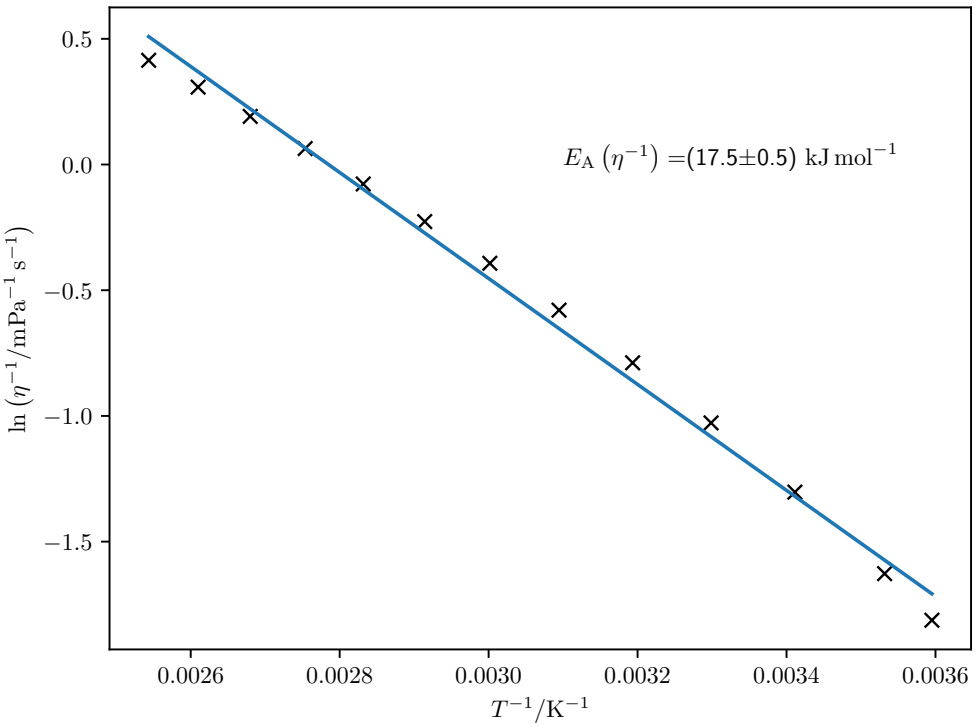

Figure A.1.: Arrhenius plot of the fluidity of bulk DEI.

A.1. MATLAB script

```
clc
clear all
close all
addpath('C:\Users\emeyer.MMC-NET\Documents\Promotion_Enno_Meyer\Matlab_easyspin\easyspin-5.2.33\easyspin')
easyspin

filename = 'C:\Users\emeyer.MMC-NET\Documents\Promotion_Enno_Meyer\Forschung\Styrol_DMA\EPR_Daten\2022_03_07\PLP_4_Sty-d8_DMA_0.25_99.75_0.1M_DCP_293K.txt';
startRow = 2;

formatSpec = '%10f%21f%f%[^\n\r]';
fileID = fopen(filename,'r');

textscan(fileID, '%[^\n\r]', startRow-1, 'WhiteSpace', '', 'ReturnOnError', false, 'EndOfLine', '\r\n');
dataArray = textscan(fileID, formatSpec, 'Delimiter', '', 'WhiteSpace', '', 'TextType', 'string', 'EmptyValue', NaN, 'ReturnOnError', false);
fclose(fileID);
spektrumdma = [dataArray{1:end-1}];

B = dataArray{:, 2};
spc = dataArray{:, 3};
%plot(B,spc)
clearvars filename delimiter formatSpec fileID dataArray ans;

Exp.ModAmp = 0.3;
Exp.mwFreq = 9.419034; % GHz
Exp.Range = [330 350]; %mT


%System 1 Definition
%Styrene-d8
Sys1.g = 1.99137;
A1 =0.598124;%MHz
%A1= mt2mhz(A1,2.0023193043617);
A2 =5.82129;%MHz
%A2= mt2mhz(A2,2.0023193043617);
Sys1.Nucs = '2H,2H';
Sys1.A = [A1 A2];
Sys1.n = [2 1];
Sys1.lw = [0.463654 0.476]; %mT

%System 2 Definition
%DMA Conformer A
Sys2.g = 1.99137;
A1 =1.58;%mT
A1= mt2mhz(A1,2.0023193043617);
A2 =0.63;%mT
A2= mt2mhz(A2,2.0023193043617);
A3 =2.23;%mT
A3= mt2mhz(A3,2.0023193043617);
Sys2.Nucs = '1H,1H,1H';
Sys2.A = [A1 A2 A3];
Sys2.n = [1 1 3];
Sys2.lw = [0.163654]; %mT

%System 3 Definition
%DMA Conformer B
Sys3.g = 1.99137;
A1 =2.35;%mT
A1= mt2mhz(A1,2.0023193043617);
A2 =0.02;%mT
A2= mt2mhz(A2,2.0023193043617);
A3 =2.23;%mT
A3= mt2mhz(A3,2.0023193043617);
```

```
Sys3.Nucs = '1H,1H,1H';
Sys3.A = [A1 A2 A3];
Sys3.n = [1 1 3];
Sys3.lw = [0.163654]; %mT


%Variation of Parameters

Vary1.g = [0.02];
Vary2.g = [0.02];
Vary3.g = [0.02];

Sys1.weight = 0.5;
Sys2.weight = 0.25;
Sys3.weight = 1-Sys1.weight-Sys2.weight;

Vary1.weight = 0.4;
Vary2.weight = 0.2;
Vary3.weight = 0.2;

%Fitting
SimOpt.Method = 'perturb';
FitOpt.Method = 'genetic fcn';
FitOpt.Scaling = 'maxabs';
esfit('garlic',spc,{Sys1,Sys2,Sys3},{Vary1,Vary2,Vary3},Exp,SimOpt,FitOpt);
```

A.2. DRACO code

DRACO.py

```
#!/usr/bin/python3
# All mole fractions etc refer to Monomer 1
import csv
from dataclasses import dataclass
from functools import cached_property
from typing import Callable
from typing_extensions import Self
import corner
import lmfit
import matplotlib as mpl
import numpy as np
from lmfit import Minimizer, Parameter, Parameters, fit_report, minimize
from matplotlib import pyplot as plt
from scipy.constants import R
from monomers import DMA, MMA, Monomer, Styrene_d8, DEI

# In case you want to use Arrhenius expressions, enter the temperature here
T_meas = 273.15 + 37.6

# Define your monomers
monomer_1 = Styrene_d8
monomer_2 = MMA


def kp_arrhenius(monomer: Monomer, temp: float = T_meas):
    return monomer.kp_A * np.exp(-monomer.kp_E_A / (R * temp))


def kp_constant(monomer: Monomer):
```

```
    if monomer is Styrene_d8:
        return 68.8
    if monomer is DMA:
        return 432.5
    if monomer is DEI:
        return 7.37
    if monomer is MMA:
        return 454.2
    raise RuntimeError(f"No constant kp value defined for monomer {Monomer}")

# Decide whether to use Arrhenius expressions or manually defined kp values. Typically manually defined values work better.
kp = kp_constant


def normalize(data: np.ndarray) -> np.ndarray:
    return (data - np.min(data)) / (np.max(data) - np.min(data))


def scale_uncertainty(data: np.ndarray, unc: np.ndarray) -> np.ndarray:
    return np.sqrt((1 / (np.max(data) - np.min(data)) * unc) ** 2 + (
            (data - np.max(data)) / (np.max(data) - np.min(data)) ** 2 * unc[np.argmin(data)]) ** 2 + (
                    (np.min(data) - data) / (np.max(data) - np.min(data)) ** 2 * unc[np.argmax(data)]) ** 2)


@dataclass(frozen=True)
class Dataset:
    f: np.ndarray
    observable: np.ndarray
    uncertainty: np.ndarray
    equation: Callable[[np.ndarray, Parameters], np.ndarray]

    @cached_property
    def normalized_observable(self) -> np.ndarray:
        return normalize(self.observable)

    @cached_property
    def normalized_uncertainty(self) -> np.ndarray:
        return scale_uncertainty(self.observable, self.uncertainty)


# DEFINE SHORTCUT EQUATIONS FOR THE MODEL
def r_avg(monomer: Monomer, f_1: np.ndarray, pars: Parameters) -> np.ndarray:
    f_2 = 1 - f_1
    if monomer is monomer_1:
        r_prime = pars['rprime_1'].value
        r_1 = pars['r_1'].value
        return r_prime * (r_1 * f_1 + f_2) / (r_prime * f_1 + f_2)
    else:
        r_prime = pars['rprime_2'].value
        r_2 = pars['r_2'].value
        return r_prime * (r_2 * f_2 + f_1) / (r_prime * f_2 + f_1)


def kp_avg(monomer: Monomer, f_1: np.ndarray, pars: Parameters) -> np.ndarray:
    f_2 = 1 - f_1
    if monomer is monomer_1:
        kp_monomer = pars['kp_1']
        r_1 = pars['r_1'].value
        s_1 = pars['s_1'].value
        return kp_monomer * (r_1 * f_1 + f_2) / (r_1 * f_1 + f_2 / s_1)
    else:
        kp_monomer = pars['kp_2']
        r_2 = pars['r_2'].value
        s_2 = pars['s_2'].value
        return kp_monomer * (r_2 * f_2 + f_1) / (r_2 * f_2 + f_1 / s_2)

# READ DATA AND STORE IN DATACLASS
```

```
97  # Data for propagating radical fraction
98
99  data_radical_fraction = np.genfromtxt('Exp_data/Sty_MMA/Sty_MMA_Phi.txt',skip_header=1)
100
101 f_1_Phi = data_radical_fraction[:, 0]
102 data = data_radical_fraction[:, 1]
103 unc = data*0.05
104
105
106 def Phi_vs_f_1(f_1: np.ndarray, pars: Parameters) -> np.ndarray:
107     f_2 = (1 - f_1)
108     term_1 = kp_avg(monomer_2, f_1, pars) * r_avg(monomer_1, f_1, pars) * f_1
109     term_2 = kp_avg(monomer_1, f_1, pars) * r_avg(monomer_2, f_1, pars) * f_2
110     return term_1 / (term_1 + term_2)
111
112
113 phi_data = Dataset(
114     f=f_1_Phi,
115     observable=data,
116     uncertainty=unc,
117     equation=Phi_vs_f_1,
118 )
119
120 # Data for copolmyer composition
121
122 data_composition= np.genfromtxt('Exp_data/Sty_MMA/Sty_MMA_composition.txt',skip_header=1)
123 f_1_composition = data_composition[:, 0]
124 composition = data_composition[:, 1]
125 unc_comp = composition * 0.05
126
127
128 def composition_vs_f_1(f_1: np.ndarray, pars: Parameters) -> np.ndarray:
129     f_2 = (1 - f_1)
130     numerator = r_avg(monomer_1, f_1, pars) * f_1 ** 2 + f_1 * f_2
131     denominator = r_avg(monomer_1, f_1, pars) * f_1 ** 2 + 2 * f_1 * f_2 + r_avg(monomer_2, f_1, pars) * f_2 ** 2
132     return numerator / denominator
133
134
135 comp_data = Dataset(
136     f=f_1_composition,
137     observable=composition,
138     uncertainty=unc_comp,
139     equation=composition_vs_f_1,
140 )
141
142 # Data for kpcopo
143
144 data_kpcopo= np.genfromtxt('Exp_data/Sty_MMA/Sty_MMA_kpcopo.txt',skip_header=1)#Sty_MMA
145 f_1_kpcopo = data_kpcopo[:, 0]
146 kpcopo = data_kpcopo[:, 1]
147 unc_kpcopo = kpcopo * 0.05
148
149
150 def kpcopo_vs_f_1(f_1: np.ndarray, pars: Parameters) -> np.ndarray:
151     f_2 = (1 - f_1)
152     numerator = r_avg(monomer_1, f_1, pars) * f_1 ** 2 + 2 * f_1 * f_2 + r_avg(monomer_2, f_1, pars) * f_2 ** 2
153     denominator = (
154             (r_avg(monomer_1, f_1, pars) * f_1 / kp_avg(monomer_1, f_1, pars))
155             + (r_avg(monomer_2, f_1, pars) * f_2 / kp_avg(monomer_2, f_1, pars))
156     )
157     return numerator / denominator
158
159
160 kpcopo_data = Dataset(
161     f=f_1_kpcopo,
162     observable=kpcopo,
163     uncertainty=unc_kpcopo,
```

```
    equation=kpcopo_vs_f_1,
)


# MODEL PARAMETERS
# Explicit penultimate model
explicit_model_params = Parameters()
explicit_model_params.add('r_1', value=1, min=0.01, max=100)
explicit_model_params.add('r_2', value=1, min=0.01, max=100)
explicit_model_params.add('rprime_1', value=1, min=0.01, max=100)
explicit_model_params.add('rprime_2', value=1, min=0.01, max=100)
explicit_model_params.add('s_1', value=1, min=0.01, max=100)
explicit_model_params.add('s_2', value=1, min=0.01, max=100)
explicit_model_params.add('kp_1', value=kp(monomer_1), min=kp(monomer_1)*0.90, max=kp(monomer_1)*1.10,vary=True)
explicit_model_params.add('kp_2', value=kp(monomer_2), min=kp(monomer_2)*0.90, max=kp(monomer_2)*1.10,vary=True)

# Implicit penultimate model
implicit_model_params = Parameters()
implicit_model_params.add('r_1', value=1, min=0.01, max=100)
implicit_model_params.add('r_2', value=1, min=0.01, max=100)
implicit_model_params.add('rprime_1', expr='r_1')
implicit_model_params.add('rprime_2', expr='r_2')
implicit_model_params.add('s_1', value=1, min=0.01, max=100)
implicit_model_params.add('s_2', value=1, min=0.01, max=100)
implicit_model_params.add('kp_1', value=kp(monomer_1), min=kp(monomer_1)*0.90, max=kp(monomer_1)*1.10,vary=True)
implicit_model_params.add('kp_2', value=kp(monomer_2), min=kp(monomer_2)*0.90, max=kp(monomer_2)*1.10,vary=True)

# Terminal model
terminal_model_params = Parameters()
terminal_model_params.add('r_1', value=1, min=0.01, max=100)
terminal_model_params.add('r_2', value=1, min=0.01, max=100)
terminal_model_params.add('rprime_1', expr='r_1')
terminal_model_params.add('rprime_2', expr='r_2')
terminal_model_params.add('s_1', expr='1')
terminal_model_params.add('s_2', expr='1')
terminal_model_params.add('kp_1', value=kp(monomer_1), min=kp(monomer_1)*0.90, max=kp(monomer_1)*1.10,vary=True)
terminal_model_params.add('kp_2', value=kp(monomer_2), min=kp(monomer_2)*0.90, max=kp(monomer_2)*1.10,vary=True)

# Choose your model here
params = explicit_model_params


# SET UP AND PERFORM THE FIT WITH LMFIT
# Defne the objective function to be minimised. In order to fit only a subset of observables, comment the unneeded ones in the
↪  concatenate function.
def objective(pars: Parameters, phi: Dataset, comp: Dataset, kpcopo: Dataset) -> np.ndarray:
    def residuals(dataset: Dataset, model_iteration: np.ndarray) -> np.ndarray:
        chi = (dataset.normalized_observable - normalize(model_iteration)) / dataset.normalized_uncertainty
        return chi ** 2 / dataset.observable.size

    return np.concatenate(
        (
            residuals(phi, model_iteration=Phi_vs_f_1(phi.f, pars)),
            residuals(comp, model_iteration=composition_vs_f_1(comp.f, pars)),
            residuals(kpcopo, model_iteration=kpcopo_vs_f_1(kpcopo.f, pars)),
        )
    )

# Define a class for storing the obtained results
@dataclass(frozen=True)
class FitParameterResult:
    name: str
    value: float
    delta: float

    @classmethod
    def from_param(cls, param: Parameter) -> Self:
```

```
230             return cls(
231                 name=param.name,
232                 value=param.value,
233                 delta=param.stderr,
234             )
235
236
237     for monomer in (monomer_1, monomer_2):
238         print("kp initial", monomer.name, kp(monomer))
239     print()
240
241     # Run the fit
242     fit_args = (phi_data, comp_data, kpcopo_data)
243     minimizer = Minimizer(objective, params, fcn_args=fit_args)
244     fit = minimizer.minimize(
245         method='nelder', options={'adaptive': True, 'fatol': 1e-100, 'xatol': 0.001}, max_nfev=1000000
246     )
247
248     print(fit_report(fit))
249
250     # Calculate confidence ellipsoids
251     mc = minimize(objective, fit.params, method='emcee', args=fit_args, nan_policy='omit', is_weighted=True, progress=False)
252
253     # Store obtained results
254     r_1 = FitParameterResult.from_param(fit.params["r_1"])
255     r_2 = FitParameterResult.from_param(fit.params["r_2"])
256     rprime_1 = FitParameterResult.from_param(fit.params["rprime_1"])
257     rprime_2 = FitParameterResult.from_param(fit.params["rprime_2"])
258     s_1 = FitParameterResult.from_param(fit.params["s_1"])
259     s_2 = FitParameterResult.from_param(fit.params["s_2"])
260     kp_1 = FitParameterResult.from_param(fit.params["kp_1"])
261     kp_2 = FitParameterResult.from_param(fit.params["kp_2"])
262
263     ########################################
264     # Calculate and print individual propagation constants
265
266     print('Values of determined kp in L/(mol*s)')
267     print('kp 112', kp_1.value / r_1.value)
268     print('kp 221', kp_2.value / r_2.value)
269     print('kp 211', kp_1.value * s_1.value)
270     print('kp 122', kp_2.value * s_2.value)
271     print('kp 212', kp_1.value * s_1.value / rprime_1.value)
272     print('kp 121', kp_2.value * s_2.value / rprime_2.value)
273
274     # Write results to file
275     with open('results.txt', 'w') as f:
276         csv_writer = csv.DictWriter(f, fieldnames=["name", "value", "delta"])
277         csv_writer.writeheader()
278         for param in (r_1, r_2, rprime_1, rprime_2, s_1, s_2, kp_1, kp_2):
279             csv_writer.writerow(dict(name=param.name, value=param.value, delta=param.delta))
280
281     ########################################
282     # CREATE PLOTS
283
284     # These style options require a LaTeX installation to be in the path. They can be turned off if necessary. If so, change the labels
    ↪  or you will get errors
285     mpl.rcParams['text.usetex'] = True
286     mpl.rc('text.latex', preamble=r'\usepackage{siunitx}\usepackage{amsmath}')
287     mpl.rcParams['mathtext.fontset'] = 'cm'
288
289
290     fig, axs = plt.subplots(nrows=2, ncols=3)
291     f_grid = np.linspace(0, 1, 1000)
292
293     def plot_dataset(
294             axis: plt.Axes, f_grid: np.ndarray, dataset: Dataset, params: Parameters, *, scaled: bool = False
295     ) -> None:
```

```
        model = dataset.equation(f_grid, params)
        if scaled:
            model = normalize(model)
            y = dataset.normalized_observable
            error = dataset.normalized_uncertainty
        else:
            y = dataset.observable
            error = dataset.uncertainty

        axis.plot(f_grid, model)
        axis.errorbar(dataset.f, y, yerr=error, fmt="kx", ms=1)


    # Row 1: unchanged data
    axs[0, 0].set_ylabel("unchanged")
    plot_dataset(axs[0, 0], f_grid, phi_data, fit.params)
    plot_dataset(axs[0, 1], f_grid, comp_data, fit.params)
    plot_dataset(axs[0, 2], f_grid, kpcopo_data, fit.params)

    # Row 2: normalized data
    axs[1, 0].set_ylabel("normalized")
    plot_dataset(axs[1, 0], f_grid, phi_data, fit.params, scaled=True)
    plot_dataset(axs[1, 1], f_grid, comp_data, fit.params, scaled=True)
    plot_dataset(axs[1, 2], f_grid, kpcopo_data, fit.params, scaled=True)

    # Column labels
    axs[0, 0].set_title(r'$\phi_1$')
    axs[0, 1].set_title(r'$F_1$')
    axs[0, 2].set_title(r'$\langle k_{\mathrm{p}}\rangle/\si{\litre\per\mole\per\second}$')

    fig.tight_layout()
    fig.savefig('plot_grid.pdf')
    fig.show()

    ########################################
    # CONFIDENCE ELLIPSOIDS AND ERRORS

    # Plot the acceptance fraction of the emcee method wlaker. It should be roughly between 0.2 and 0.5
    plt.figure()
    plt.plot(mc.acceptance_fraction, 'o')
    plt.xlabel('walker')
    plt.ylabel('acceptance fraction')
    plt.show()

    emcee_plot = corner.corner(mc.flatchain, labels=(r'$r_1$',r'$r_2$',r'$r^\prime_1$',r'$r^\prime_2$',r'$s_1$', r'$s_2$',
    ↪  r'$k_{\mathrm{p}}^{111}$',
    ↪  r'$k_{\mathrm{p}}^{222}$'),label_kwargs=dict(fontsize=16),truths=list(mc.params.valuesdict().values()),quantiles=[0.95])
    emcee_plot.show()
    emcee_plot.savefig('emcee_plot.pdf')
    print('median of posterior probability distribution')
    print('---------------------------------------')
    print(fit_report(mc.params))
```

monomers.py

```
from dataclasses import dataclass

import numpy as np


@dataclass(frozen=True)
class Monomer:
    name: str
```

```
    kp_A: float
    kp_E_A: float


Styrene = Monomer("Sty", kp_A=10**7.63, kp_E_A=32510)
Styrene_d8 = Monomer("Sty-d8", kp_A=3.63*10**7, kp_E_A=31500)
DEI = Monomer("DEI", kp_A=1.1 * 10**4, kp_E_A=17500)

# kp data for MMA, taken from Buback 1997 Macromol. Chem. Phys. 198,1545-1560 (1997)
MMA = Monomer("MMA", kp_A=10**6.425, kp_E_A=22330)

# kp data for DMA, taken from Buback 1997 Macromol. Chem. Phys. 198,3451-3464 (1997)
DMA = Monomer("DMA", kp_A=np.exp(14.71), kp_E_A=21100)
```

A.3. Results of DRACO tests

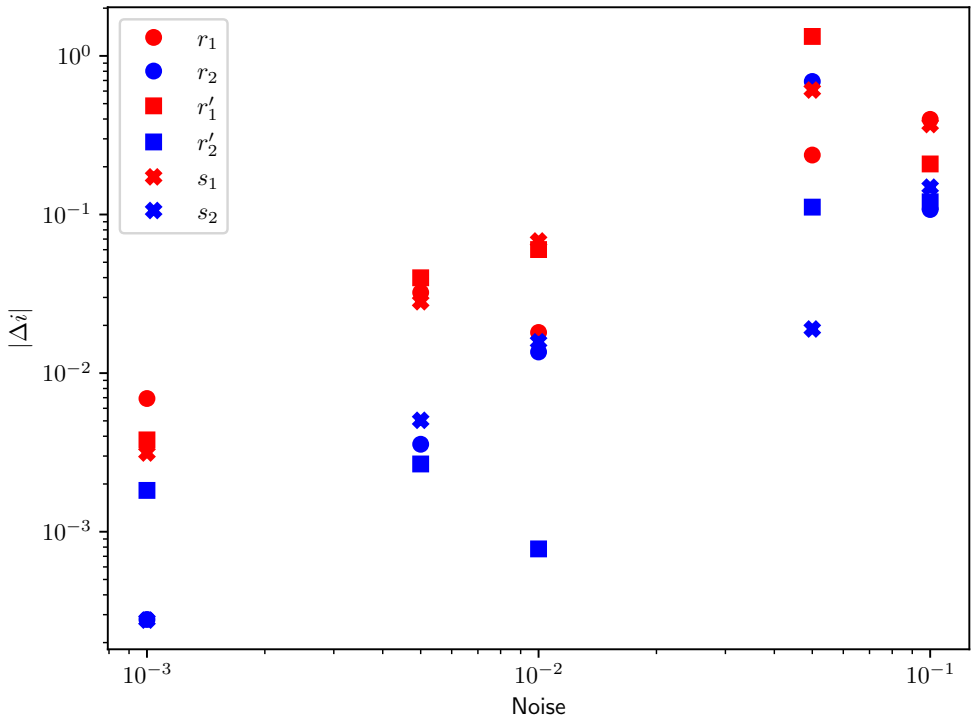

Figure A.2.: Test 2: Absolute values of the deviation of the obtained RR from the true values in table 6.5 as a function of noise added to the data with a samle size of 50.

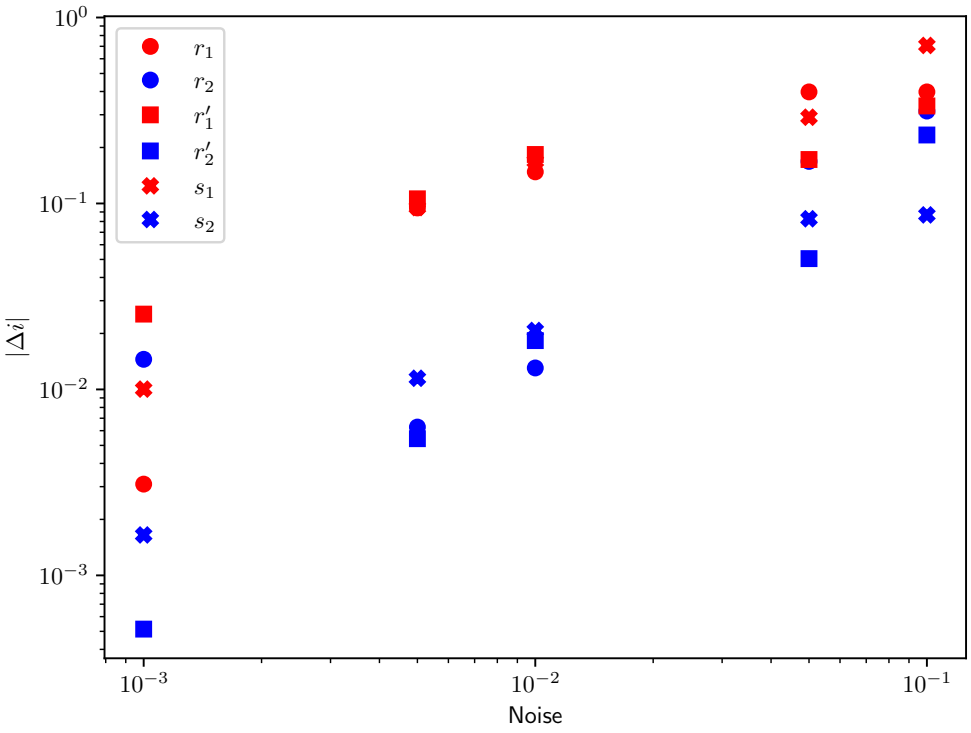

Figure A.3.: Test 2: Absolute values of the deviation of the obtained RR from the true values in table 6.5 as a function of noise added to the data with a samle size of 10000.

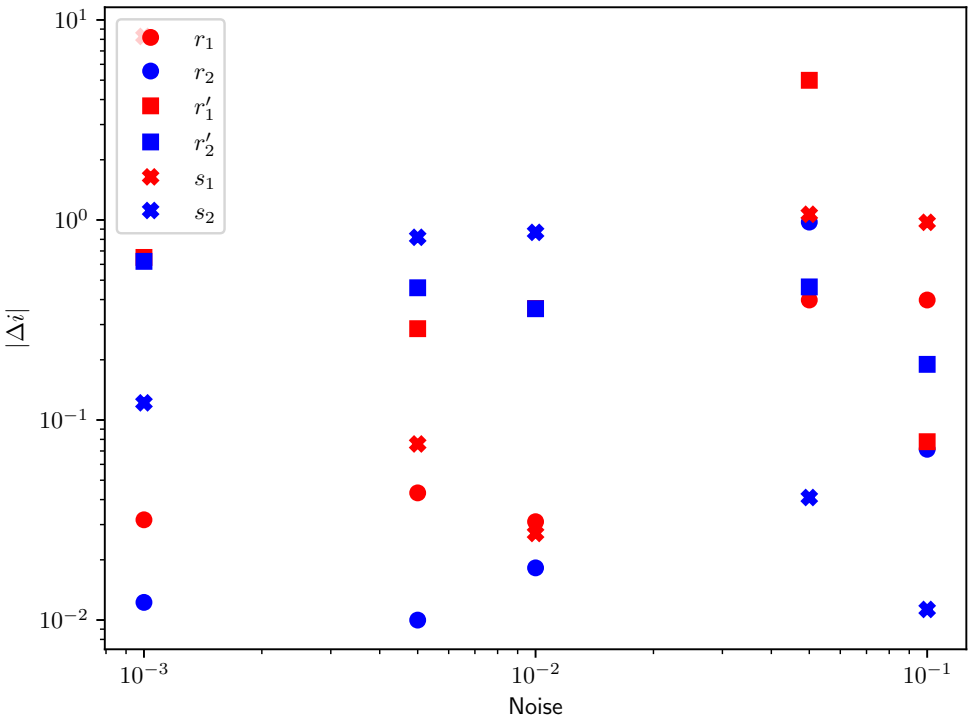

Figure A.4.: Test 3: Absolute values of the deviation of the obtained RR from the true values in table 6.5 as a function of noise added to the data when not including the PRF in the fit for a sample size of 50.

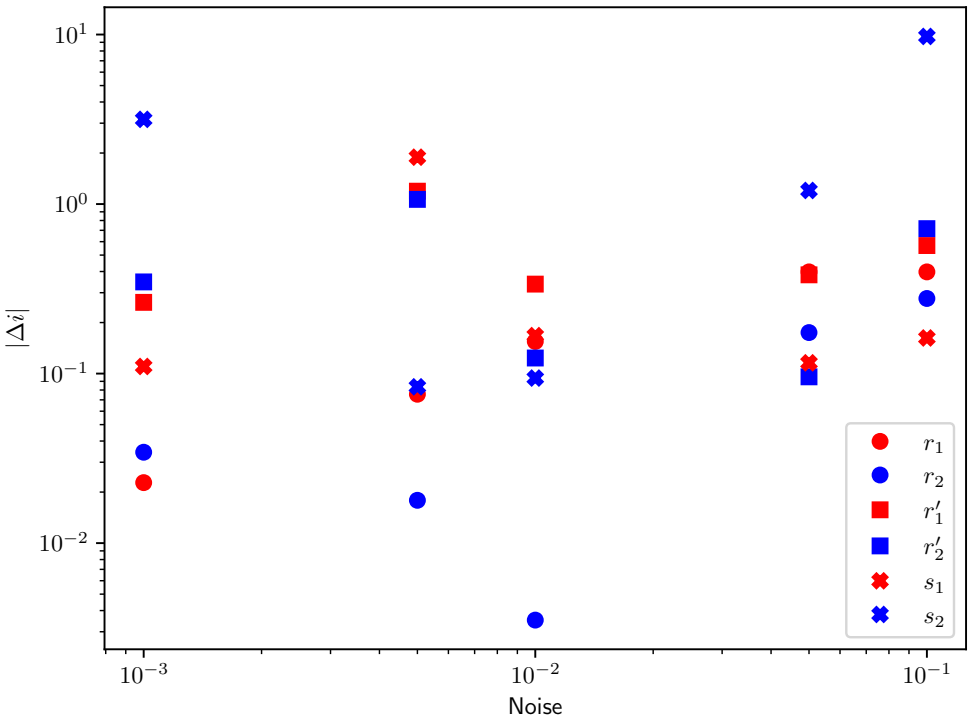

Figure A.5.: Test 3: Absolute values of the deviation of the obtained RR from the true values in table 6.5 as a function of noise added to the data when not including the PRF in the fit for a sample size of 10000.

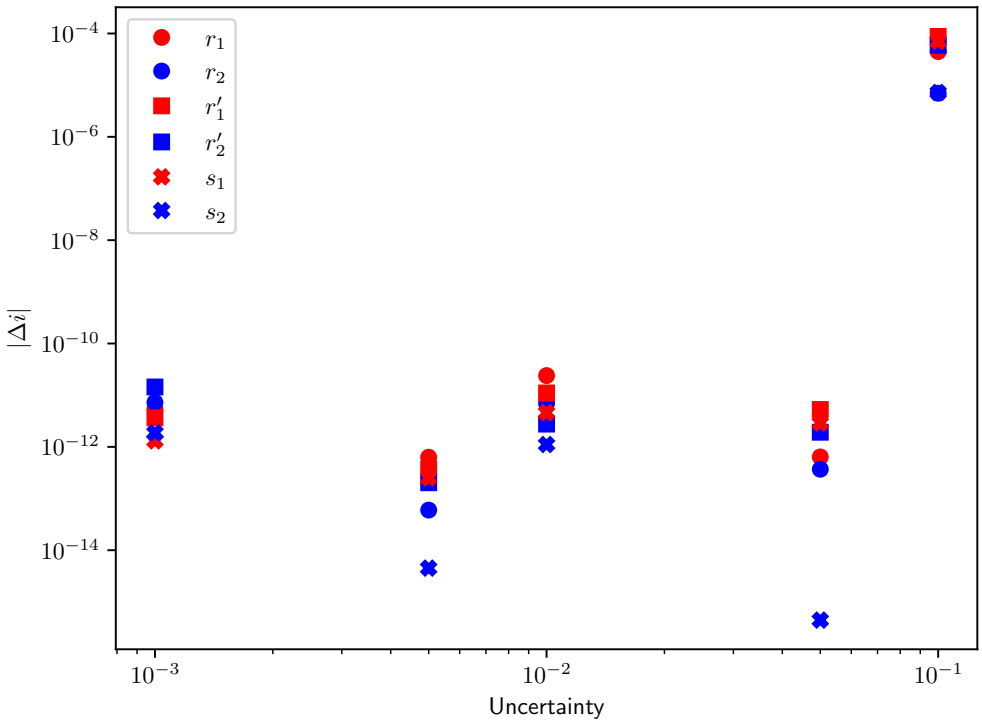

Figure A.6.: Test 4: Absolute values of the deviation of the obtained RR from the true values in table 6.5 as a function of the uncertainty given to perfectly accurate data for a sample size of 50.

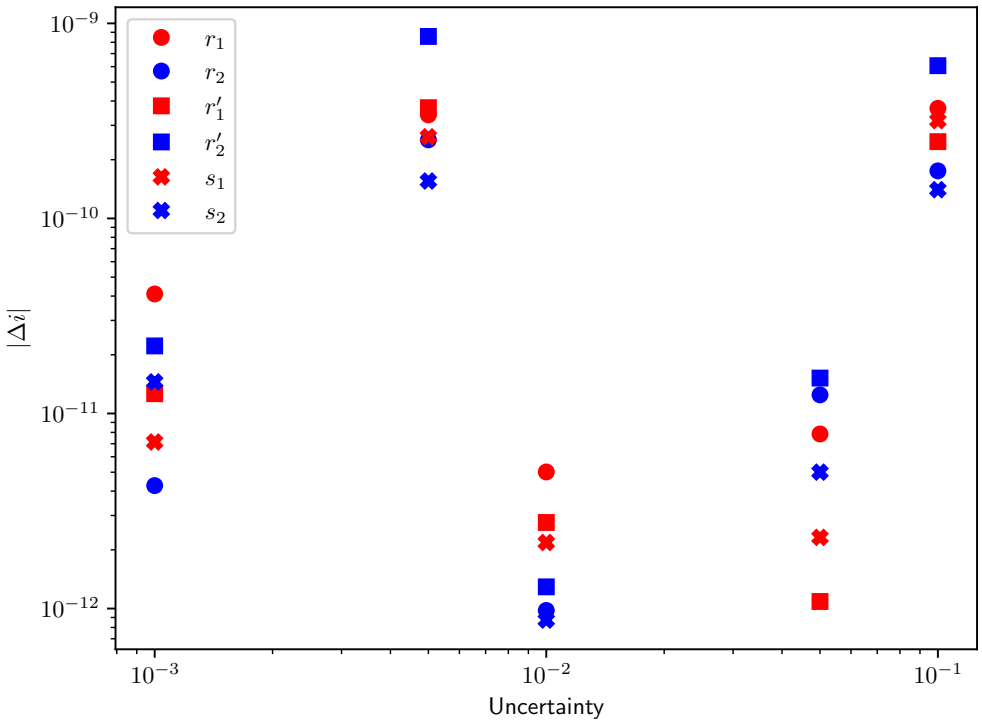

Figure A.7.: Test 4: Absolute values of the deviation of the obtained RR from the true values in table 6.5 as a function of the uncertainty given to perfectly accurate data for a sample size of 10000.

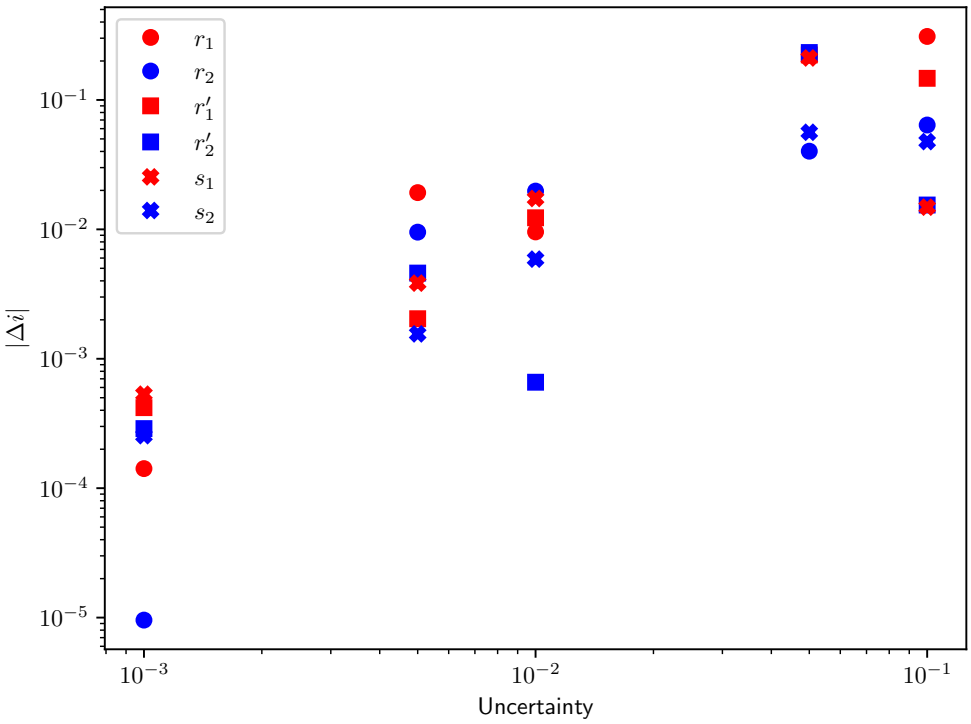

Figure A.8.: Test 5: Absolute values of the deviation of the obtained RR from the true values in table 6.5 as a function of the uncertainty and noise added to the data for a sample size of 50.

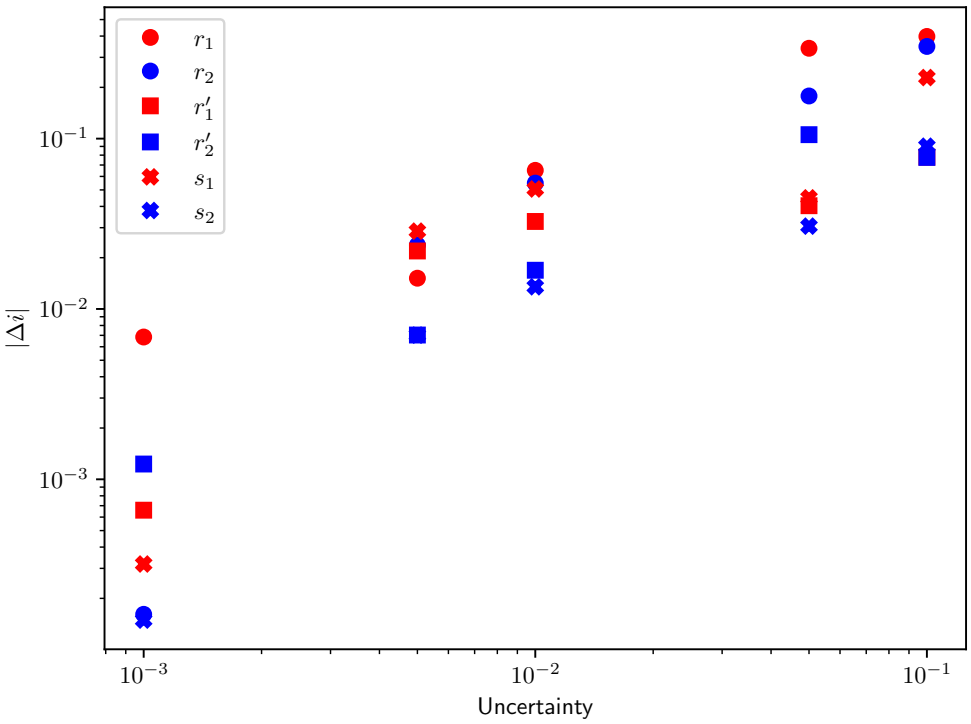

Figure A.9.: Test 5: Absolute values of the deviation of the obtained RR from the true values in table 6.5 as a function of the uncertainty and noise added to the data for a sample size of 10000.

A.4. Software versions

python	3.10.10
corner	2.2.2
lmfit	1.2.0
matplotlib	3.7.1
scipy	1.10.1
MATLAB	R2020a
easyspin	5.2.33

List of Figures

List of Tables

List of mathematical symbols

Symbol	Description
χ	conversion
E	energy
h	Planck constant
ν	frequency
k_B	Boltzmann constant
A	pre-exponential Arrhenius factor
E_A	Arrhenius activation energy
f_A	fraction of monomer A in the reaction feed
F_A	fraction of monomer A in the copolymer
ϕ_A	propagating radical fraction of monomer A
k_p	propagation rate coefficient
k_p^ij	propagation rate coefficient of a macroradical with monomer i at the end, attacking monomer j
$\langle k_\mathrm{p} \rangle$	overall rate coefficient in a copolymerisation
k_t	termination rate coefficient

Symbol	Description
$k_t^{i,j}$	termination rate coefficient for macroradicals with chain lengths i and j
$k_t^{1,1}$	termination rate coefficient for two monomer radicals
k_t^0	termination rate coefficient for two (hypothetically) coiled monomer radicals
α_s	composite model parameter or the short-chain regime
α_l	composite model parameter or the long-chain regime
i_c	crossover-chainlength

List of Abbrevations

DMI dimethyl itaconate

DEI diethyl itaconate

DPI di-*n*-propyl itaconate

DBI di-*n*-butyl itaconate

DCHI dicyclohexyl itaconate

MA methyl acrylate

BA butyl acrylate

BMA butyl methacrylate

BzMA benzyl methacrylate

DMA dodecyl methacrylate

2-EHMA 2-ethylhexyl methacrylate

MMA methyl methacrylate

NaMA sodium methacrylate

PnMA n-pentyl methacrylate

TMAEA trimethylaminoethyl acrylate chloride

Sty styrene

Sty-h8 styrene-h8

Sty-d8 styrene-d8

MAn maleic anhydride

AIBN azobisisobutyronitrile

DCP Dicumylperoxide

DMPA 2,2-Dimethoxy-2-phenylacetophenone

MMMP 2-Methyl-4′-(methylthio)-2-morpholinopropiophenone

TEMPO 2,2,6,6-Tetramethylpiperidin-1-oxyl

VAc vinyl acetate

VPiv vinyl pivalate

DME 1,2-dimethoxyethane

TD translational diffusion

SD segmental diffusion

CTA chain transfer agent

MCR mid-chain radical

GMM geometric mean model

HMM harmonic mean model

DMM diffusion mean model

DRACO determining reactivity ratios with a conjoined scalable fit

PRF propagating radical fraction

PUM penultimate model

RR reactivity ratios

TM terminal model

EPR electron paramagnetic resonance

PLP pulsed laser polymerisation

PLP–SEC Pulsed laser polymerisation–size exclusion chromatography

SP–PLP–EPR Single–pulse pulsed–laser–polymerisation with EPR spectroscopy

S/N signal-to-noise ratio

TS transition state

TST transition state theory

Acknowledgements

I would like to thank Prof. Dr. Philipp Vana for supervising this work, useful discussions and the trust put in me. Without his continued support this work would not have been possible. Of course, a special thanks go to the whole thesis advisory committee, consisting of Prof. Dr. Philipp Vana, Prof. Dr. Thomas Zeuch and Prof. Dr. Dirk Schwarzer for much valued input in the annual meetings. Furthermore, I would like to thank Prof. Dr. Thomas Zeuch for being the second reviewer of this thesis and Prof. Dr. Dirk Schwarzer, Jun.-Prof. Dr. Daniel Obenchain, Jun.-Prof. Dr. Anna Krawczuk and Dr. Tim Schäfer for being a part of examination committee.

Dr. Florian Ehlers helped me with the experimental SP–PLP–EPR setup, laser tuning and pulse controller methods for which I am grateful. Dr. Holger Gibhardt and Prof. Dr. Burkhard Geil gave me useful insights on statistical analysis which were very helpful for the development of DRACO for which I thank both of them. Dr. Hendrik Kattner is greatly acknowledged for his helpfulness in discussions about the SP–PLP–EPR technique. Dr. Jürgen Grotheer and Dr. Barbara von der Lühe gave me access to the gas pycnometry system of the geological department for which I am thankful.

Many student interns contributed to this work, namely Daniel Meleschko, Tobias Weege, Franziska Otto and Daniel Kösters which is thankfully acknowledged. Also my bachelor student Milena Waldhoff is greatly acknowledged for her excellent work and contribution to this thesis. For proofreading the thesis, I would like to thank Robert Dallinger and Daniel Kösters.

Special thanks are in order to Luise Fanslau, Robert Dallinger and Daniel Kösters for useful scientific discussions. But also the whole AK Vana for being excellent colleagues and for many fun talks over a beer, fun games and barbecues. In this context, especially the Activity Arrangement Administrator Luise Fanslau and the Bierboxbehüter Robert Dallinger shall be mentioned.

Without my supportive family, I would not have been able to reach this point in my life. My parents, step-parents and brothers are owed great thanks for being incredibly supportive of my studies. Last but not least I would like to thank my girlfriend Lena for motivating during the writing process. I am lucky to have you in my life.